

การสังเคราะห์อนุภาคระดับนาโนเมตรที่มีสมบัติแม่เหล็กและการแทรกซึมผ่านแผ่นเนื้อฟันด้วย
สนามแม่เหล็กเพื่อประยุกต์ในการนำส่งยาสูโพรงฟัน

นางสาววิชชุดา อินจำปา



บทคัดย่อและแฟ้มข้อมูลฉบับเต็มของวิทยานิพนธ์ตั้งแต่ปีการศึกษา 2554 ที่ให้บริการในคลังปัญญาจุฬาฯ (CUIR)
เป็นแฟ้มข้อมูลของนิสิตเจ้าของวิทยานิพนธ์ ที่ส่งผ่านทางบัณฑิตวิทยาลัย

The abstract and full text of theses from the academic year 2011 in Chulalongkorn University Intellectual Repository (CUIR)
are the thesis authors' files submitted through the University Graduate School.

วิทยานิพนธ์นี้เป็นส่วนหนึ่งของการศึกษาตามหลักสูตรปริญญาวิทยาศาสตรมหาบัณฑิต
สาขาวิชาเคมี ภาควิชาเคมี
คณะวิทยาศาสตร์ จุฬาลงกรณ์มหาวิทยาลัย
ปีการศึกษา 2557
ลิขสิทธิ์ของจุฬาลงกรณ์มหาวิทยาลัย

SYNTHESIS OF MAGNETIC NANOPARTICLES AND INFILTRATION
THROUGH DENTINE DISC WITH MAGNETIC FIELD FOR APPLICATION IN DRUG DELIVERY
TO DENTAL PULP

Miss Wishulada Injumba



A Thesis Submitted in Partial Fulfillment of the Requirements
for the Degree of Master of Science Program in Chemistry
Department of Chemistry
Faculty of Science
Chulalongkorn University
Academic Year 2014
Copyright of Chulalongkorn University

Thesis Title	SYNTHESIS OF MAGNETIC NANOPARTICLES AND INFILTRATION THROUGH DENTINE DISC WITH MAGNETIC FIELD FOR APPLICATION IN DRUG DELIVERY TO DENTAL PULP
By	Miss Wishulada Injumpa
Field of Study	Chemistry
Thesis Advisor	Numpon Insin, Ph.D.

Accepted by the Faculty of Science, Chulalongkorn University in Partial Fulfillment of the Requirements for the Master's Degree

.....Dean of the Faculty of Science
(Professor Supot Hannongbua, Dr.rer.nat.)

THESIS COMMITTEE

.....Chairman
(Associate Professor Vudhichai Parasuk, Ph.D.)

.....Thesis Advisor
(Numpon Insin, Ph.D.)

.....Examiner
(Associate Professor Nongnuj Muangsin, Ph.D.)

.....External Examiner
(Suwussa Bamrungsap, Ph.D.)

วิชุลดา อินจำปา : การสังเคราะห์อนุภาคระดับนาโนเมตรที่มีสมบัติแม่เหล็กและการแทรกซึมผ่านแผ่นเนื้อฟันด้วยสนามแม่เหล็กเพื่อประยุกต์ในการนำส่งยาสู่โพรงฟัน (SYNTHESIS OF MAGNETIC NANOPARTICLES AND INFILTRATION THROUGH DENTINE DISC WITH MAGNETIC FIELD FOR APPLICATION IN DRUG DELIVERY TO DENTAL PULP) อ.ที่ปรึกษาวิทยานิพนธ์หลัก: นำพล อินสิน, 81 หน้า.

ในงานวิจัยชิ้นนี้ ได้สังเคราะห์อนุภาคคอมโพสิตระดับนาโน (MNCs) ที่มีสมบัติทางแม่เหล็กเคลือบด้วยพอลิพอลิเอททิลีนไกลคอลเมทาอะคริเลต (Polypoly(ethylene glycol) monomethyl ether methacrylate, PPEGMA) การเคลือบผิวของอนุภาคนี้ด้วย PPEGMA ใช้ปฏิกิริยาอะตอมทรานสเฟอร์เรดิคัลพอลิเมอไรเซชัน (Atom Transfer Radical Polymerization, ATRP) อนุภาคที่สังเคราะห์ได้มีขนาดในช่วง 20-200 นาโนเมตร อนุภาคคอมโพสิตระดับนาโนเคลือบด้วย PPEGMA เหล่านี้สามารถกระจายตัวได้ดีในน้ำและยังสามารถเข้ากันได้กับระบบชีวภาพอีกด้วย มากไปกว่านั้นอนุภาคคอมโพสิตระดับนาโนที่เคลือบด้วย PPEGMA ยังรักษาความเป็นซูเปอร์พาราแมกเนติก (superparamagnetism) ของอนุภาคแม่เหล็กเริ่มต้นแต่มีความเป็นแม่เหล็กน้อยกว่า กล้องจุลทรรศน์อิเล็กตรอนแบบส่องผ่าน (Transmission electron microscopy, TEM) ใช้เป็นเครื่องมือตรวจสอบขนาดของอนุภาคคอมโพสิตระดับนาโน พบว่าอนุภาค MNCs ขนาดต่าง ๆ ที่ได้ ได้แก่ขนาด 24.86 ± 4.38 , 45.24 ± 5.00 , 98.10 ± 8.88 และ 202.22 ± 6.70 นาโนเมตร เทอร์โมกราวิเมตริกส์แอลอโลยีซิส (Thermogravimetric analysis) ถูกใช้เพื่อหาร้อยละโดยน้ำหนักของพอลิเมอร์ที่เคลือบบนผิวของอนุภาคคอมโพสิตระดับนาโนพบว่าน้ำหนักของพอลิเมอร์ร้อยละเท่ากับ 86, 64, 33 และ 30 สำหรับอนุภาคคอมโพสิตระดับนาโนขนาด 20, 40, 100 และ 200 นาโนเมตรตามลำดับ และในงานวิจัยชิ้นนี้ได้นำอนุภาคคอมโพสิตระดับนาโนเหล่านี้ไปศึกษาผลของขนาดอนุภาคแม่เหล็กในการแทรกซึมผ่านแผ่นฟันแต่อนุภาคเหล่านี้ไม่สามารถแทรกซึมผ่านแผ่นฟันด้วยการเหนี่ยวนำจากแม่เหล็กภายนอกได้ นอกเหนือจากนี้งานวิจัยชิ้นนี้ได้นำอนุภาคแม่เหล็กระดับนาโนที่ไม่ผ่านการเคลือบสองแบบไปศึกษาการแทรกซึมผ่านแผ่นฟัน แบบแรกคืออนุภาคที่มีกรดโอเลอิกเป็นตัวทำให้อนุภาคแม่เหล็กเริ่มต้นเสถียรและสามารถกระจายตัวในโซโคลเฮกเซน แบบที่สองมีอะมิโนเอททอกซีไซเลน (APS) เป็นตัวทำให้อนุภาคแม่เหล็กระดับนาโนเสถียรและสามารถกระจายตัวในเอทานอล การแทรกซึมผ่านแผ่นฟันของอนุภาคแม่เหล็กเริ่มต้นทั้งสองแบบสามารถแทรกซึมผ่านแผ่นฟันได้ร้อยละ 2.87 และ 0.65 เมื่อเทียบกับความเข้มข้นเริ่มต้นสำหรับอนุภาคแม่เหล็กเริ่มต้นแบบที่หนึ่งและแบบที่สองตามลำดับ ผลการศึกษาการแทรกซึมผ่านแผ่นฟันของอนุภาคคอมโพสิตระดับนาโนพบว่าอนุภาคคอมโพสิตระดับนาโนไม่สามารถแทรกซึมผ่านแผ่นฟันได้เป็นเพราะอนุภาคเหล่านี้มีความเป็นแม่เหล็กน้อยมาก และผลจากการแทรกซึมผ่านแผ่นฟันของอนุภาคแม่เหล็กระดับนาโนเริ่มต้นทั้งสองแบบทำให้ทราบว่าอนุภาคระดับนาโนที่มีแรงแม่เหล็กมากพอมีความสามารถในการแทรกผ่านแผ่นฟันสำหรับการพัฒนาระบบรักษารากฟันแบบใหม่และงานวิจัยชิ้นนี้ยังเป็นประโยชน์ในอนาคตต่องานทางด้านทันตกรรมอีกด้วย

ภาควิชา เคมี ลายมือชื่อนิสิต

สาขาวิชา เคมี ลายมือชื่อ อ.ที่ปรึกษาหลัก

5572109523 : MAJOR CHEMISTRY

KEYWORDS: ATOM TRANSFER RADICAL POLYMERIZATION (ATRP) / MONODISPERSITY / PRISTINE MAGNETIC NANOPARTICLES / ROOT CANAL TREATMENTS / SUPERPARAMAGNETISM

WISHULADA INJUMPA: SYNTHESIS OF MAGNETIC NANOPARTICLES AND INFILTRATION THROUGH DENTINE DISC WITH MAGNETIC FIELD FOR APPLICATION IN DRUG DELIVERY TO DENTAL PULP. ADVISOR: NUMPON INSIN, Ph.D., 81 pp.

In this work, Polypoly(ethylene glycol) monomethyl ether methacrylate (PPEGMA) coated magnetic nanocomposite (PPEGMA-MNCs) size series were synthesized. The MNCs were coated with PPEGMA via Atom Transfer Radical Polymerization (ATRP). Their sizes are in the range of 20-200 nm. All of them are well-dispersed in water-based solution and biocompatible. Moreover, after they were coated with PPEGMA, they still exhibited magnetic response with superparamagnetic character but weaker than pristine magnetic NPs. The MNCs of 24.86 ± 4.38 , 45.24 ± 5.00 , 98.10 ± 8.88 and 202.22 ± 6.70 nm in diameter were obtained as measured by transmission electron microscopy (TEM). Thermogravimetric analysis (TGA) was used for determination of % weight of PPEGMA on MNCs showing the weight loss of 86%, 64%, 33% and 30% for PPEGMA-MNCs for the MNCs of 20, 40, 100 and 200 nm, respectively. These MNC size series were studied for the infiltration through a dentine disc. The results indicated that they cannot be infiltrated through dentine discs with an external magnet. Additionally, we studied the infiltration of the pristine magnetic NPs (MNPs) in two systems. In the first system, MNPs were stabilized with oleic acid and dispersed in cyclohexane (M_c), while the other MNPs were stabilized with aminoethoxysilane (APS) and dispersed in ethanol (M_e). The infiltration results indicated that MNPs can pass through dentine discs for 2.87% and 0.65% of the starting concentration for the infiltration of M_c and M_e , respectively. The differences in magnetization of MNPs and MNCs suggested that the MNCs cannot be infiltrated through dentine discs because their magnetic property is very weak. From these studies, we demonstrate that the magnetic nanoparticles with enough magnetization can be applied in the development of new techniques for root canal treatments and can be useful in as a new clinical approach in dentistry.

Department: Chemistry

Student's Signature

Field of Study: Chemistry

Advisor's Signature

Academic Year: 2014

ACKNOWLEDGEMENTS

Firstly, I would like to appreciate Dr. Numpon Insin who is my thesis advisor, gave me valuable assistance to achieve my thesis successfully complete.

For valuable comment and advices, I would to thank my thesis committee, associate professor Dr.Vudhichai Parasuk, associate professor Dr.Nongnuj Muangsin and Dr. Suwussa Bamrungsup. This research would have not been completed without all of their kindness.

In addition, I would special thank to all of members of Materials Chemistry and Catalyst Research Unit who are always helpful. Particularly, Mr. Sarawuth Phaenthong, Miss Chalatan Saengruengrit, Mr. Korakot Niyomsat, Miss Pavisara Nanthasurasuk, Miss Padtaraporn Chunhom, Miss Jamonpan Yangcharoenyuenyong and Mr. Phranot Ajkidkarn

Other special group is my family who gave me everything for my life and moreover, they are my encouragement for working on this research.

Finally, this work was partly funded by the Thailand Research Fund (MRG5680091), the Grants for Development of New Faculty Staff, the 90th Anniversary of Chulalongkorn University, Ratchadaphiseksomphot Endowment Fund, Chulalongkorn University, and the Science Achievement Scholarship of Thailand (SAST), additionally; we would like to thank Department of Chemistry, Faculty of Science, and Chulalongkorn University for laboratory facilities and instruments.

CONTENTS

	Page
THAI ABSTRACT.....	iv
ENGLISH ABSTRACT.....	v
ACKNOWLEDGEMENTS	vi
CONTENTS.....	vii
LIST OF TABLES	xi
LIST OF FIGURES.....	xii
LIST OF ABBREVIATIONS	xviii
CHAPTER I INTRODUCTION.....	1
1.1 statement of the problem.....	1
1.2 Objectives of this thesis.....	2
1.3 Scope of this thesis.....	2
1.4 The benefits of this thesis.....	2
CHAPTER II THEORIES AND LITERATURE REVIEWS	3
2.1 Materials	3
2.1.1 Magnetic materials	3
2.1.1.1 Origin of magnetism	3
2.1.1.2 Types of magnetic materials.....	3
2.1.1.3 Iron oxides	5
2.1.1.3.1 Iron oxide nanomaterials	5
2.1.2 Biocompatible materials.....	6
2.1.3 Dentine.....	6
2.2 Principle of synthesis.....	7

	Page
2.2.1 Magnetite nanoparticles (Fe_3O_4 or MNP)	7
2.2.2 Synthesis of silica nanoparticles (NPs).....	8
2.2.3 Coating silica on nanoparticles surface	9
2.2.4 Biocompatible polymer-coated MNPs (M@P).....	10
2.2.4.1 ATRP on silanol materials particles	13
2.3 Literature reviews.....	15
2.3.1 Applications of MNPs	15
2.3.2 PEGylation on MNPs	17
2.3.3 Infiltration of dentine discs	18
CHAPTER III EXPERIMENTS.....	23
3.1 The instrument	23
3.2 Chemicals	24
3.3 Synthesis and characterization of magnetic nanoparticles size series.....	25
3.3.1 Synthesis of magnetite (Fe_3O_4) NPs.....	26
3.3.2 Synthesis of core-shell magnetite-silica magnetic nanocomposites (M@S MNCs).....	28
3.3.3 Synthesis of magnetite-decorating silica particles (S-M) MNCs	29
3.3.3.1 Synthesis of bare silica NPs	29
3.3.3.2 Preparation of magnetite solution (M solution)	29
3.3.3.3 Attachment of magnetite NPs on silica particles (preparation of S-M MNCs)	29
3.3.4 Preparation of Polypoly(ethylene glycol) monomethyl ether methacrylate (PPEGMA)-coated S-M MNCs and M@S MNCs (Si-M@P and M@S@P MNCs)	30

	Page
3.3.4.1 NH ₂ -functionalization on S-M and M@S MNCs surface.....	31
3.3.4.2 Initiator-functionalization on S-M-NH ₂ and M@S-NH ₂ MNCs surfaces	31
3.3.4.3. Synthesis of PPEGMA-coated on S-M-Br and M@S-Br MNCs surface	31
3.4 Characterization of synthesized-MNPs and MNCs	32
3.5 Preparation of dentine disc	33
3.6 Study of particles infiltration through dentine discs	33
3.6.1 Data analyses.....	35
CHAPTER IV RESULTS AND DISCUSSIONS	36
4.1 Characterization of synthesized MNP and synthesized MNCS size series	36
4.1.1 Characterization of synthesized MNP and synthesized MNCS size series with X-ray diffraction	36
4.1.2 Preparation of dentine disc.....	53
4.2 The investigation of the infiltration through dentine discs.....	55
4.2.1 The investigation of the infiltration through dentine discs of the two types of pristine magnetite samples	55
4.2.2 The investigation of the infiltration through dentine disc of PPEGMA- MNC size series.	57
4.2.3 The investigation of the effect of time on the infiltration through dentine discs of the pristine magnetites	59
4.2.4 The investigation of the effect from dentine thickness on the infiltration through the dentine disc of the pristine magnetites	60
4.2.5 The investigation of magnetic field strength on the infiltration through the dentine discs of the pristine magnetites.....	61

	Page
4.2.6 The investigation of infiltration through different dentine discs of the pristine magnetites.....	62
CHAPTER V CONCLUSION.....	64
REFERENCES.....	66
VITA	81



LIST OF TABLES

Table	Page
3.1 List of instrument.....	23
3.2 List of chemical	24
3.3 Temperature program for the preparation of monodispersed magnetite NPs (MNPs).....	28
4.1 The sizes of PPEGMA-MNCs, PPEGMA-coated M@S MNCs PPEGMA-M@S MNCs (PPS-20 and PPS-40 for the sizes of 20 nm and 40 nm respectively), PPEGMA-S-M MNCs (PPS-100 and PPS-200 for the sizes of 100 nm and 200 nm respectively) as measured by the Zetasizer ZSP analyzer	51
4.2 The summary for the infiltration of different sizes of PPEGMA-MNCs (PPS) through dentine discs (PPS-20, PPS-40, PPS-100 and PPS-200 with the MNC sizes of 20, 40 100 and 200 nm in diameters, respectively) for 8.0 h.	58

LIST OF FIGURES

Figure	Page
2.1 Demonstration of magnetic moment in an atom, (a) magnetic moment from orbital moment and (b) magnetic moment from spin moment.....	3
2.2 Diagrams presenting superparamagnetic behavior of MNPs.....	6
2.3 Illustration of tooth anatomy[28].....	7
2.4 Mechanism for a sol-gel formation of silica[48]	9
2.5 Schematic diagram of synthesis of silica-coated MNPs (M@SiO ₂) by reverse microemulsion [53]	10
2.6 Common synthetic pathways to immobilized ATRP initiator on material surface [65].....	11
2.7 Common chemical structures of ATRP monomer [65].....	12
2.8 Mechanism of halogen exchange in ATRP[67].....	13
2.9 The mechanism of the reaction between Ninhydrin and APS [69].....	14
2.10 Schematic illustration of polymerization through ATRP[67].	15
2.11 Example of multimodal imaging [74].....	16
2.12 Illustration of synthesis of Dox SMNPs and their cellular functions for drug release and tumor imaging. FRET=fluorescence resonant energy transfer[75].....	17
2.13 Direct MNPs synthesis using PEG precursor or graft copolymer [77].....	18
2.14 MNCs synthesis using modified-PEG with unsaturated polymers [47].....	18
2.15 (a) Scanning electron micrograph of intact dentine surface. Showing opened dentinal tubules (b) Scanning electron micrograph of caries affected dentine surface occluded dentinal tubules [2].	19
2.16 Diagram of the experimental system for hydraulic conductance measurement [2]	20

LIST OF FIGURES (Continued)

Figure	Page
2.17 HIFU experimental arrangement used for <i>in vitro</i> experiment on dentine sample [1].....	21
2.18 (A-G) The collapse of a spark discharge bubble of maximum bubble radius, $R_{\max} = 3.3$ mm (taken horizontally from frame B, $t = 0.46$ milliseconds), on top of a tubular channel of 3.3-mm diameter. The timing for each frame in milliseconds [3].	21
2.19 (a) The cross-section of the dentine samples with the exposed dentinal tubules does not show antibacterial-nanoparticles within the lumen, (b) Field Emission scanning electron micrographs of dentinal tubules from the HIFU treatment group samples and (c) showing aggregation of antibacterial nanoparticles of 100 - 200nm sizes [3].....	22
3.1 Schematic presentation for the synthesis of magnetic nanoparticles size series...26	
3.2 Schematic presentation of PPEGMA coated on MNCs (MNC@PPEGMA MNCs) size series	30
3.3 Illustration of experiment setup for infiltration through the dentine disc, (a) strong magnetic field (32.59×10^2 gauss) and (b) stronger magnetic field (36.86×10^2 gauss).....	35
4.1 The XRD patterns of the synthesized magnetic nanoparticles (MNPs) (purple), M@S (M@S-20) (orange), M@S-40 (pink) for the composites with the sizes of 20 and 40 nm in diameter, respectively, and S-M MNCs (S-M-100 (green), S-M-200 (blue) for the composites with the sizes of 100 and 200 nm in diameter, respectively. In comparison with the standard pattern files JCPDS 19-0629 (black) of magnetite and JCPDS 29-0085 (red) of amorphous silica.....	36

LIST OF FIGURES (Continued)

Figure	Page
4.2 IR spectra of MNCs, M@S MNCs (M@S-20 (a), M@S-40 (b) for the MNCs with the sizes of 20 and 40 nm in diameter, respectively), and S-M MNCs (S-M-100 (c), S-M-200 (d) for the MNCs with the sizes of 100 and 200 nm in diameter, respectively).....	38
4.3 IR spectra of NH ₂ -functionalized MNCs, NH ₂ -functionalized M@S MNCs (M@S-NH ₂ -20 (a), M@S-NH ₂ -40 (b) for the MNCs with the sizes of 20 and 40 nm in diameter, respectively.) and NH ₂ -S-M MNCs (S-M-NH ₂ -100 (c), S-M-NH ₂ -200 (d) for the MNCs with the sizes of 100 and 200 nm in diameter, respectively)	38
4.4 IR spectra of initiator attached MNCs, BiBB attached M@S MNCs (M@S-Br-20 (a), M@S-Br-40 (b) for the MNCs with the sizes of 20 and 40 nm in diameter, respectively.) and BiBB attached S-M MNCs (S-M-Br-100 (c), S-M-Br-200 (d) for the MNCs with the sizes of 100 and 200 nm in diameter, respectively).....	39
4.5 IR spectra of monomer (PEGMA) (P), PPEGMA coated MNCs, PPEGMA-M@S MNCs (PPEGMA-M@S-20 (a), PPEGMA-M@S-40 (b) for the MNCs with the sizes of 20 and 40 nm in diameter, respectively.) and PPEGMA coated S-M MNCs (PPEGMA-S-M-100 (c), PPEGMA-S-M-200 (d) for the MNCs with the sizes of 100 and 200 nm in diameter, respectively).....	40
4.6 Schematic presentation of the mechanism of Ninhydrin reacting with APS.....	42
4.7 Results for Ninhydrin test of NH ₂ -functionalized MNCs and BiBB attached MNCs, M@S-NH ₂ (a), M@S-Br (b) and APS (c), DI water blank (d) for the MNCs with the size of 20 nm in diameter.	43
4.8 Results for Ninhydrin test of NH ₂ -functionalized MNCs and BiBB attached MNCs, M@S-NH ₂ (a), M@S-Br (b) and APS (c), DI water blank (d) for the MNCs with the size of 40 nm in diameter.	44

LIST OF FIGURES (Continued)

Figure	Page
4.9 Results for Ninhydrin test of NH ₂ -functionalized MNCs and BiBB attached MNCs, S-M-NH ₂ (a), S-M -Br (b) and APS (c), DI water blank (d) for the MNCs with the size of 100 nm in diameter.....	45
4.10 Results for Ninhydrin test of NH ₂ -functionalized MNCs and BiBB attached MNCs, S-M-NH ₂ (a), S-M -Br (b) and APS (c), DI water blank (d) for the MNCs with the size of 200 nm in diameter.	46
4.11 TEM images of MNPs (a), M@S MNCs (b and c for the sizes of 20 nm and 40 nm respectively), S-M MNCs (d and e for the sizes of 100 nm and 200 nm respectively) and pure silica (f and g for the sizes of 100 nm and 200 nm respectively).....	48
4.12 TEM images of PPEGMA-coated on MNCS, PPEGMA-coated M@S MNCs PPEGMA-M@S MNCs (a and b for the sizes of 20 nm and 40 nm respectively), PPEGMA-S-M MNCs (c and d for the sizes of 100 nm and 200 nm respectively).....	50
4.13 TGA curves of particles with PPEGMA coated on MNCs, PPEGMA-coated M@S MNCs PPEGMA-M@S MNCs (PPS-20 and PPS-40 for the sizes of 20 nm and 40 nm respectively), PPEGMA-S-M MNCs (PPS-100 and PPS-200 for the sizes of 100 nm and 200 nm respectively)	51
4.14 Show magnetization of pristine magnetites (M) (black) and PPEGMA-M@S MNCs (PPS-20 and PPS-40 for the sizes of 20 nm and 40 nm respectively), PPEGMA-S-M MNCs (PPS-100 and PPS-200 for the sizes of 100 nm and 200 nm respectively).	52
4.15 SEM images of the three dentine discs labelling (1), (2) and (3), respectively,.....	54
4.16 The dispersions of the pristine magnetites, a) the dispersion of M _c and b) the dispersion of M _e	55

LIST OF FIGURES (Continued)

Figure	Page
4.17 Diagram for the percent quantity of iron (Fe) when compare with the starting Fe that passed through dentine discs for 8.0 h starting from 0.453 mg of Fe in M_c and 0.505 mg of Fe in M_e injected to the apparatus.	56
4.18 Diagram for the percent quantity of iron (Fe) in M_c that pass through dentine discs for 0.5, 2.0, 4.0, 6.0 and 8.0 h.....	59
4.19 Diagram for the percent quantity of iron (Fe) in M_c that passed dentine disc using the different dentine discs (0.45, 0.68 and 0.95 mm) for 4.0 h with 0.453 mg of starting Fe quantity injected to apparatus as shown in Figure 3.3.	60
4.20 Diagram for the percent quantity of iron (Fe) in M_c that passed dentine disc using the same dentine discs with the thickness of 0.45 mm for 0.5 h and 1.287 mg of Fe injected to the apparatus.....	61
4.21 Diagram for the percent quantity of iron (Fe) in M_c that passed dentine disc using different dentine discs for 8.0 h with 0.453 mg of starting Fe injected to experiment setup.	62
A1 Distribution graph of PPS-20 from DLS analysis	76
A2 Distribution graph of PPS-40 from DLS analysis	76
A3 Distribution graph of PPS-100 from DLS analysis	77
A4 Distribution graph of PPS-200 from DLS analysis	77
A5 Distribution graph of PPS<20 from DLS analysis	78
A6 TEM image of PPS<20	78
A7 Photographs comparing the dispersity of MNCs (left) and PPEGMA coated MNCs dispersions (right).;figures (a), (b), (c), and (d) are for NPs of the size 20, 40, 100 and 200 nm in diameter, respectively.	79
A8 Photographs of the preparation process of the dentine discs, (a) The dentine disc casting in a resin and (b) the dentine disc cutting.....	80

LIST OF FIGURES (Continued)

Figure	Page
A9 Images of the pristine magnetite dispersion (M_c , left) and (M_e right), (a) without a strong magnet and (b) with a strong magnet.....	80



LIST OF ABBREVIATIONS

M	=	magnetite
M _c	=	magnetite was stabilized with oleic acid and dispersed in cyclohexane
M _e	=	magnetite was stabilized with AP and dispersed in ethanol
MNPs	=	magnetic nanocomposites
M@SiO ₂ (M@S)	=	magnetite was coated with silica
M@SiO ₂ (S-M)	=	silica was attached with magnetite
PPS<20	=	MNCs size less than 20 nm in diameter was coated with PPEGMA
PPS-20	=	MNCs size 20 nm in diameter was coated with PPEGMA
PPS-40	=	MNCs size 40 nm in diameter was coated with PPEGMA
PPS-100	=	MNCs size 100 nm in diameter was coated with PPEGMA
PPS-100	=	MNCs size 100 nm in diameter was coated with PPEGMA
h	=	hour
min	=	minute
g	=	gram
mg	=	milligram
L	=	liter
mL	=	milliliter

CHAPTER I

INTRODUCTION

1.1 statement of the problem

Root canal inflammation is considered as one of many dangerous inflammation types. The inflammation is normally treated with antibacterial drug. Also, in the present day, the well-known technique for root canal treatment is the endodontic therapy. This technique is claimed to be able to treat root canal inflammation completely; however, it could leave some side effects [1-3]. The process for the treatment is very complex because several steps have to be done. Moreover, each step takes long time to complete, making the patient extensively agonized by root canal inflammation. Secondly, these techniques can also destroy large area of dentine. Another effect would be the highly expensive instruments so that patient would have to spend much money for the treatment. Problems mentioned above encourage many researchers to find a simpler and cheaper method for root canal treatment. In previous trials [1-3], many tests failed due to unsuccessful delivery systems of antibacterial drugs to the inflamed area (below the root canal). Therefore, this work would focus on the use of magnetic nanoparticles in delivery system which is proposed for a better delivery to the affected area.

Drug delivery system in this work is using magnetic nanoparticles (MNPs) as a carrier. MNPs display the behavior, called the superparamagnetic behavior, which is a greater character compared to large magnetic particles in many aspects. When MNPs are not induced by an external magnetic field, MNPs do not exhibit ferromagnetic property; however, it can show strong magnetic response in the presence of an external magnetic field. Such behavior makes MNPs the best candidate for drug delivery system in root canal therapy. This work aims to use their special magnetic character for inducing drugs to target area with an external magnet.

1.2 Objectives of this thesis

1.2.1 To synthesize magnetic nanocomposites (MNCs) with biocompatible polymers with various sizes in a series.

1.2.2 To investigate infiltration of MNPs size series through dentine discs with magnetic field for application in drug delivery to dental pulp.

1.3 Scope of this thesis

First of all, we synthesized MNPs size series using a process of four parts. The first part includes the synthesis of magnetite nanoparticles as MNPs, synthesis of core-shell magnetic nanocomposites (M@S MNCs), preparation of magnetic NPs solution (MP solution), synthesis of bare silica and synthesis of M immobilized on bare silica MNCs (S-M MNCs). Second part is the amine functionalization on the surface of core-shell MNPs. Third part is initiator functionalization, and the final part is the polymerization. For all parts, nanoparticles were characterized by transmission electron microscope (TEM) and Fourier transmission infrared spectroscopy (FT-IR). Moreover, ninhydrin test was conducted to confirm the amine functionalization. Next, we investigated the infiltration through a dental disc. We studied six factors affecting infiltration. Those factors included solvent which MNCs dispersed, the differences in sizes of MNCs, time consuming, the different dentine thickness, the strength of an external magnetic field and the different dentine disc for the infiltration. The investigation of infiltration was done by atomic absorption spectroscopy (AAS).

1.4 The benefits of this thesis

1. Polymer-coated MNCs size series in the range of 20 -200 nm can be obtained.
2. This work can provide new methods for root canal therapy.
3. We can understand effects of factors to infiltration of MNPs size series through a dentine disc, which can be applied to other filtering systems

CHAPTER II

THEORIES AND LITERATURE REVIEWS

2.1 Materials

2.1.1 Magnetic materials

2.1.1.1 Origin of magnetism

Magnetic properties of materials come mostly from magnetic moments of an individual electron. Each electron has magnetic moment which is originated from two sources [4] as show in Figure 2.1. One is called “orbital moment” as show in Figure 2.1b which is a result from electrons that orbit around nucleus. Another is electron spin or electron rotating around itself leading to a so-called “spin moment” as show in Figure 2.1a. The orbital moment generates very small magnetic moment when compare to the spin moment as show in Figure 2.1. Therefore, spin moment contributes to most of magnetic moment of the materials.

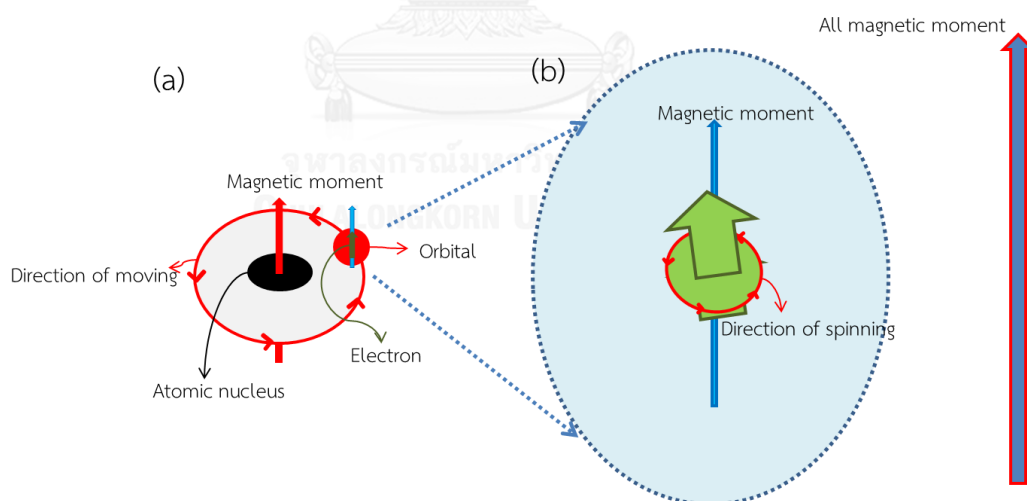


Figure 2.1 Demonstration of magnetic moment in an atom, (a) magnetic moment from orbital moment and (b) magnetic moment from spin moment

2.1.1.2 Types of magnetic materials

All magnetic materials can be classified into three classes by their different properties [4]. Types of materials are diamagnetic, paramagnetic and ferromagnetic

materials. In addition, antiferromagnetism and ferrimagnetism are subclasses of ferromagnetism. Magnetic materials can be divided by the magnetization (M_z). When the materials have high magnetization, they show strong magnetic responses. The magnetization of materials depends on magnetic susceptibility (χ_m) and magnetic field strength (H) as shown in Equation 2.1.

$$M_z = \chi_m H \quad (2.1)$$

For diamagnetism, it is a type of magnetic materials with the weakest magnetism. Its magnetic moment is only generated from the orbital moment because the spin moment is cancelled by pairing up of electrons with spin up and spin down arrangements. Thus, its volume susceptibility is very low (-10^{-5}) [5]. When diamagnetic materials are placed near strong magnets, they are attracted to the weakest area of the field, or they are extremely repulsed from strong magnets [5].

Paramagnetism is stronger form of magnetism comparing to diamagnetism. The volume susceptibility would be at around 10^{-5} - 10^{-2} [5]. It is induced by magnetic moment of both orbital moment and spin moment, but spin moment is the dominant factor. Due to magnetic momentous directions which are arranged randomly, net moment is mostly cancelled out. When paramagnetic materials are placed in a magnetic field, random magnetic moments are arranged into same direction with the external magnetic field. Thus, they are attracted while placed near a magnet. On the other hand, once paramagnetic materials are placed outside a magnetic field, magnetic moments are random, resulting in a non-permanent magnetization.

Ferromagnetism is the strongest form of magnetism. The volume susceptibilities of ferromagnetic materials are as high as 10^6 . Their magnetizations are permanent even in the absence of magnetic fields. Permanent magnetic moments are resulted of both of orbital moment and spin moment like in paramagnetic form; however,

spin moments of each unpaired electron are aligned in the same direction. In addition, each magnetic moment is coupled together, and the materials maintain their permanent magnetization. Ferromagnetism consists of other two subclasses, ferrimagnetism and antiferromagnetism. Ferrimagnetism is a type which some of unpaired electrons align in opposite direction with the net magnetic moment. Therefore, the ferrimagnetic materials would respond to external magnetic field more weakly than ferromagnetic materials of the same quantity. For antiferromagnetism, all unpaired electrons align in opposite direction and the magnetic moment is cancelled out. Therefore, the net magnetic moment is zero in antiferromagnetic materials. When antiferromagnetic materials are placed in magnets, some the unpaired electrons is induced to align the same direction with magnetic moments and resulted in a little permanent magnetization[4, 6].

2.1.1.3 Iron oxides

Iron oxide compounds are common found in 3 major crystalline phases, which are magnetite (Fe_3O_4), maghemite ($\gamma\text{-Fe}_2\text{O}_3$) and hematite ($\alpha\text{-Fe}_2\text{O}_3$). Magnetite and maghemite possess a ferrimagnetic property, while hematite is an antiferromagnetic[7]. Magnetite and maghemite are of our focus because of their magnetic property that leads to strong responses to an external magnetic field.

2.1.1.3.1 Iron oxide nanomaterials

When ferromagnetic and ferrimagnetic are synthesized in nanoscale, they present a special behavior which is called superparamagnetism [6]. This behavior is similar to paramagnetic behavior in absence of an external magnetic field, but superparamagnetic materials are attracted to magnetic fields much more strongly than paramagnetic materials. The superparamagnetic materials will be attracted to a magnet or exhibit ferromagnetic response in a presence of an external magnetic field, but their magnetic responses disappear when the external magnetic field is removed as shown in Figure 2.2.

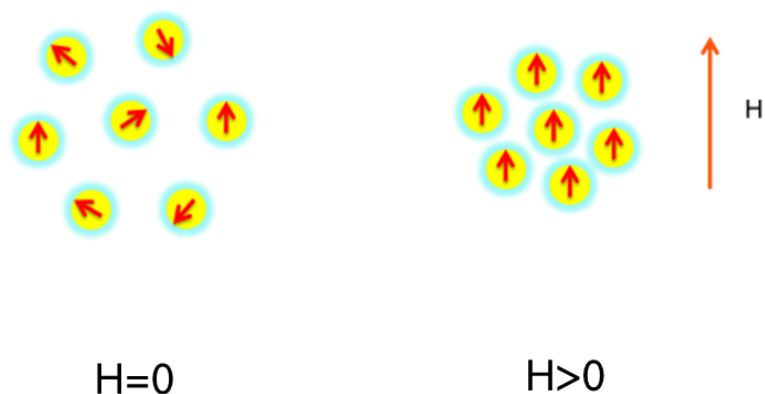


Figure 2.2 Diagrams presenting superparamagnetic behavior of MNPs.

2.1.2 Biocompatible materials

Biocompatible materials are materials which are engineered by controlling of the interactions with components of living systems. Therefore, biocompatible materials can be compatible with biology. Furthermore, these materials are water-soluble and stable in hydrophilic solution. Therefore, the biomaterials are applied as stabilizers and bio-coatings [8].

In order to develop magnetic materials used in biological application, such materials are necessary to be biocompatible. In the present days, biocompatible materials can be made from both of inorganic compounds[9, 10] and organic compounds[11]. Examples of biocompatible inorganic compounds are silica[12], titanium, silicones and hydroxyapatite. For organic compounds[13-16], there are teflon, polyurethane, poly(ethylene glycol)[17, 18], poly (polyethylene glycol) methacrylate[19-21], polyamidoamine-type Dendron-b-poly(2-dimethylaminoethyl methacrylate)-b-poly(N-isopropylacrylamide) (PAMAM-b-PDMAEMA-b-PNIPAM)[22] and poly(lactic-glycolic acid)[23, 24] as samples of commonly used materials. In addition, multi-functionalized materials are of interest as well because these materials can be widely and more diversely used in biological applications. Factors for choosing the suitable materials depend on applications; for example, in coating application would use stable silica and polymer, while for releasing application, porous materials [24] and degradable polymers would be considered [25].

2.1.3 Dentine

Dentine is a main component of teeth as shown in Figure 2.3. It is a second layer covered by enamel. Dentine covers a pulp cavity which is adjacent to tissues that contain

nerves and blood vessels. The dentine thickness is about 3-10 mm[26], and it consists of tiny tubules which are connected between enamel and pulp cavity. Dentine can be divided into 3 types which are primary, secondary and tertiary dentines. Primary dentine is a layer that is closest to enamel, while secondary dentine is a layer that is next to primary dentine. Tertiary dentine is a layer which is closest to pulp cavity. Tiny tubules in dentine have the size range of about 2-3 micrometers in diameter[27].

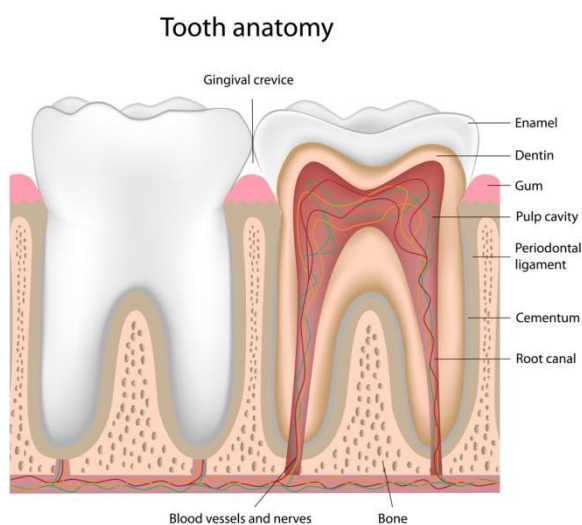
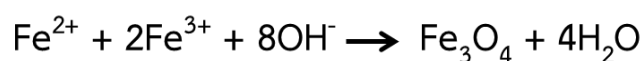


Figure 2.3 Illustration of tooth anatomy[28]

2.2 Principle of synthesis

2.2.1 Magnetite nanoparticles (Fe_3O_4 or MNP)

There are many techniques that are used for synthesis of MNPs. These techniques include co-precipitation of iron salts, microemulsion and thermal decomposition. Co-precipitation technique is the simplest method, but the product has polydispersity and low crystallinity. The overall reaction might be written as shown in Equation (2.1) [29]. For microemulsion technique, the product is better monodispersity than the products from co-precipitation, but the product still exhibits low crystallinity. The product from thermal decomposition technique is the best in the properties of monodispersity and high crystallinity[30].



(2.1)

Therefore, the synthesis of magnetite nanoparticles in this thesis was mainly done using thermal decomposition method to obtain the best properties of the magnetic nanoparticles [31-33]. Ferric oleate was used as a precursor. Temperature which was used for the decomposition is 320 °C. Finally, after heated to 320 °C [31], they were left to oxidize in ambient air condition. Moreover, this method use others precursor which are ferric complex such as $\text{Fe}(\text{CO})_5$ [34], $\text{Fe}(\text{acac})_3$ (acac = acetylacetonate)[35], iron oleate[36], $\text{Fe}(\text{Cup})_3$ (Cup = N-nitrosophenylhydroxylamine) [37, 38], Prussian blue ($\text{Fe}_4[\text{Fe}(\text{CN})_6]_3 \cdot 14\text{H}_2\text{O}$)[39, 40], Fe-urea complex ($[\text{Fe}(\text{CON}_2\text{H}_4)_6](\text{NO}_3)_3$)[38], ferrocene ($\text{Fe}(\text{C}_5\text{H}_5)_2$)[41], and $\text{Fe}_3(\text{CO})_{12}$ [42].

2.2.2 Synthesis of silica nanoparticles (NPs)

The well-known method used for synthesis of silica is sol-gel method. This process is based on the hydrolysis and condensation of molecular precursors in solution, originating a “sol” of NPs. Then, condensation and inorganic propagation lead to a three-dimensional NPs network denominated (gel) [43]. Silica product from this method can be varied in sizes depending on such parameters as type of solvent, amount of solvent, amount of TEOS and amount of catalyst (ammonia) [44-46]. Reverse emulsion technique is also attractive because this technique can control silica size by the size of micelle. Moreover, silica from this technique is monodispersity as well [47]. Micelles are easily prepared with polyethylene glycol tert-octylphenyl ether (triton x-100) as surfactant, 1-hexanol as co-surfactant, water as polar solvent and cyclohexane as non-polar solvent. NH_4OH and H_2O act as catalysts, and TEOS acts as silica source or reactant [47]. Mechanism of silica formation by hydrolysis followed by condensation of TEOS is shown below (Figure 2.4).

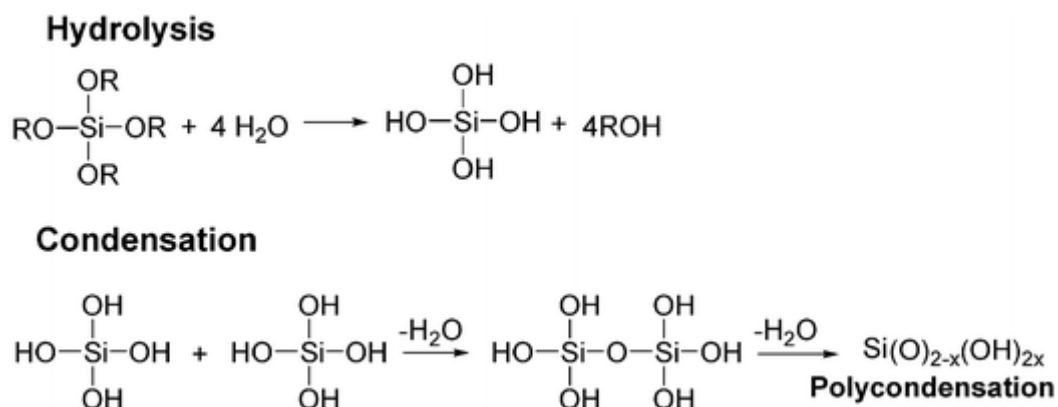


Figure 2.4 Mechanism for a sol-gel formation of silica[48]

2.2.3 Coating silica on nanoparticles surface

Silica is one of biocompatible materials that is widely used as coating materials because it can be easily formed by hydrolysis of commonly starting chemical (tetraethyl orthosilicate, TEOS), and it can be easily multi-functionalized on its surface [49]. Silica has been used for metal nanoparticles (NPs) coating, such as on Au, Ag, Cu and Pt [43, 50, 51]. Silica coating on the nanoparticles surface in water solution is done by electrostatic interaction. On the other hand, metals, metal oxides (magnetite) and quantum dots (QDs) NPs, which are synthesized and dispersed in organic solvent or hydrophobic NPs, cannot be used in bio-application directly. Silica coating on their NPs surface can make all of them water soluble, and they then can be used in bio-applications [52].

One method used for silica coating on magnetite is a reverse emulsion method [53]. In generally, emulsion is generated using a surfactant or fabricant [54-56]. The surfactant contains two parts; one is hydrophobic, and the other one is a hydrophilic part. Normally, two solvents which are non-polar solvent and polar solvent were mixed in order to make emulsion in which amount of the polar solvent should be extremely more than amount of non-polar solvent. The surfactant is added into the mixture and emulsion is formed [57]. On the other hand, reverse emulsion was formed by the opposite method in which the amount of non-polar solvent is much

more than amount of polar solvent[58]. For the formation of silica, silica is formed by hydrolysis and condensation of TEOS (Figure 2.4) [59, 60]. In this method, silica will be coated on the particles surface when the particles are located at the center of reverse emulsion and no interaction between magnetite NPs (MNPs) and silica. MNPs surface is coated with silica via the like-dissolve-like explanation.

The reverse emulsion method is widely used for silica coating on magnetite surface because the size of core-shell MNCs can be controlled, and the MNCs are monodispersity as well [61, 62]. Three main steps are generaling conducted for coating of silica on magnetite via reverse emulsion. At the beginning, reverse micelle was formed with cyclohexane and polyoxyethylene (5) nonylphenylether (Igepal CO-520) were mixed. After that, MNPs were added into the mixture and ammonium hydroxide (NH_4OH) as a catalyst for silane coupling. At last, TEOS was added as silica source. Finally, M@SiO_2 magnetic nanocomposites (MNCs) were obtained after silane coupling of TEOS as shown in Figure 2.5

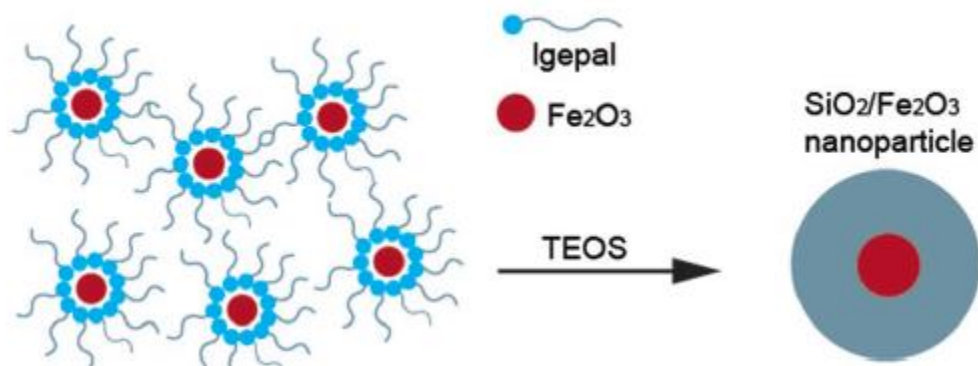


Figure 2.5 Schematic diagram of synthesis of silica-coated MNPs (M@SiO_2) by reverse microemulsion [53]

2.2.4 Biocompatible polymer-coated MNPs (M@P)

The MNPs are toxic for human [63]. It can be coated with biomaterials to reduce the toxicity. In previous studies, biopolymers were used for MNPs coating. There are two methods which are used for polymers coating on MNPs. The simplest method is co-precipitation where iron salts were precipitated in the presence of the polymers [64]. This method used no chemical interaction between MNPs and the polymers.

The polymers on the MNPs are not stable in this method. Another method is atom transfer radical polymerization (ATRP) method [65]. The methods rely on radical polymerization. There are 2 main steps; in the beginning, generation radical on materials surface which is coated by catalyst (Cu^+). In this step, materials need to immobilize initiator on their surface. The initiator mostly used is alkyl halides (C-Br and C-Cl) as shown in Figure 2.6. Due to this method relying on radical polymerization, the monomer is needed to consist of conjugated double bond as shown in Figure 2.7. Next, polymerization of monomer is started. Finally, polymer completely coated on the materials [65]

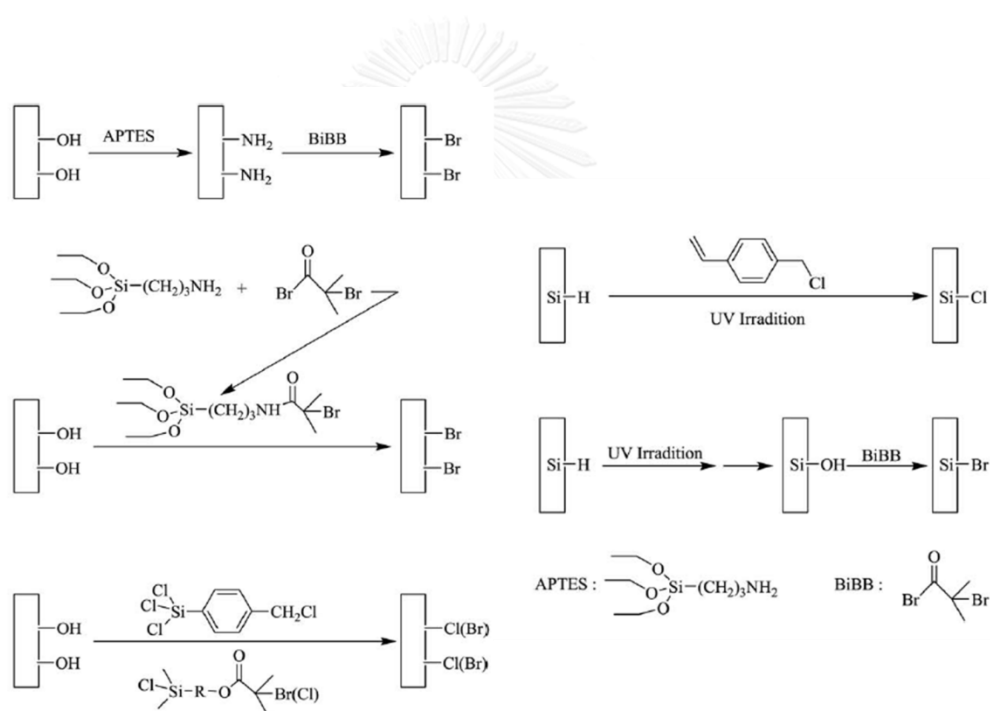


Figure 2.6 Common synthetic pathways to immobilized ATRP initiator on material surface [65].

The ATRP is widely well-known for polymer coating because this technique can control polymer chains by adjusting the amount of monomer used and time consumed [65, 66]. The polymers bind to the MNPs via covalent or coordinate

bonds, so the polymers strongly coat on the MNPs. Therefore, the ATRP method is widely used for the polymers coating on the MNPs surface.

Although, the silica coated MNPs (M@S) are biocompatible, they are not stable enough in water solution where it can be used for bio-applications. The biopolymers are not only biocompatible but also act as a stabilizer for MNPs and others NPs [63]. The M@S is needed to be coated with biopolymers for improvement their stability for applying in biological fields

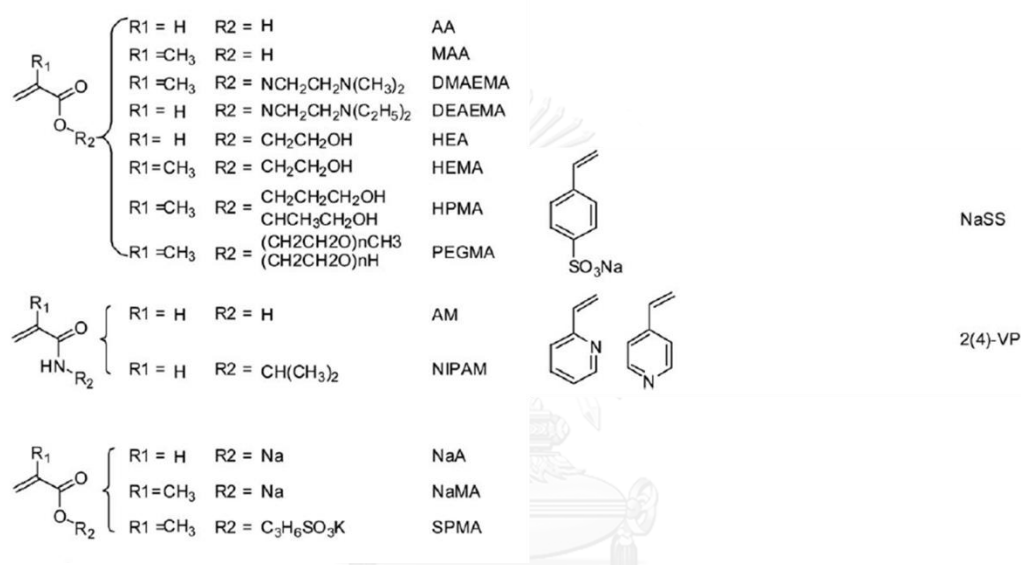


Figure 2.7 Common chemical structures of ATRP monomer [65]

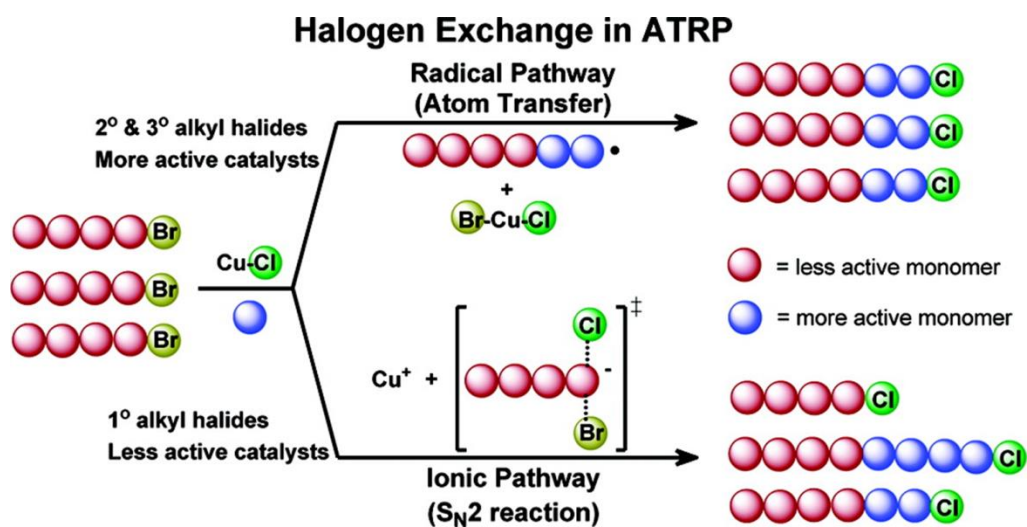


Figure 2.8 Mechanism of halogen exchange in ATRP[67]

2.2.4.1 ATRP on silanol materials particles

Generally, 3-aminopropyl silane (APS) chemical is used for NH_2 -functionalization of the materials particles with silanol groups ($-\text{Si-OH}$) and similar groups on their surface, such as silica and iron oxide [16, 68] before applying ATRP initiator immobilization as shown in Figure 2.8. The APS act as a source of amino group. The material particles with silanol groups on surface can react with silanol group on hydrolyzed APS. The reaction is proceeded by silane coupling (hydrolysis-condensation). NH_2 -functionalized particles is obtained (M-NH_2).

The amino group of a primary amine can be characterized by a colorimetric reaction. The amino group can form a purple compound with ninhydrin, a reaction used to detect amino compound or a ninhydrin test [69]. This reaction can be applied for the detection of NH_2 functionalization on the particle surfaces. The mechanism of formation of the purple compound for the reaction starting with APS and ninhydrin was shown in Figure 2.9

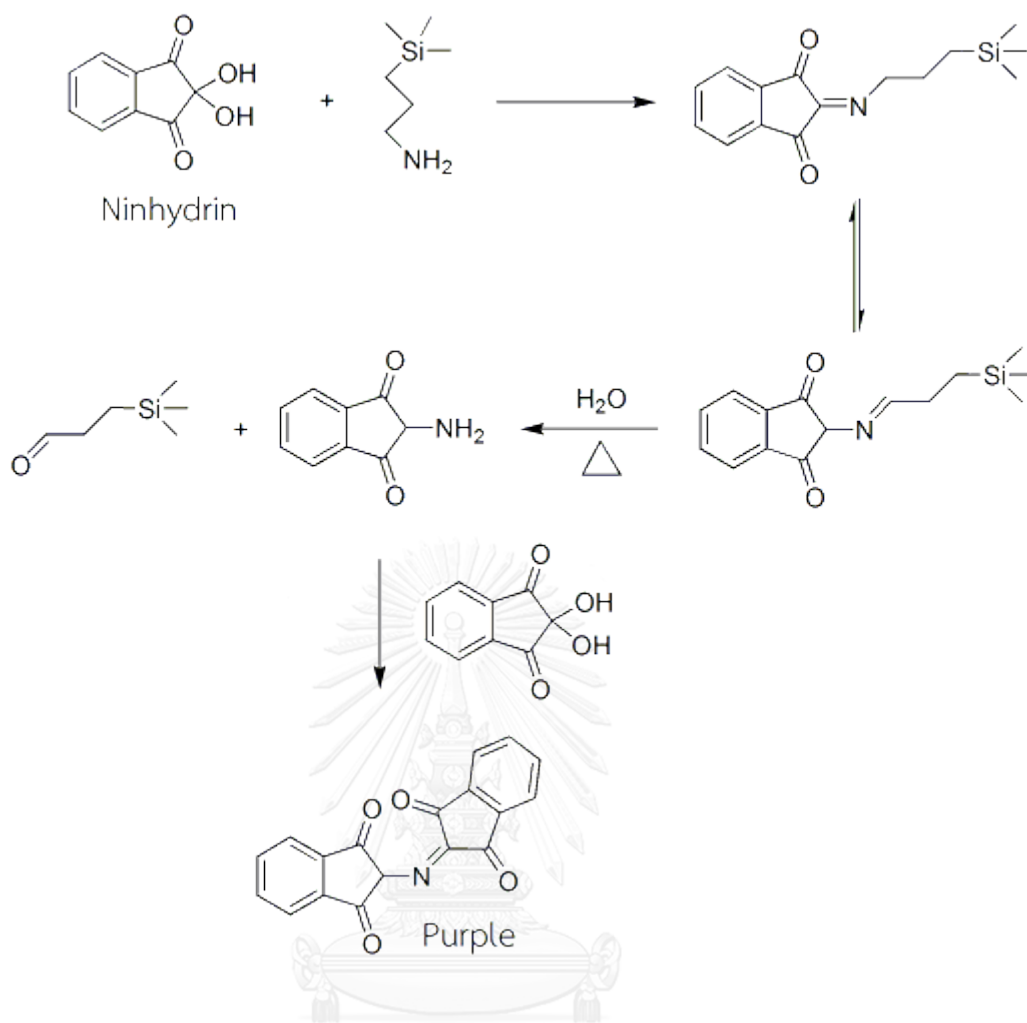


Figure 2.9 The mechanism of the reaction between Ninhydrin and APS [69].

Commonly, the ATRP initiator that is used for immobilization on the M-NH₂ is 2-bromo isobutylylbromide (BiBB) [66, 67] because it consists of halogen (Br) as shown in Figure 2.6. Structure of the compound extremely supports the generation of radical because the radical is stabilized by delocalization on carbonyl group. Moreover, Br-C bond was easily broken due to big differences between electronegativity (EN) of the two atoms. After the reaction, material particles were completely immobilized with initiator (BiBB) to form (M-NH₂-Br) [47]. M-NH₂-Br has C-Br bond on the surface. The bond can be broken by a reducing agent. When a radical is generated on the particle surface, ATRP starts taking place as shown in Figure 2.10

Finally, the silanol group on the material surfaces is completely coated with the polymers.

For polymer-coated MNPs, PPEGMA is claimed to be a biocompatible polymer with a long-term circulation in human body [70]. In addition, MNPs that were coated with PPEGMA can circulate for a long time in blood system[71]. The MNPs were reported to be coated with PPEGMA via ATRP [67, 72] using $\text{Cu}^{(+)}$ as catalyst.

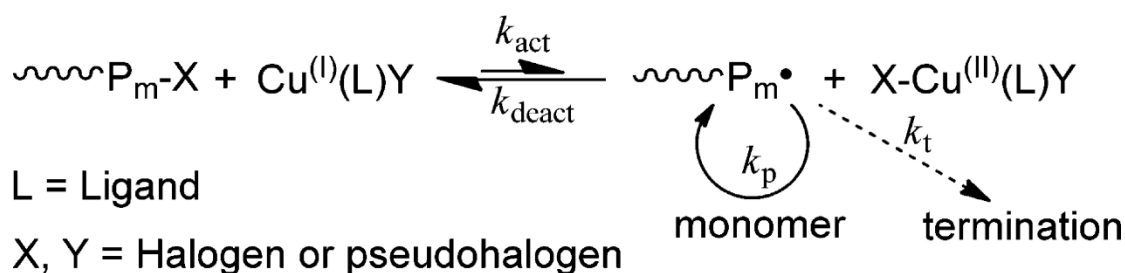


Figure 2.10 Schematic illustration of polymerization through ATRP[67].

2.3 Literature reviews

2.3.1 Applications of MNPs

The MNPs and magnetic nanocomposites (MNCs) were synthesized by many ways depending on the use. For biological applications, the MNCs must consist of biomolecules or biocompatible materials as coating agents because they are toxic [64]. There are a broad range of various coatings on toxic materials surface resulting in a group of materials called biocomposites[73]. The coating was used for synthesis of MNCs as well. The biological molecule-coated MNPs still exhibit both magnetic property and biocompatible properties. The choices of coating agent that is coated on MNPs surface to be MNCs or biocomposites are depended on their applications. For example, the MNCs that were used in magnetic resonance imaging (MRI) as contrast agent (Figure 2.11) were synthesized via MNPs fluorophores as coating agents. MRI studies using organic fluorophores-coated MNPs resulted in a high resolution MRI with high sensitivity [74]

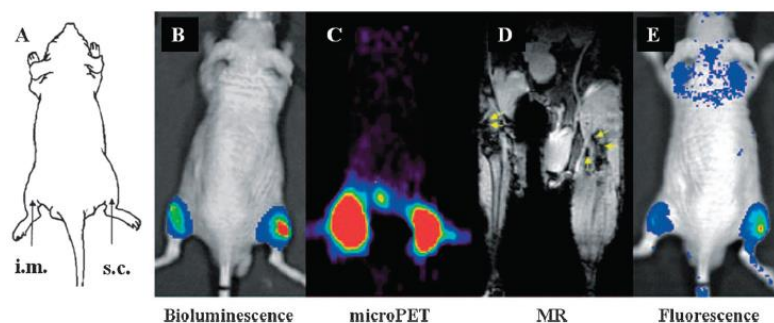


Figure 2.11 Example of multimodal imaging [74]

The MNCs are used in many drug delivery systems[75]. For examples, the MNPs were surface modified for conjugation with such drugs as Doxorubicin (Dox). The MNPs were coated with silica which was called core-shell $M@SiO_2$ MNCs, and then the MNCs were multifunctionalized. At the last step, Dox-conjugated-M MNCs were obtained via click reaction (Figure 2.12). When the MNPs were coated with silica, they can be widely modified because silica surfaces contain silanol groups (Si-OH) which can condense among their similar groups. Moreover, silanol groups (Si-OH) react with carbonyl group easily under mild conditions as well.

In addition, the MNPs were rapid cleared by reticuloendothelial system (RES) from body while drugs on MNPs surfaces were released. For permeation and retention, the MNPs must be long circulation in order to release drugs completely[73] So, the MNPs are needed to coat with coating agents to make them circulated for a longer time in the body. PEG was chosen because it has the best performance to be conjugated with both organic and inorganic nanocomposites in terms of solubility, stability, capability to shield the surface charge and biocompatibility[76].

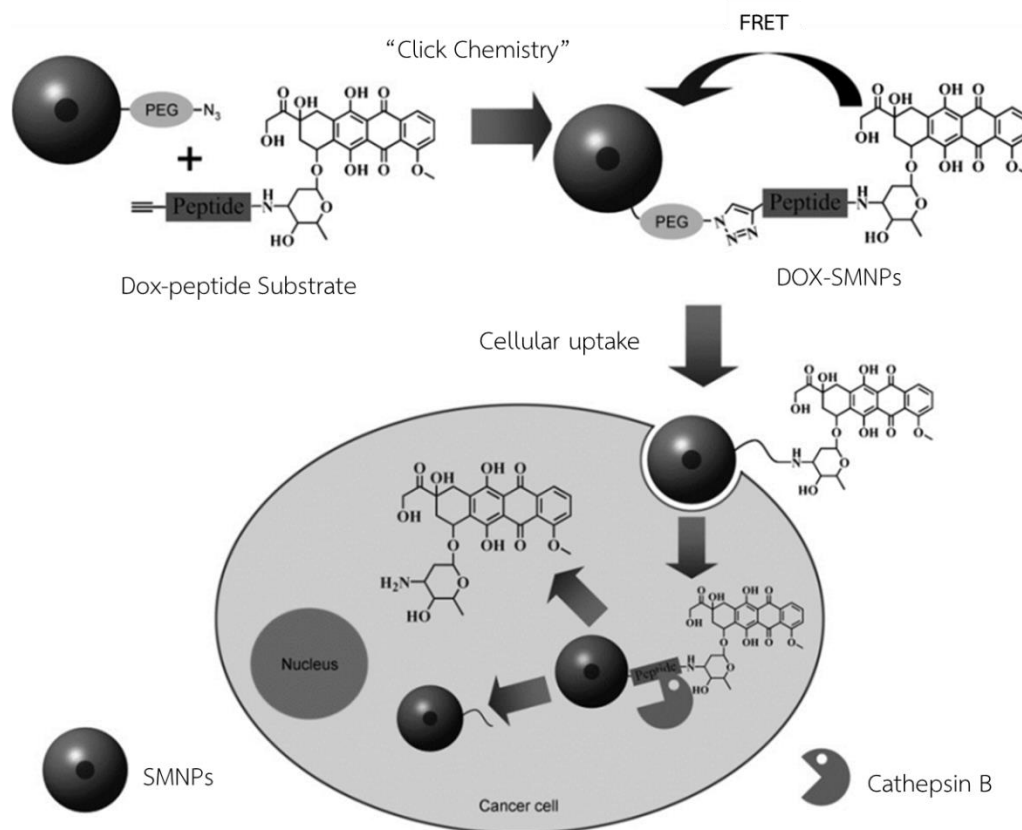


Figure 2.12 Illustration of synthesis of Dox SMNPs and their cellular functions for drug release and tumor imaging. FRET=fluorescence resonant energy transfer[75]

2.3.2 PEGylation on MNPs

Poly (ethylene glycol), PEG was widely used to be a coating because it is biocompatible [75]. Coating PEG on materials surface is called PEGylation. PEGylation can be done using two main strategies, Firstly, direct MNPs synthesis used PEG precursors as solvent or complexant called graft copolymer [77]. In general, the direct strategy is called "co-precipitation" (as in Figure 2.13). In this method, PEG interacts with material surface via weak interactions. Therefore, the PEG can be easily lost out the materials.

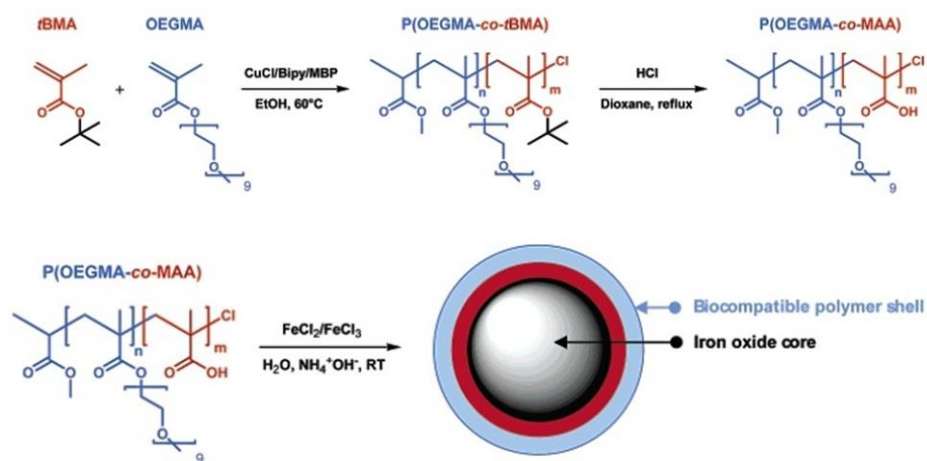


Figure 2.13 Direct MNPs synthesis using PEG precursor or graft copolymer [77]

Another strategy, material surface conjugated PEG molecules by modified with suitable anchoring ligands. For iron oxide NPs, their surface were modified with silica and amino. After that, they were immobilized with BiBB for ATRP [47] (as in Figure 2.14). In this way, the PEG strongly interacted with the material surface via coordination or covalent bonds. Therefore, The PEG was not lost out of the material surfaces.

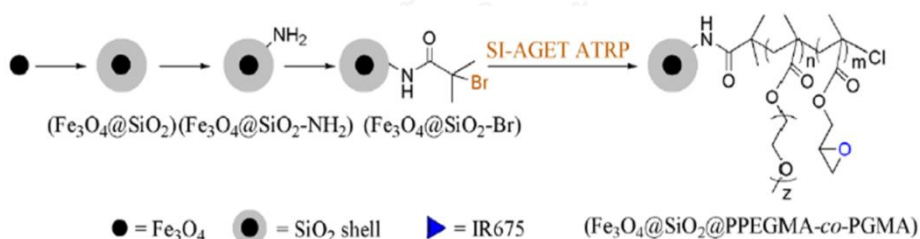


Figure 2.14 MNCs synthesis using modified-PEG with unsaturated polymers [47]

2.3.3 Infiltration of dentine discs

There are many previous works that investigated about infiltration through dentine discs. They used 2 main techniques for this investigation which are iontophoresis and pressure techniques.

For the first technique, iontophoresis is technique which uses electric current to move or deliver ion. Iontophoresis was used to deliver drug with was ionized (ionized drug) through dentinal tubules into the pulp [2]. The technique could enhance ionized drugs through both intact and caries-affect dentine (Figure 2.15). In addition, for infiltration, due to first study about infiltration of drug through dentine disc by iontophoresis, new experiment set-up was designed. The experiment set-up is close to the real condition of dentinal tubules as in Figure 2.16 This technique used for only *in vitro* studies and *in vivo* improvement is needed.

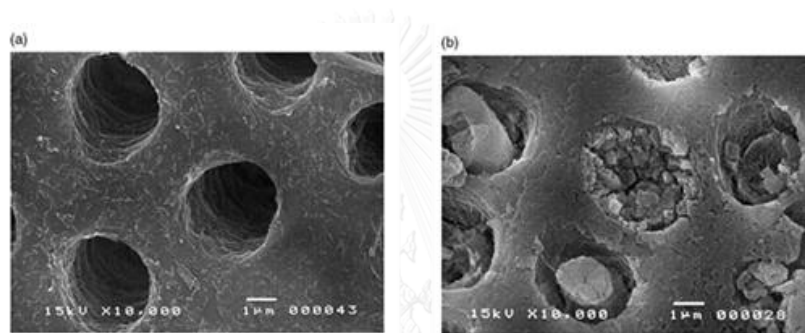


Figure 2.15 (a) Scanning electron micrograph of intact dentine surface. Showing opened dentinal tubules (b) Scanning electron micrograph of caries affected dentine surface occluded dentinal tubules [2].

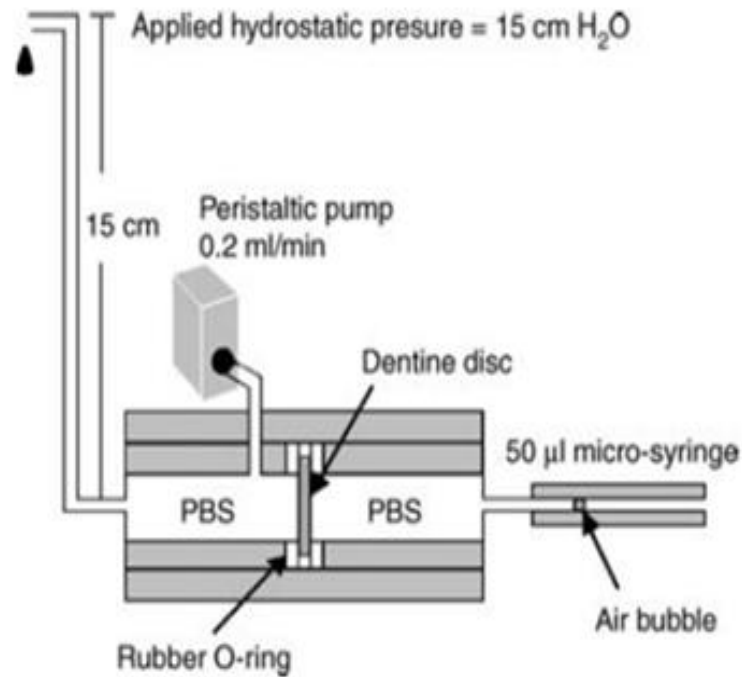


Figure 2.16 Diagram of the experimental system for hydraulic conductance measurement [2]

The second technique is called Pressure technique. Pressure was used to deliver antibacterial NPs into dentinal tubules[3]. The process for applying pressure is by the high-intensity focused ultrasound (HIFU). The HIFU is a process that produces collapsing cavitation bubbles. HIFU experimental setup was designed for delivery of antibacterial NPs into dentinal tubules as shown in Figure 2.17. In the process, the spark bubbles was generated by discharging a capacitor at first[1]. Next, HIFU was generated by voltage applier. After the different pressure occurred, the higher pressure pressed the bubbles which are of lower pressure than the liquid media. At the last step, antibacterial NPs in media were immersed on dentinal tubules (Figure 2.18). This works showed that applying pressure or HIFU could deliver antibacterial NPs into dentinal tubules or dentine discs, but antibacterial NPs were aggregated and blocked the infiltration of NPs through dentine discs (as in Figure 2.19), which limiting the use of this technique.

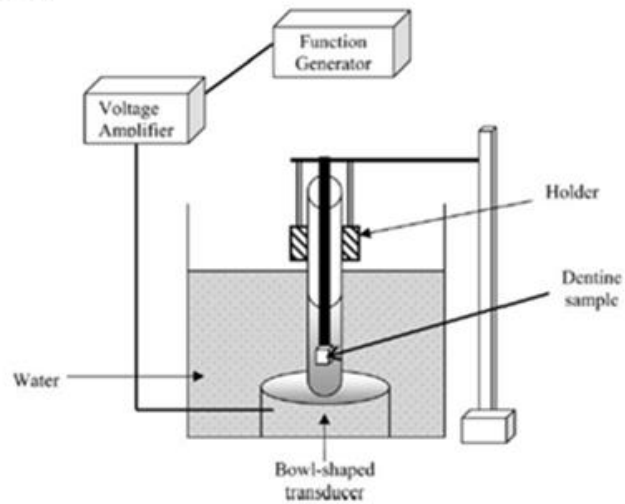


Figure 2.17 HIFU experimental arrangement used for *in vitro* experiment on dentine sample [1]

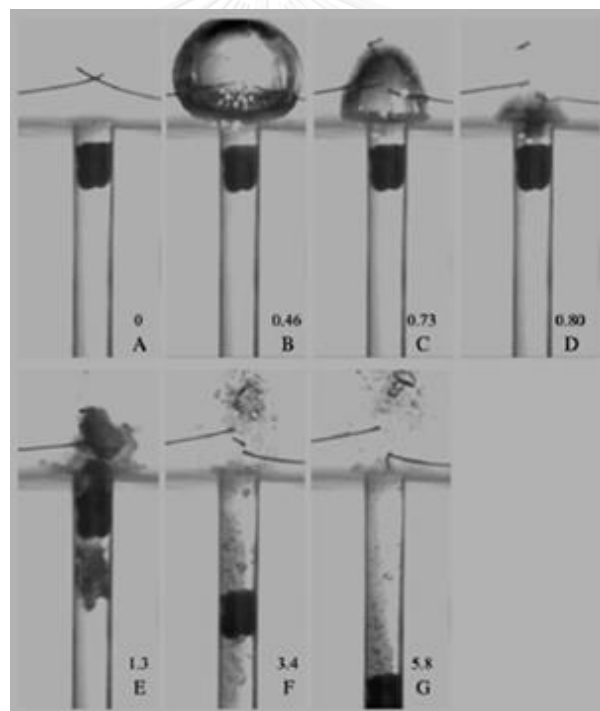


Figure 2.18 (A-G) The collapse of a spark discharge bubble of maximum bubble radius, $R_{\max} = 3.3$ mm (taken horizontally from frame B, $t = 0.46$ milliseconds), on top of a tubular channel of 3.3-mm diameter. The timing for each frame in milliseconds [3].

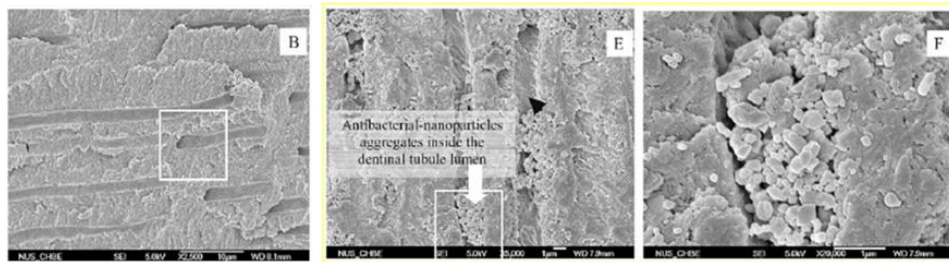


Figure 2.19 (a) The cross-section of the dentine samples with the exposed dentinal tubules does not show antibacterial-nanoparticles within the lumen, (b) Field Emission scanning electron micrographs of dentinal tubules from the HIFU treatment group samples and (c) showing aggregation of antibacterial nanoparticles of 100 - 200nm sizes [3].



CHAPTER III

EXPERIMENTS

The experimental section is divided into two parts. First part is the synthesis of magnetic nanoparticle size series, and the last part is the study of infiltration of the magnetic nanoparticles size series through dentine discs.

The instrument and chemicals which are used for the synthesis of magnetic nanoparticle size series and the study of their infiltration through dentine discs were listed below.

3.1 The instrument

Table 3.1 List of instrument

Characterization techniques	Models
X-ray powder diffraction spectrometer (XRD)	DMAX2200/Ultima+ (Rigaku)
Transmission electron microscope (TEM)	JEM-2100 (JOEL)
Fourier transform infrared spectrometer (FTIR)	Impact 410 (Nicolet)
Inductively Coupled Plasma Optical Emission Spectrometer (ICP-OES)	Perkin Elmer Optima 2100
Scanning electron microscope (SEM)	JSM-5410
Centrifuge	Centaur 2 (Sanyo)
Magnetic stirrer	MS 101 (Gem)
Thermogravimetric analyzer (TGA)	Pyris 1 TGA (Perkin Elmer)
Vibrating-sample magnetometer (VSM)	LakeShore Model 7404
Dynamic light scattering analyzer (DLS)	Zetasizer Nano ZSP (Malvern)

3.2 Chemicals

Table 3.2 List of chemical

Chemicals	Supplier
Iron (III) chloride (FeCl ₃), AR grade	Aldrich
Oleic acid (C ₁₆ H ₃₄ O ₂), AR grade	Merck
Sodium hydroxide (NaOH), pellet for analysis	Merck
Ethanol (C ₂ H ₅ OH), AR grade	Merck
n-Hexane (C ₆ H ₁₄), AR grade	Carlo erba
1-octadecene (C ₁₈ H ₃₆), technical grade	Aldrich
Cyclohexane (C ₆ H ₁₂), AR grade	Lab scan
Tetraethyl orthosilicate (TEOS), purum>98%	Fluka
ammonium hydroxide (NH ₄ OH), AR grade 25%	Merck (AR grade 25%)
polyoxyethylene (5) nonylphenylether (Igepal CO-520), reagent grade	Aldrich
Triton X-100, laboratory grade	Aldrich
1-hexanol (C ₆ H ₁₄ O), reagent grade 98%	Aldrich
Triethylamine, reagent grade	Riedel de haën
5-amino-pentanol (AP), reagent grade	Aldrich
3-aminopropyltriethoxysilane (APS)	Aldrich
2-propanol, AR grade	Univar
Dichloromethane (CH ₂ Cl ₂), AR grade	Lab scan
12-hydroxydodecanoic acid (HDC), reagent grade	Aldrich

2-bromoisobutyl bromide, For synthesis	Merck
Methanol (CH ₄ O), AR grade	Lab scan
Copper(I) bromide (CuBr) , 99.9999%	Aldrich (
Phosphoric acid, AR grade 72%)	Merck (
N, N, N', N'', N'''-Pentamethyl-diethylenetriamine (PMDTA), reagent grade	Aldrich
poly(ethylene glycol) monomethyl ether methacrylate (PEGMA), reagent grade	Aldrich (Average Mn 360)

3.3 Synthesis and characterization of magnetic nanoparticles size series

The synthesis of PPEGMA coated MNCs (MNC@PPEGMA) was divided into 2 pathways. The first part, synthesis of the smaller MNC@PPEGMA sizes 20-40 nm in diameters, another pathway, synthesis of the bigger MNC@PPEGMA sizes 100-200 nm in diameters as shown in Figure 3.1

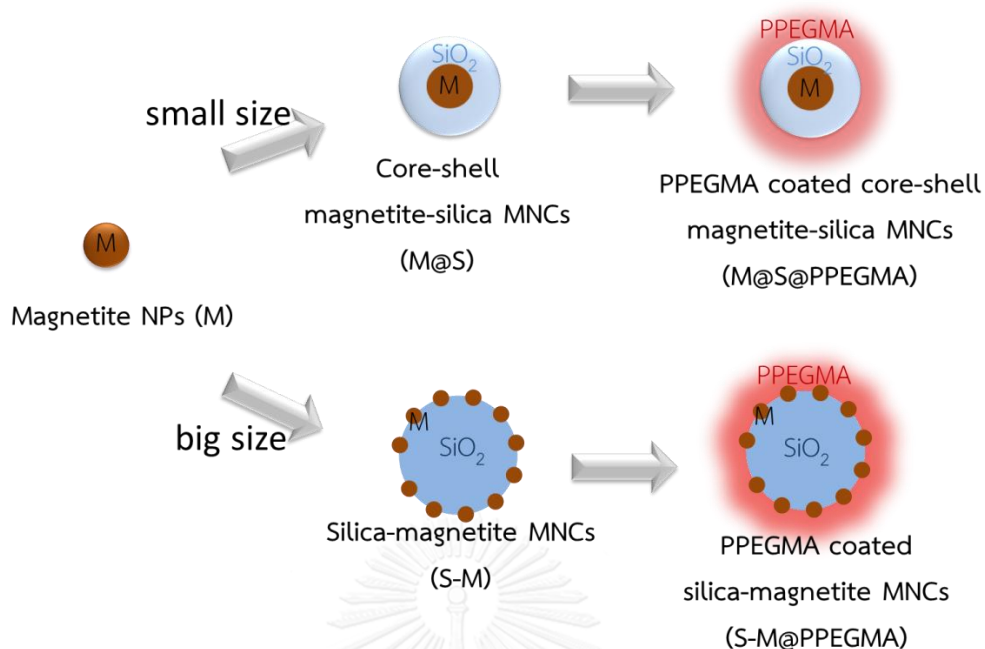
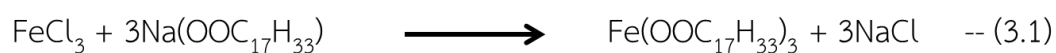


Figure 3.1 Schematic presentation for the synthesis of magnetic nanoparticles size series

The synthesis of MNC@PEGMA 20-200 nm in diameters was divided into 3 steps. Beginning with magnetite NPs or pristine magnetic NPs (MNPs) was synthesized. They act as starting materials for synthesis of magnetic nanocomposites (MNCs) in the next step. Finally, All of MNCs were coated with PEGMA (MNC@PEGMA) via ATRP method.

3.3.1 Synthesis of magnetite (Fe₃O₄) NPs

Thermal decompose technique was used for synthesis of magnetite (Fe₃O₄) NPs. The synthesis consisted of two steps according to reactions in Equations 3.1 and 3.2.



For the synthesis of monodispersed magnetite NPs (M) [31], we started with the preparation of Fe(oleate)_3 as a precursor from iron (III) chloride and oleic acid. In the preparation, 8 mmol of iron (III) chloride was dissolved in 10 mL of de-ionized (DI) water, and 24 mmol of sodium hydroxide was dissolved in 10 mL of DI water. Then 24 mmol of oleic acid and the sodium hydroxide solution were added in a round bottom flask, yielding the sodium oleate solution. Finally, iron (III) chloride solution and a mixture of DI water:ethanol:hexane in ratio of 12:16:28 by volume (mL) were added into the oleate solution. The mixture was refluxed at 70°C for 4 h. After that, the mixture was extracted by 3 times of 6.0 mL of DI water. Fe(oleate)_3 was then dispersed in the hexane layer. The Fe(oleate)_3 dispersion was collected and was evaporated to obtain the Fe(oleate)_3 as dark brown fluid.

For the step of the synthesis of MNPs by thermal decomposition process, a mixture of oleic acid : Fe(oleate)_3 : 1-octadecene as 1.0 : 6.0 : 38 by mol was prepared. The mixture was gradually heated as controlled by a temperature controller to 320°C with the rate of 3.3°C per minute and was held at this temperature for 30 minutes under inert gas (N_2 gas).

Table 3.3 Temperature program for the preparation of monodispersed magnetite NPs (MNPs)

Step	Temperature (°C)	Duration (h)	Condition
1	50	0.15	vacuum
2	50	1.00	vacuum
3	320	1.21	at 100°C start flowing the N ₂
4	320	0.30	under N ₂ gas
5	160	0.05	under N ₂ gas
6	160	2.00	under air
7	40	0.05	under air

After last step, MNPs dispersion were washed several time by 2-propanol using a centrifuge; All of the dispersion was separated into about 10 factions and using a centrifuge for washing with 40 mL of isopropanol for each faction and then the precipitated-part or MNPs of each faction was collected. Finally, The MNPs were re-dispersed in n-hexane or cyclohexane and kept in this form for storage.

3.3.2 Synthesis of core-shell magnetite-silica magnetic nanocomposites (M@S MNCs)

To begin with the preparation of reverse micelles, 84 mL of cyclohexane and 9.8 g polyoxyethylene (5) nonylphenylether (Igepal CO-520) were mixed using a magnetic stirrer until obtaining a clear mixture. After that 0.8 mL of (110 mg/mL) magnetite in cyclohexane was added in the reverse micelle mixture. Next, 1.5 mL of 25 %

ammonium hydroxide (NH_4OH) was added following by continuous stirring for 10 min. At the last step, 0.6 or 3.0 mL of tetraethylorthosilicate (TEOS) was dropwised and kept stirring for 16 h. M@S MNCs were then obtained and washed for 3 times with 30 mL of ethanol before kept for later used.

3.3.3 Synthesis of magnetite-decorating silica particles (S-M) MNCs

3.3.3.1 Synthesis of bare silica NPs

Firstly, a reverse emulsion was used for the synthesis of bare silica NPs. The emulsion was prepared using mixtures of 25.0 to 37.5 mL of polyethylene glycol tert-octylphenyl ether (triton x-100), 16.0 to 24.0 mL of 1-hexanol and 75.0 mL of cyclohexane. The mixtures were mixed by sonication for 30 min. Then, 6.00 mL of DI water was added into the mixtures. The mixtures were stirred until obtaining clear mixtures. Next, 1.25 mL of 25% NH_4OH was added into the emulsion. After stirring for 2 h, 3.9 or 4.2 mL of TEOS was added. TEOS acted as a silica source. Finally, bare silica NPs were obtained after emulsion was stirred for 24 h and was washed by centrifugation-precipitation for 3 times with 30 mL of ethanol.

3.3.3.2 Preparation of magnetite solution (M solution)

As-synthesized magnetites NPs were removed of surfactants to be more free magnetites using centrifugation. In order to become attachable on bare silica surfaces, free magnetites were then modified with multifunctional ligand systems. For the modification, 35 mg of free magnetites was dispersed in 0.50 mL of ethanol. Then, 95 mg of 12-hydroxydodecanoic acid (HDC) was added into the magnetite dispersion. After that, the dispersion was sonicated for 30 min or until the dispersion becoming clear. Next, 415 mg of 5-amino-pentanol (AP) and 400 mg of 3-aminopropyltriethoxysilane (APS) was added respectively. The mixture was stirred for 20 min. After that M solution as a clear brown solution was observed.

3.3.3.3 Attachment of magnetite NPs on silica particles (preparation of S-M MNCs)

100 mg of bare silica NPs (from 3.1.3.1) was dispersed in 120 mL of ethanol, and then 0.4 – 0.6 mL of M solution (from 3.1.3.2) was added dropwise into the

dispersion. The mixture was stirred for 20 min. Then, 0.1 mL of DI water and 0.1 mL of 25% NH_4OH were added respectively. After stirring for 5 min, 0.2 mL of TEOS was added into the dispersion, and then the dispersion was continuously stirred for another 16 h. After washed for 3 times with 30 mL of ethanol, S-M MNCs were obtained.

3.3.4 Preparation of Polypoly(ethylene glycol) monomethyl ether methacrylate (PPEGMA)-coated S-M MNCs and M@S MNCs (Si-M@P and M@S@P MNCs)

The preparation of all of PPEGMA coated on MNCs was divided into 3 steps as shown in Figure 3.2 via ATRP. The first steps, all of MNPs (S-M and M@S) were NH_2 -functionalization with amine source (APS) and form MNC-NH_2 . Next, the MNC-NH_2 was immobilization with ATRP initiator (BiBB) and form MNC-Br and the last step, MNC-Br was coated with PPEGMA and form (MNC@PPEGMA).

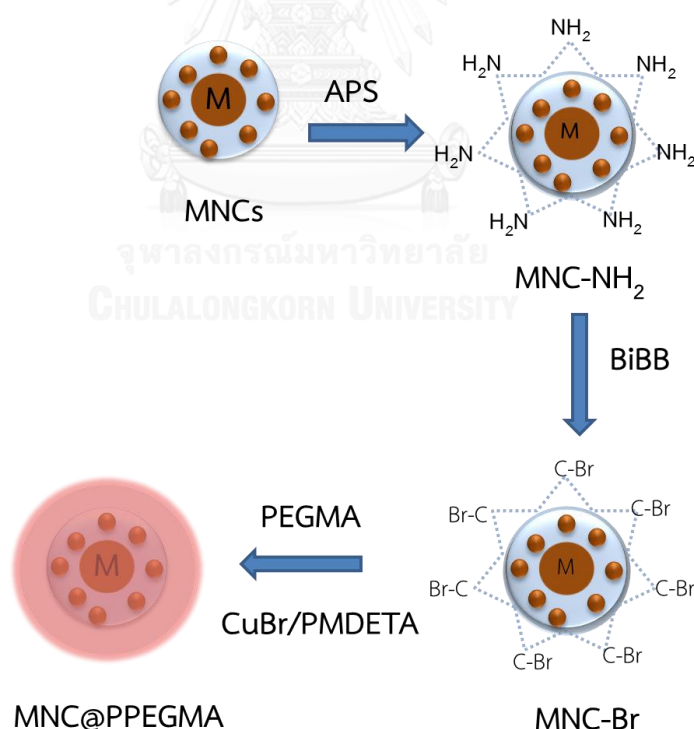


Figure 3.2 Schematic presentation of PPEGMA coated on MNCs (MNC@PPEGMA MNCs) size series

3.3.4.1 NH₂-functionalization on S-M and M@S MNCs surface

250 mg of M@S or S-M MNCs were dispersed in 100 mL of 2-propanol, and then 2.00 mL of APS was added dropwise. The mixture was continuously stirred for 24 h to get M@S-NH₂ or S-M-NH₂ MNCs. Before used in the next steps, the MNCs were washed with 25 mL of 2-propanol for twice and 25 mL of dichloromethane for 2 times respectively.

3.3.4.2 Initiator-functionalization on S-M-NH₂ and M@S-NH₂ MNCs surfaces

300 mg of S-M-NH₂ or M@S-NH₂ MNCs were dispersed in 30 mL of dichloromethane. 1 mL of triethylamine was added into the dispersion. The dispersion was immersed into ice bath under nitrogen atmosphere. After 10 min, 0.3 mL of 2-bromoisobutylylbromide (BiBB) was added dropwise. The mixture was stirred at 0°C for 2 h under N₂ gas and then continuous stirring for another 20 h. Lastly, S-M-NH₂-Br and M@S-NH₂-Br MNCs were obtained. Before continued to the next step, they were washed with 30 mL of dichloromethane for 3 times, 30 mL of ethanol twice and 30 mL of water twice, respectively.

3.3.4.3. Synthesis of PPEGMA-coated on S-M-Br and M@S-Br MNCs surface

300 mg of S-M-Br or M@S-Br MNCs were dispersed into mixture of 5 mL of DI water and 30 mL of methanol. The dispersion was immersed into ice bath and magnetically stirred. Then the atmosphere above the dispersion was pumped-refilled with N₂ for 3 cycles. Next, 2 mL of PEGMA or the monomer was added dropwise into the dispersion. Then, 0.1 mg of copper (I) bromide and 1 mL of N, N, N', N'', N''-pentamethyl-diethylenetriamine (PMDETA) were added respectively. the atmosphere above the dispersion was pumped-refilled with N₂ for another 3-cycles. After that, the mixture was stirred under N₂ for 16 h Lastly, S-M@PPEGMA and M@S@PPEGMA MNCs were obtained, they were washed with 30 mL of ethanol twice and 30 mL of DI water twice, respectively. The samples were then collected and kept in DI water.

It was washed with 30 mL of ethanol for 3 times, 30 mL of methanol twice and 30 mL of DI water twice, respectively.

3.4 Characterization of synthesized-MNPs and MNCs

The crystalline phases of MNPs and MNCs were characterized using X-ray powder diffraction (XRD). X-ray powder diffraction (XRD) analyses were performed using Rigaku D/MaX-2200 Ultima-plus instrument with Cu K radiation (1.5418 Å source (40kV, 30mA). The powdered samples were placed on glass holder. The scans were performed at 25°C in steps of 0.03° over 2-theta range from 20° to 70°.

The sizes and shapes of MNPs and MNCs in this work were monitored by transmission electron microscopy (TEM) with JEM-2010 microscope at accelerating voltage of 120 kV (Japan). The dispersed sample of MNPs and MNCs were deposited on carbon film with 300 mesh copper grids.

Fourier transform infrared spectra (FTIR) were recorded on Nicolet 6700 FT-IR spectrometer. The powdered samples (MNPs and MNCs) were mixed with KBr (ratio 1:1000). The mixed powder was compressed using hydraulic compressor into pellet. This instrument was used for finding function groups on the samples.

Ninhydrin test was used for detecting NH₂ functionalization on MNCs surfaces. Ninhydrin interacted with primary amine to form a compound of 2-[(1-Hydroxy-3-oxo-2,3-dihydro-1H-inden-2-yl)imino]-1H-indene-1,3(2H)-dione as purple compound [69]. 30 mg of ninhydrin was dissolved in 3 mL of water and dropped on a filter paper which have sample and then were heated 10 min at 100°C.

Thermogravimetric analysis TGA was carried out on a TA Instruments *Pyris 1* TGA. The powder samples were placed on ceramic holders. Samples weighing between 3 and 11 mg. were heated from 50°C to 700°C under nitrogen atmosphere with a heating rate of 10°C per min. The instrument was used determination of percent weight of PPEGMA on MNCs.

A vibrating-sample magnetometer (VSM-7407, LakeShore, USA) was used at room temperature to measure magnetization of MNPs and MNCs.

3.5 Preparation of dentine disc

Dentine discs were prepared from both the dentine beneath a carious lesion without any sign of pulp exposure and the intact dentine. Before used, the teeth were stored in 0.01 M of phosphate buffered saline (PBS) at 4°C for not more than 4 weeks. Carious dentine was removed using a low speed round steel bur. The dentine thickness between the cavity floor and pulpal horn is not less than 0.7 mm. The dentine discs were sliced as close as possible to the pulp chamber. The discs were polished on an abrasive rotator. The smear layers were removed using 35% of phosphoric acid for 10 s. The surfaces of the discs were rinsed with DI water for 5 min and then the discs were sonicated for 10 min.

Scanning electron microscopy (SEM) was used to observe morphology of dentine discs. The pore sizes were observed under scanning electron microscope (JSM-5410 JEOL, Japan).

3.6 Study of particles infiltration through dentine discs

For the investigation of infiltration through dentine discs, MNPs and MNCs were prepared. Firstly, pristine magnetite nanoparticles (pMNPs), which were dispersed in cyclohexane (M_c) and in ethanol (M_e), and PPEGMA-MNCs were prepared as following paragraphs.

For the preparation of pristine magnetite nanoparticles (pMNPs) dispersed in cyclohexane (M_c), pMNPs were synthesized similar to the process mentioned in 3.1.1, but the different part is the pMNPs were dispersed in cyclohexane for storage. The M_c dispersion was concentrated and measured quantity of Fe by ICP. The concentration of Fe in M_c is 4.530 mg/L. This concentration was used for investigation of the effects of many factors for infiltration through dentine discs with 100 μ L of M_c dispersion for each experiment, and the results were shown in Chapter IV.

For the preparation of pMNPs dispersed in ethanol (M_e), the pMNPs in cyclohexane (M_c dispersion) was washed with isopropanol in order to remove oleic acid stabilizer on MNP surfaces. M_c dispersion was separated to 1 mL and then 35

mL of isopropanol was added into M_c dispersion before centrifugation and redisperse into cyclohexane. This step was repeated for 5 times. After that free-pMNPs were dispersed into ethanol with the concentration of 3.525 mg/mL. Next, the pMNPs were modified with HDC and AP which similar to the preparation of M solution in Section 3.1.3.2, but in this preparation APS was not added in. In the last step, M_e were dispersed in ethanol and kept before used. The concentration of Fe in M_e dispersion is 5.050 mg/L for the study of infiltration.

Preparation of PPEGMA-MNCs dispersion, their dispersion was concentrated by centrifugation and re-dispersion. Finally, concentration of Fe in PPEGMA-MNPs dispersion with size of 20 40 100 and 200 nm is 0.210, 1.054, 0.115 and 0.388 mg/L, respectively.

Inductively Coupled Plasma Optical Emission Spectrometry (ICP-OES) was used for determining of quantity of Fe atom that are related with amount of MNPs. For determination of quantity of Fe, the dispersion of MNCs was digested with concentrated hydrochloric (HCl), and then the solution was filtrated with filter with 0.2 micrometers cut-off. After that the filtrates were measured by ICP-OES for analysis of quantity of Fe in the solution that through dentine disc.

For the infiltration experiment set-up, the apparatus consisted of an injection tube, a clamp, O-ring rubbers and a strong magnet. All of them were set as shown in Figure 3.3. The injection tube was designed with the length of about 6.20 cm and tiny tube width of 0.5 cm in diameter. Magnetic strength (Neodymium) is 32.59×10^2 gauss (Figure 3.3a) and 36.86×10^2 gauss (Figure 3.3b) for the investigation of the effect of magnetic field strength. The apparatus were used for infiltration and study of factors affecting the infiltration.

For the infiltration part, there are 6 factors were investigated. The first one, dentine compatible solvent comparing cyclohexane and ethanol, M_c and M_e dispersions were used for this effect. The second one is the effect of PPEGMA-MNCs sizes, the PPEGMA-MNCs size series in range 20-200 nm in diameter which were synthesized was used for second factor. The third factor is time. Time for infiltration

was set to 0.5, 2.0, 4.0, 6.0 and 8.0 h. The dentine thickness was studied for the fourth factor. There are three difference thicknesses of the discs, which were 0.45, 0.68 and 0.95 mm. The magnet strength was concerned in the fifth factor. There are 2 different magnetic strengths for this study. The a thin magnet with the strength of 32.59×10^2 gauss and another one is a stronger magnet strength of 36.86×10^2 gauss. The last factor is the dentine discs from different teeth. There are 3 discs that were used.

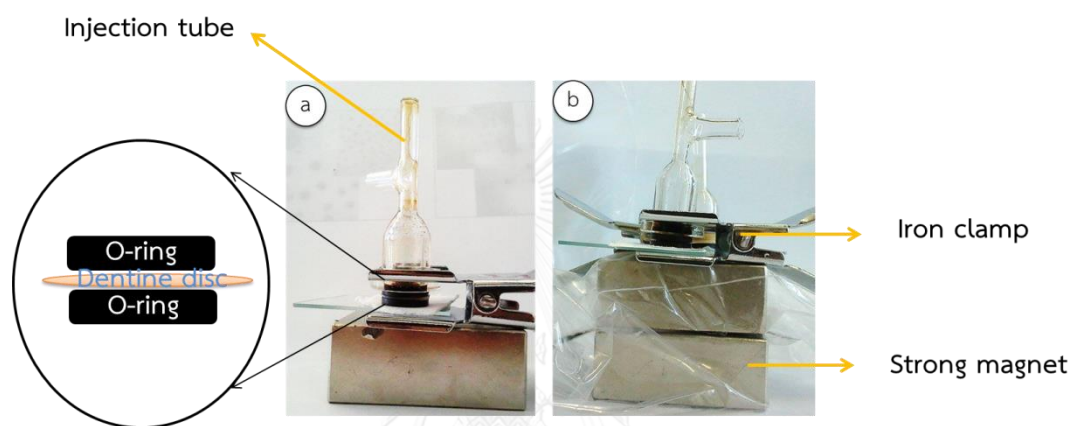


Figure 3.3 Illustration of experiment setup for infiltration through the dentine disc, (a) strong magnetic field (32.59×10^2 gauss) and (b) stronger magnetic field (36.86×10^2 gauss)

จุฬาลงกรณ์มหาวิทยาลัย
CHULALONGKORN UNIVERSITY

3.6.1 Data analyses

The SPSS Statistics 17.0 program was used for one-way ANOVA and independent t-test. A probability value of $P < 0.05$ was considered as significant. The amount of infiltrated Fe was compared via the SPSS statistics 17.0 program.

CHAPTER IV

RESULTS AND DISCUSSIONS

In first part of this work, magnetite nanoparticles (MNPs) and magnetic nanocomposite (MNCs) size series were synthesized, characterized and estimated their size. For the second part, their infiltration through dentine discs was studied. Quantities of their infiltration through the discs were determined and evaluated for the delivery systems.

4.1 Characterization of synthesized MNP and synthesized MNCS size series

4.1.1 Characterization of synthesized MNP and synthesized MNCS size series with X-ray diffraction

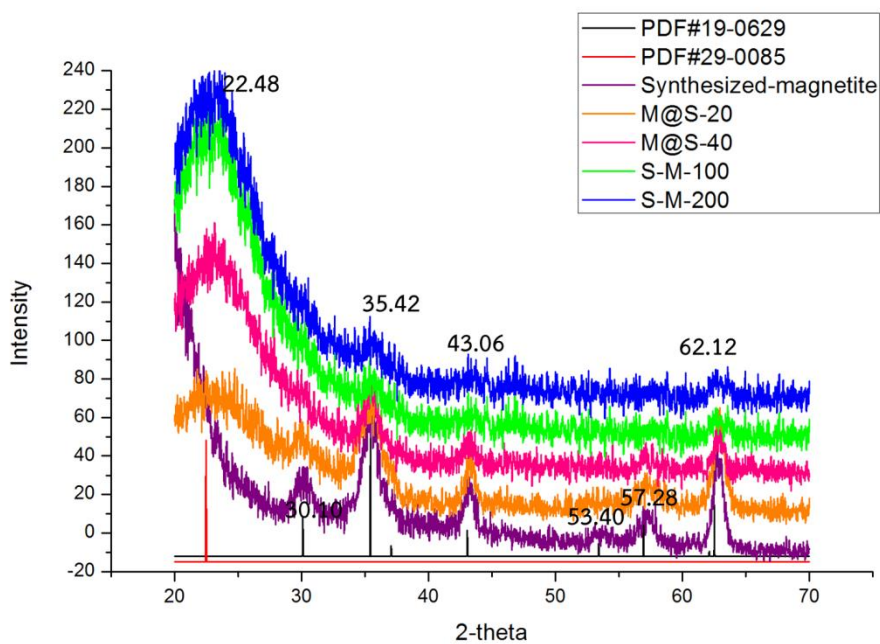


Figure 4.1 The XRD patterns of the synthesized magnetic nanoparticles (MNPs) (purple), M@S (M@S-20) (orange), M@S-40 (pink) for the composites with the sizes of 20 and 40 nm in diameter, respectively, and S-M MNCs (S-M-100 (green), S-M-200 (blue) for the composites with the sizes of 100 and 200 nm in diameter, respectively. In comparison with the standard pattern files JCPDS 19-0629 (black) of magnetite and JCPDS 29-0085 (red) of amorphous silica.

Crystalline structures of synthesized-magnetite, both of M@S-20 MNCs and M@S-40 MNCs and both of S-M-100 MNCs and S-M-200 MNCs were characterized by X-ray diffraction (XRD) analysis, and the resulted XRD pattern was shown in Figure 4.1. Compared with the standard pattern JCPDS 19-0629, the XRD pattern of the MNPs indicated a crystalline structure of Fe_3O_4 or magnetite. In addition, the XRD patterns of both different sizes of M@S and S-M MNCs were in accordance with both of standard pattern JCPDS 19-0629 and JCPDS 29-0085 (amorphous silica). All of M@S and S-M MNCs showed peak at 2-theta 35.42° , 43.06° and 62.12° , indicating that these MNCs contained magnetite. Moreover, the peak at 2-theta of 22.48° was observed. Because this peak was broad, the peak implied that the silica was not in its crystalline phase. Normally, crystal structures show sharp and high intensity XRD peaks that depended on their planes in the crystals. Therefore, observation the broad peak at 2-theta of 22.48° of all MNCs suggested that these MNCs contained amorphous silica. The compared results showed that all of MNCs contained both magnetite and amorphous silica.

4.1.3 Characterization of synthesized MNP and synthesized MNCs size series with Fourier transform infrared spectrometer (FTIR)

The IR spectra of M@S (Figure 4.2a and b) and S-M MNCs (Figure 4.2c and d) contained an absorption bands corresponding to a Si-O-Si stretching at 1070 cm^{-1} , indicating that all of MNCs consisted of silica and a absorption bands at 1632 cm^{-1} which is the bending vibration of H_2O molecules [78]. The Si-O-Si stretching band implied that all of the MNC contain SiO_2 .

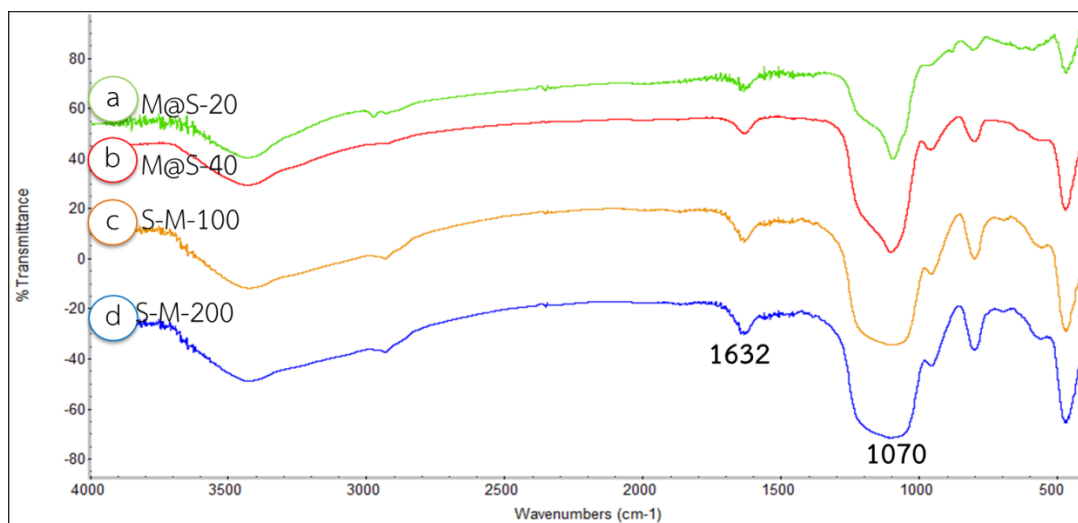


Figure 4.2 IR spectra of MNCs, M@S MNCs (M@S-20 (a), M@S-40 (b) for the MNCs with the sizes of 20 and 40 nm in diameter, respectively), and S-M MNCs (S-M-100 (c), S-M-200 (d) for the MNCs with the sizes of 100 and 200 nm in diameter, respectively)

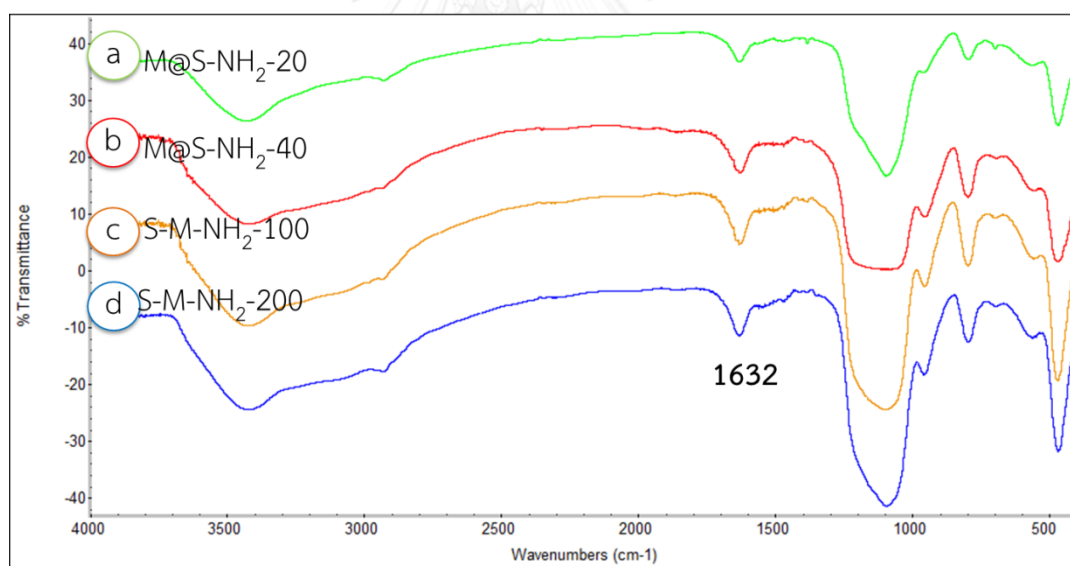


Figure 4.3 IR spectra of NH_2 -functionalized MNCs, NH_2 -functionalized M@S MNCs (M@S- NH_2 -20 (a), M@S- NH_2 -40 (b) for the MNCs with the sizes of 20 and 40 nm in diameter, respectively.) and NH_2 -S-M MNCs (S-M- NH_2 -100 (c), S-M- NH_2 -200 (d) for the MNCs with the sizes of 100 and 200 nm in diameter, respectively)

In order to follow the reaction of the amino functionalization on MNPs, we also measured the IR spectra of M@S- NH_2 and S-M- NH_2 . However, from IR spectra of

M@S-NH₂ and S-M-NH₂ MNCs (Figure 4.3), the deformation vibration of amino group stretching at about 1600 cm⁻¹ [79] was not observed because the bending vibration of H₂O molecules overlapped with this peak. Consequently, all IR spectra of MNCs could not confirm that the MNCs were successfully functionalized with amino groups.

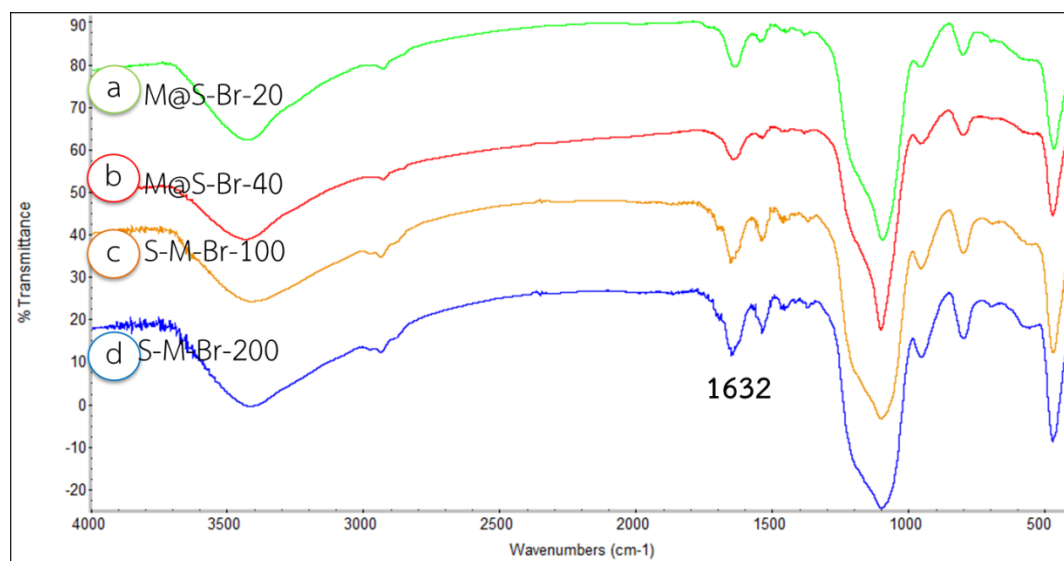


Figure 4.4 IR spectra of initiator attached MNCs, BiBB attached M@S MNCs (M@S-Br-20 (a), M@S-Br-40 (b) for the MNCs with the sizes of 20 and 40 nm in diameter, respectively.) and BiBB attached S-M MNCs (S-M-Br-100 (c), S-M-Br-200 (d) for the MNCs with the sizes of 100 and 200 nm in diameter, respectively)

Initiator functionalized MNCs (M@S-Br and S-M-Br MNCs) were detected via FT-IR spectrometer as shown in Figure 4.4. At wavenumber about 1643 cm⁻¹, which corresponded to stretching of carbonyl (-C=O) of amide group [80], were not observed because it was overlapped with peak of H₂O molecules. Moreover, the intensity of this peak is very low when compared with the peak of silica. It could not be confirmed these spectra that all of amino-functionalized MNCs (M@S-NH₂ and S-M-NH₂) were immobilized with 2-bromoisobutyl bromide (BiBB).

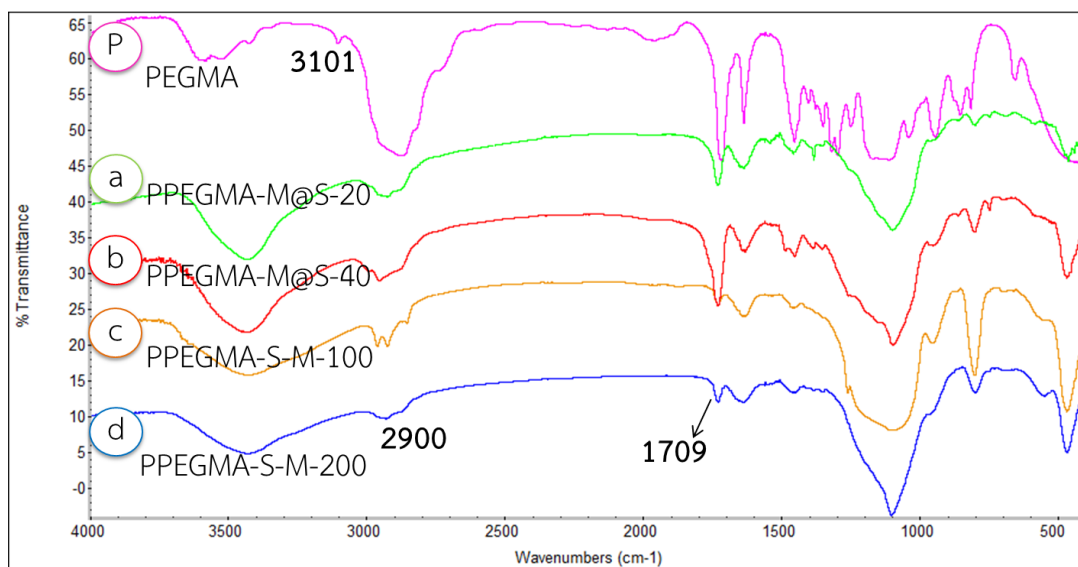


Figure 4.5 IR spectra of monomer (PEGMA) (P), PPEGMA coated MNCs, PPEGMA-M@S MNCs (PPEGMA-M@S-20 (a), PPEGMA-M@S-40 (b) for the MNCs with the sizes of 20 and 40 nm in diameter, respectively.) and PPEGMA coated S-M MNCs (PPEGMA-S-M-100 (c), PPEGMA-S-M-200 (d) for the MNCs with the sizes of 100 and 200 nm in diameter, respectively)

Figure 4.5 depicted the comparison of IR spectra between the monomer and all of PPEGMA-coated MNCs (PPEGMA-MNCs). IR stretching of terminal alkene (-C=CH) was observed at 3101 cm^{-1} for the spectrum of the monomer, while IR spectra of all of PPEGMA-coated MNCs did not show the peak at this position. The difference between the two spectra implied that the PPEGMA-coated MNCs contained PPEGMA as all the monomer was transformed into the polymer. In addition, spectra of all of PPEGMA-MNCs showed the peak at around 1700 cm^{-1} for C=O stretching (ester) and 2900 cm^{-1} for -C-H stretching. The peak at 2900 cm^{-1} of the PPEGMA-MNCs showed peak area more than area peak of MNCs without PPEGMA (nonPPEGMA-MNCs) at the same wavelength. Because the PPEGMA-MNCs consist of both of -C-H bond and C=O bonds which are the main groups in the polymer structure, these peaks of PPEGMA-MNCs indicated that MNCs were completely coated with PPEGMA.

Another method that was conducted to confirm the functionalization of NH_2 on MNCs surface was the ninhydrin test. Ninhydrin is normally used as a reagent that reacts with primary amine and changes its color to purple. NH_2 -functionalized MNCs (M@S-NH_2 and S-M-NH_2) were tested with ninhydrin as shown in Figure 4.7a – 4.10a. The figure showed that after the mixture of ninhydrin and sample (M@S-NH_2 and S-M-NH_2) was heated, purple spot was observed. In addition, the purple color was observed on only sample area or sample spot. This observation can be suggested that primary amine (APS) was immobilized on their sample surface and APS (primary amine source) were completely removed out from the NH_2 -MNCs dispersion. If APS was not completely removed out from their dispersion, the observable purple area would occur on both of sample spot and solvent area as in Figure 4.7c. This result implied that there were primary amines only on the surfaces of MNCs.

In addition, initiator (BiBB) attached on M@S-NH_2 and S-M-NH_2 MNCs (M@S-Br and S-M-Br MNCs) were the ninhydrin test too in Figure 4.7b – 4.10b. After they were heated, purple color was not observed which implies that primary amine did not locate on M@S-Br and S-M-Br MNCs surface. Moreover, the result can be concluded that M@S-NH_2 and S-M-NH_2 MNCs were initiator (BiBB) attached on their surface successfully.

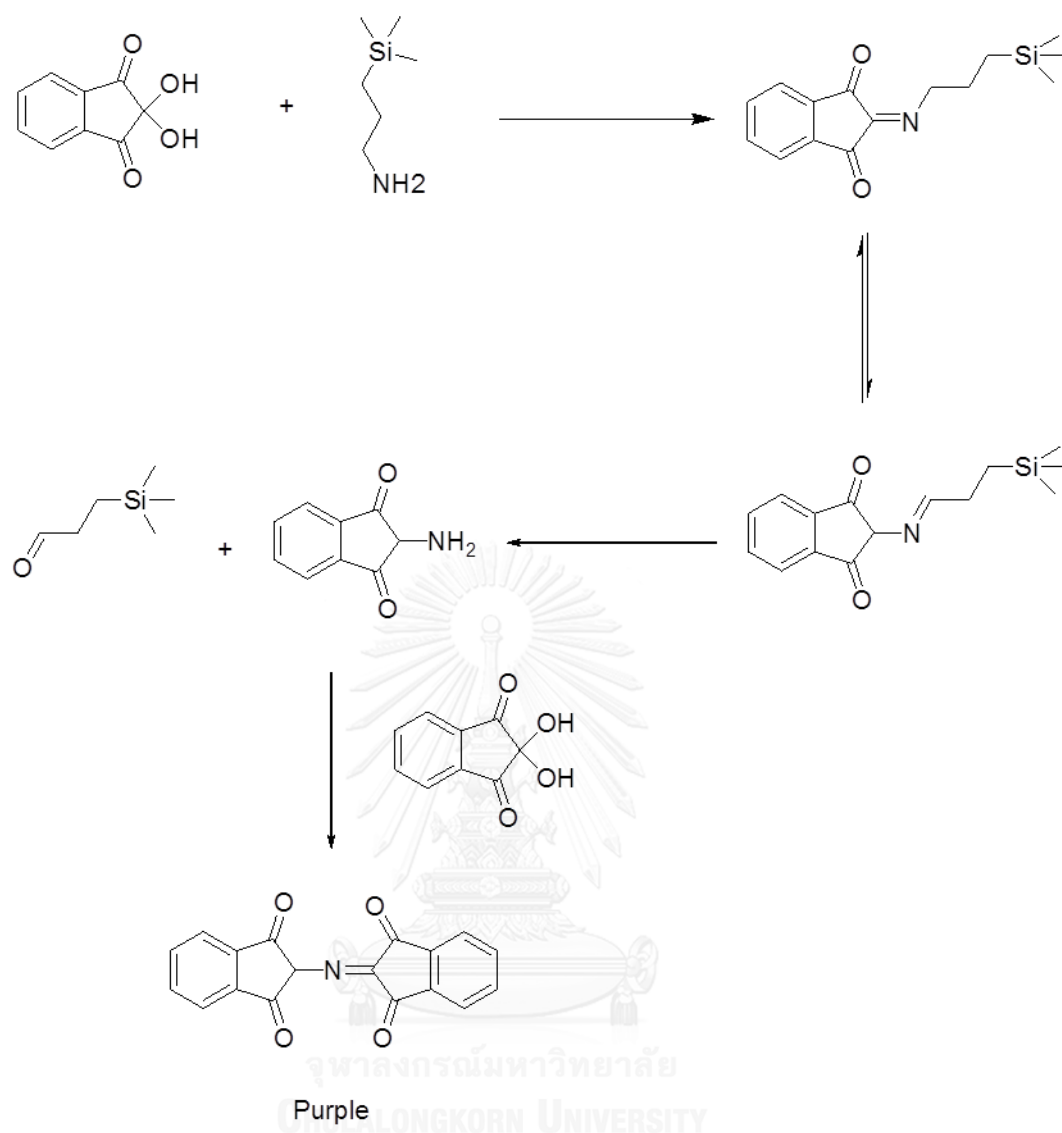


Figure 4.6 Schematic presentation of the mechanism of Ninhydrin reacting with APS

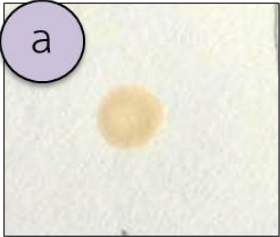
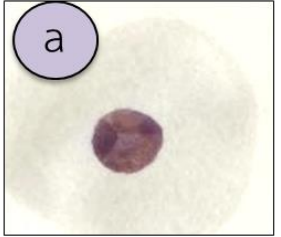
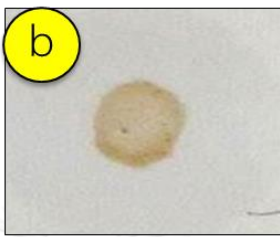
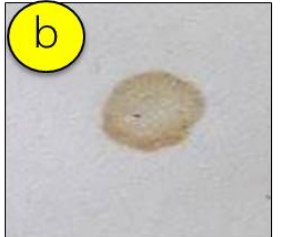
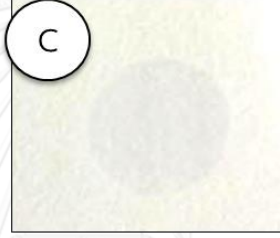
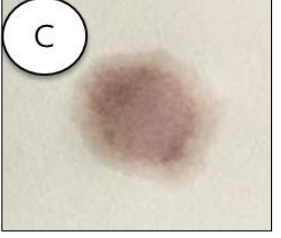
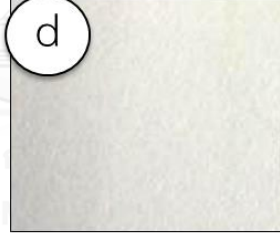
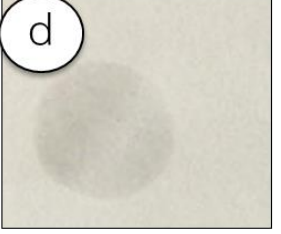
Sample	Before	After
M@S-NH ₂ -20	 A circular spot of a pale yellowish-brown color on a white background.	 A circular spot of a dark purple color on a white background.
M@S-Br-20	 A circular spot of a pale yellowish-brown color on a white background.	 A circular spot of a pale yellowish-brown color on a white background.
APS	 A circular spot of a pale yellowish-brown color on a white background.	 A circular spot of a dark purple color on a white background.
DI water	 A circular spot of a pale yellowish-brown color on a white background.	 A circular spot of a pale yellowish-brown color on a white background.

Figure 4.7 Results for Ninhydrin test of NH₂-functionalized MNCs and BiBB attached MNCs, M@S-NH₂ (a), M@S-Br (b) and APS (c), DI water blank (d) for the MNCs with the size of 20 nm in diameter.


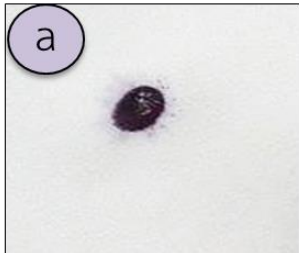
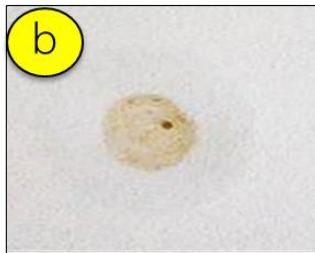
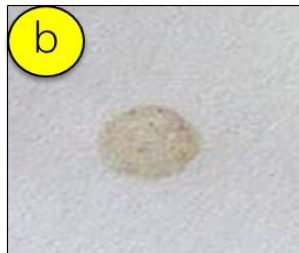
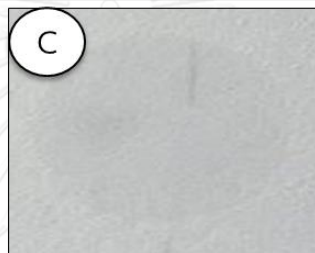

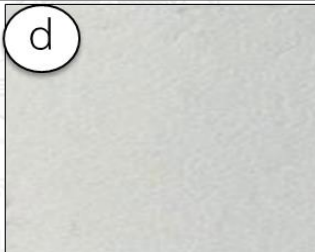
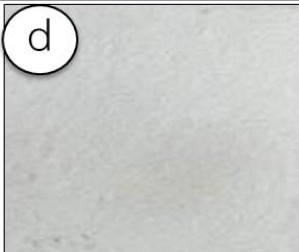
Sample	Before	After
M@S-NH ₂ -40	 A small, faint yellowish-brown spot on a white background, labeled 'a' in a purple circle.	 A dark purple, almost black, circular spot on a white background, labeled 'a' in a purple circle.
M@S-Br-40	 A larger, faint yellowish-brown spot on a white background, labeled 'b' in a yellow circle.	 A larger, faint yellowish-brown spot on a white background, labeled 'b' in a yellow circle.
APS	 A very faint, almost invisible spot on a white background, labeled 'c' in a white circle.	 A large, diffuse reddish-purple stain on a white background, labeled 'c' in a white circle.
DI water	 A completely blank white background, labeled 'd' in a white circle.	 A completely blank white background, labeled 'd' in a white circle.

Figure 4.8 Results for Ninhydrin test of NH₂-functionalized MNCs and BiBB attached MNCs, M@S-NH₂ (a), M@S-Br (b) and APS (c), DI water blank (d) for the MNCs with the size of 40 nm in diameter.

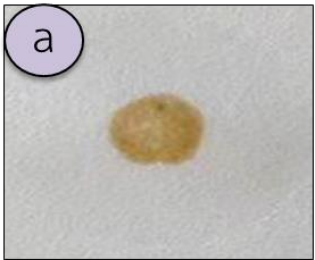
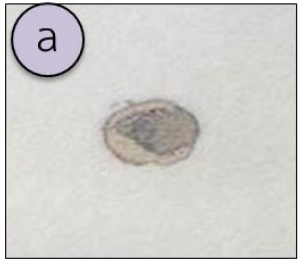
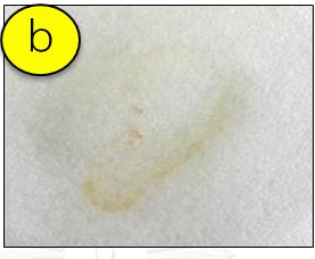
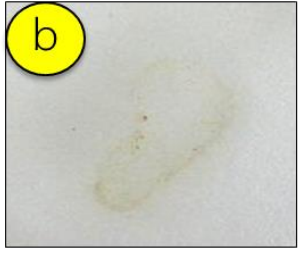

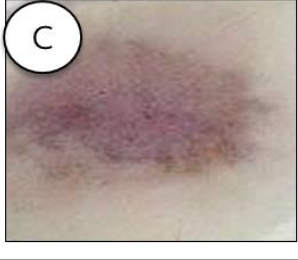
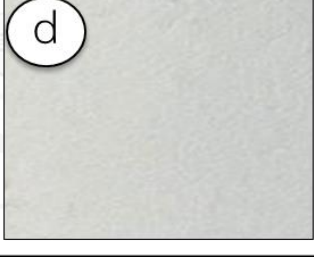
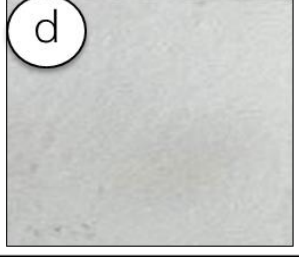
Sample	Before	After
S-M-NH ₂ -100	 A circular spot of a yellowish-brown color on a white background, labeled 'a' in a purple circle.	 A circular spot that has turned a dark purple color, labeled 'a' in a purple circle.
S-M-Br-100	 A faint, irregular yellowish spot on a white background, labeled 'b' in a yellow circle.	 A faint, irregular yellowish spot on a white background, labeled 'b' in a yellow circle.
APS	 A very faint, almost invisible spot on a white background, labeled 'c' in a white circle.	 A large, dark purple spot on a white background, labeled 'c' in a white circle.
DI water	 A blank white spot on a white background, labeled 'd' in a white circle.	 A blank white spot on a white background, labeled 'd' in a white circle.

Figure 4.9 Results for Ninhydrin test of NH₂-functionalized MNCs and BiBB attached MNCs, S-M-NH₂ (a), S-M -Br (b) and APS (c), DI water blank (d) for the MNCs with the size of 100 nm in diameter.

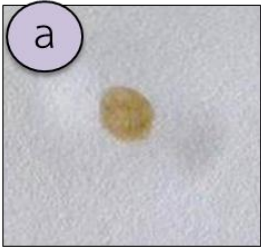
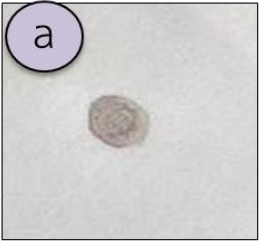
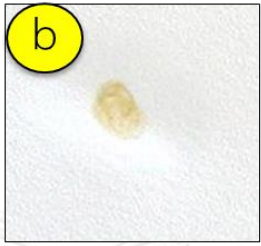
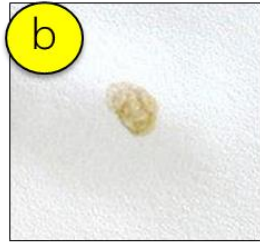
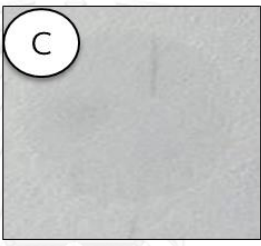
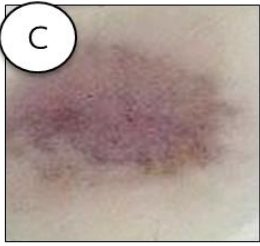

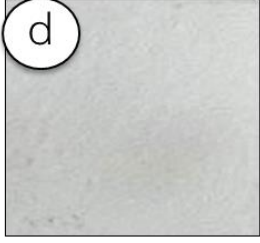
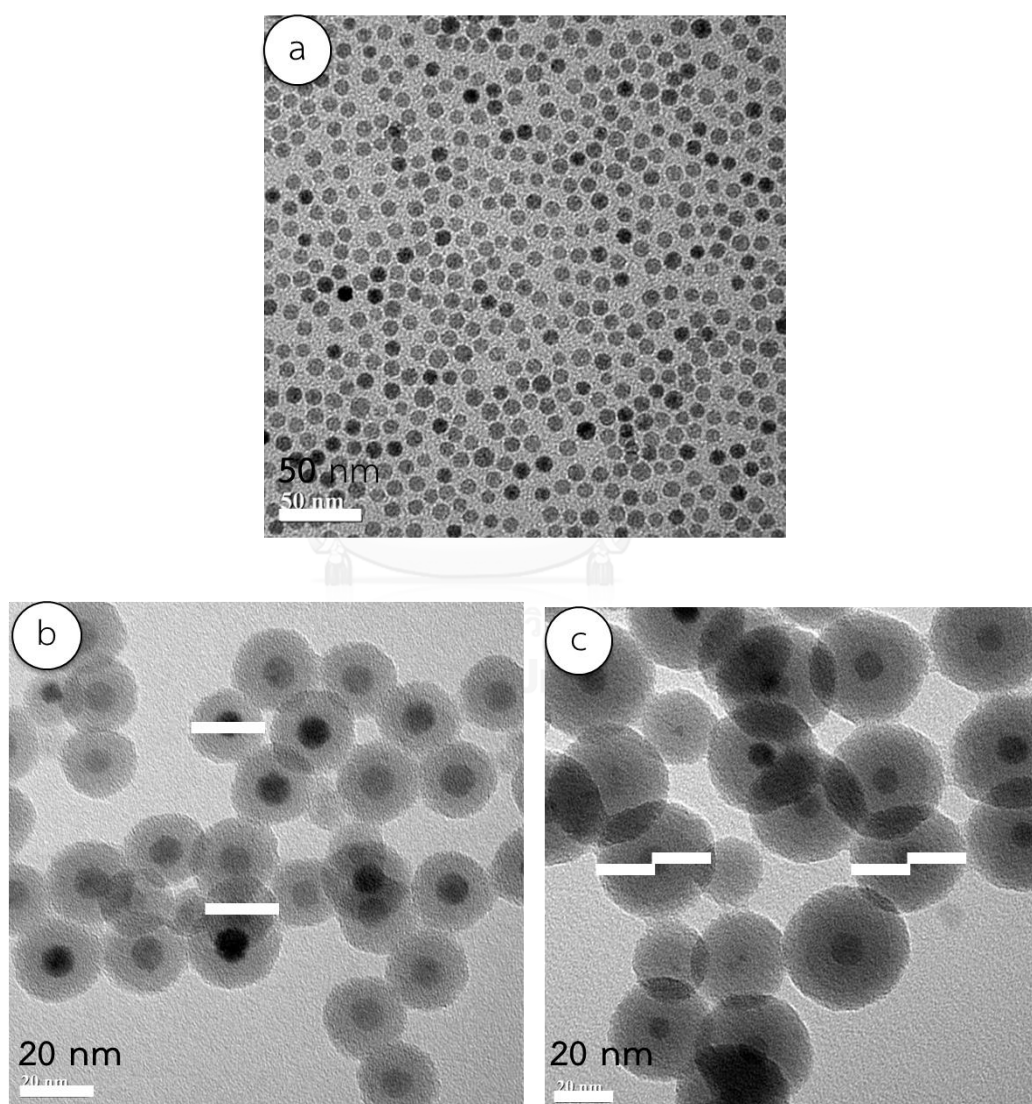
Sample	Before	After
S-M-NH ₂ -200	 A small, faint yellowish-brown spot on a white background, labeled 'a' in a purple circle.	 A larger, more distinct purple-brown spot on a white background, labeled 'a' in a purple circle.
S-M-Br-200	 A small, faint yellowish-brown spot on a white background, labeled 'b' in a yellow circle.	 A larger, more distinct yellowish-brown spot on a white background, labeled 'b' in a yellow circle.
APS	 A very faint, almost invisible spot on a white background, labeled 'c' in a white circle.	 A large, dark purple-brown spot on a white background, labeled 'c' in a white circle.
DI water	 A blank white background, labeled 'd' in a white circle.	 A blank white background, labeled 'd' in a white circle.

Figure 4.10 Results for Ninhydrin test of NH₂-functionalized MNCs and BiBB attached MNCs, S-M-NH₂ (a), S-M -Br (b) and APS (c), DI water blank (d) for the MNCs with the size of 200 nm in diameter.

Transmission electron microscopy (TEM) was used to characterize the size of all magnetic nanoparticles (MNPs, M@S MNCs, and S-M MNCs). The TEM image of MNPs (Figure 4.11a) showed particle sizes with diameters of about 10 nm, while the MNPs coated with silica (M@S) exhibited larger particle sizes of around 20 and 40 nm, as shown in Figure 4.11b and Figure 4.11c, respectively. The differences in M@S sizes were based on the quantity of TEOS used during the synthesis. In particular, 0.50 and

3.20 mL of TEOS produced 20 and 40 nm M@S, respectively. On the other hand, the TEM images of S-M MNCs (Figure 4.11d and Figure 4.11e) revealed the particle sizes of approximately 100 nm and 200 nm in diameter. The difference in S-M MNCs sizes was based on the size of bare silica particles (Figure 4.11f and Figure 4.11g), which were related to the size of reverse micelles that were prepared. The reverse micelle size was based on amount of triton x-100 and 1-hexanol in the emulsion.



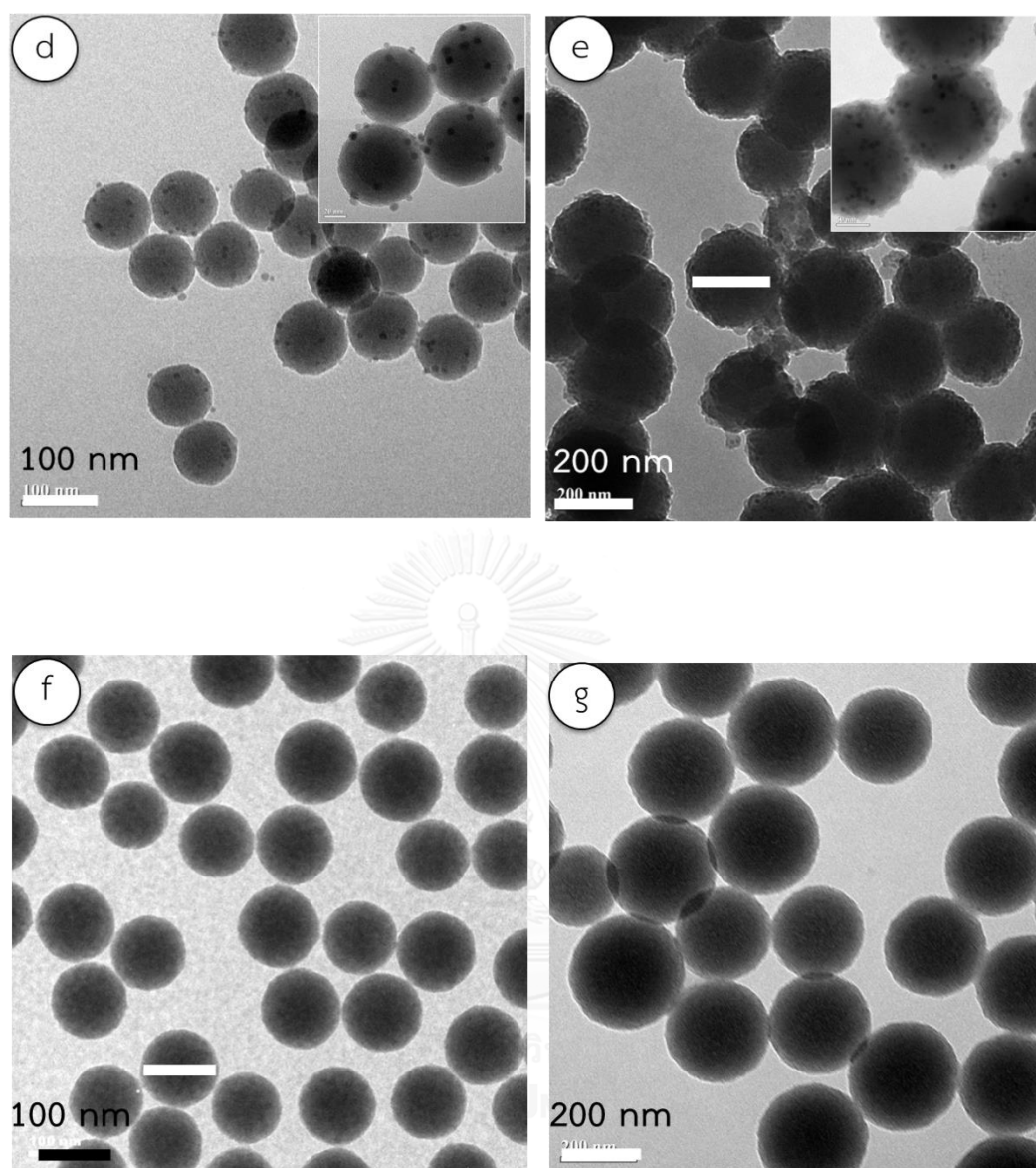


Figure 4.11 TEM images of MNPs (a), M@S MNCs (b and c for the sizes of 20 nm and 40 nm respectively), S-M MNCs (d and e for the sizes of 100 nm and 200 nm respectively) and pure silica (f and g for the sizes of 100 nm and 200 nm respectively)

In addition, TEM was used to characterize the dispersity of all of PPEGMA-coated MNCS (PPEGMA-S-M and PPEGMA-M@S MNCs) as shown in Figure 4.12. All of TEM images showed that individual particles were almost evenly separated, and the distances between individual particles were greater than those of MNCs without

PPEGMA coated (All of MNCs shown in Figure 4.11). Moreover, their surface was covered with outer layer observed as the area of lower intensity than MNCs in Figure 4.12c.

This area might be the results from PPEGMA layer. All results could suggest that MNCs were completely coated with PPEGMA to form PPEGMA-MNCs. Moreover, the PPEGMA-MNCs of 20 nm in diameter had a narrow size distribution or highly monodispersity ($PDI \leq 0.05$) and the PPEGMA-MNCs of 40, 100 and 200 nm in diameter also exhibited monodispersity ($PDI < 0.7$) as shown in Table 4.1. Additionally, it was indicated that the nanocomposites of every size were suitable for the dynamic light scattering analysis using Zetasizer Nano ZSP analyzer technique as the PDI value is less than 0.7 [81]. Monodispersity of these nanoparticles allowed us to further apply such magnetic nanocomposites for the study of size effect in the infiltration of them through dentine discs. Moreover, well-dispersity of the MNCs had advantage in preventing agglomeration that could impede activities in dentistry applications as well.

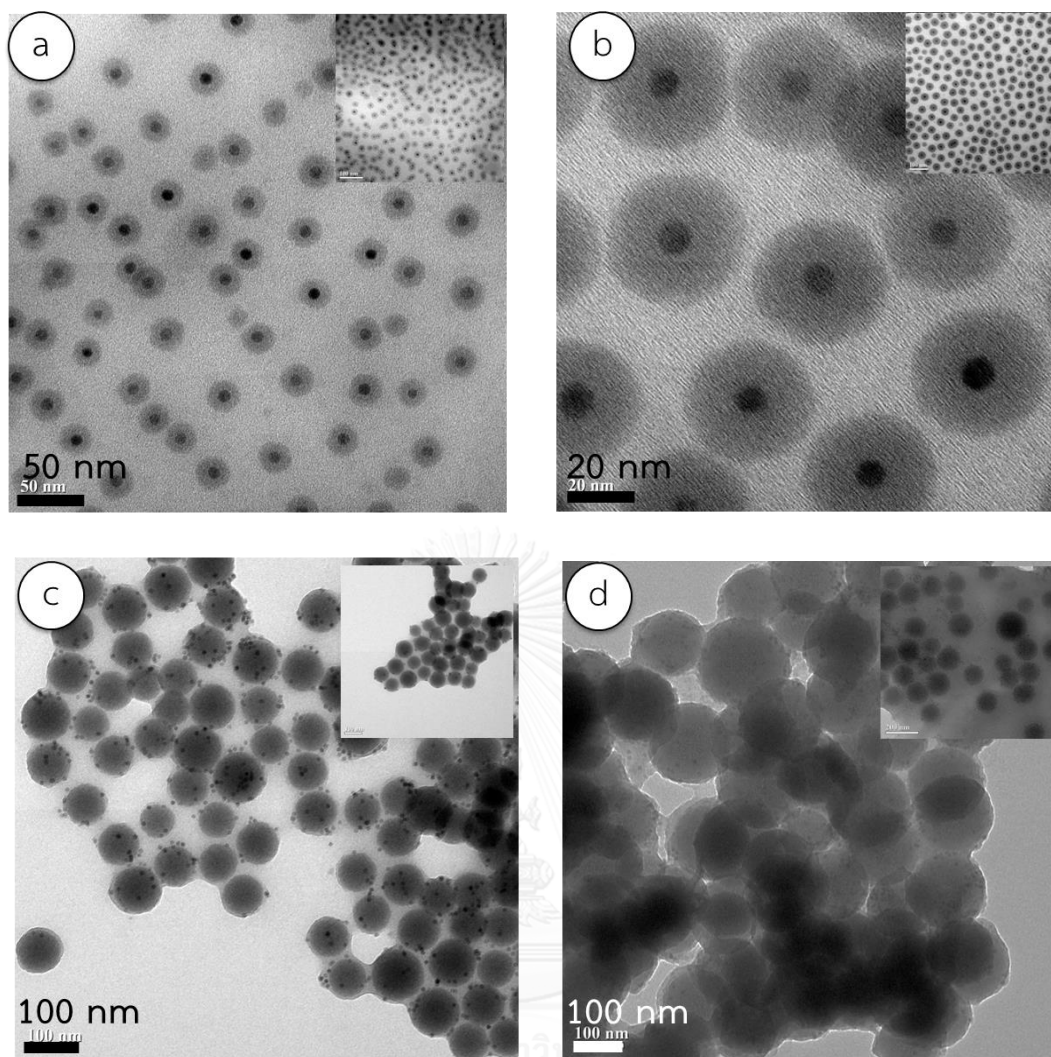


Figure 4.12 TEM images of PEGMA-coated on MNCS, PEGMA-coated M@S MNCs PEGMA-M@S MNCs (a and b for the sizes of 20 nm and 40 nm respectively), PEGMA-S-M MNCs (c and d for the sizes of 100 nm and 200 nm respectively).

	PPS-20	PPS-40	PPS-100	PPS-200
Z-Average (d.nm)	439.3	550.8	1439	2317
PDI	0.015	0.151	0.612	0.402

Table 4.1 The sizes of PPEGMA-MNCs, PPEGMA-coated M@S MNCs PPEGMA-M@S MNCs (PPS-20 and PPS-40 for the sizes of 20 nm and 40 nm respectively), PPEGMA-S-M MNCs (PPS-100 and PPS-200 for the sizes of 100 nm and 200 nm respectively) as measured by the Zetasizer ZSP analyzer

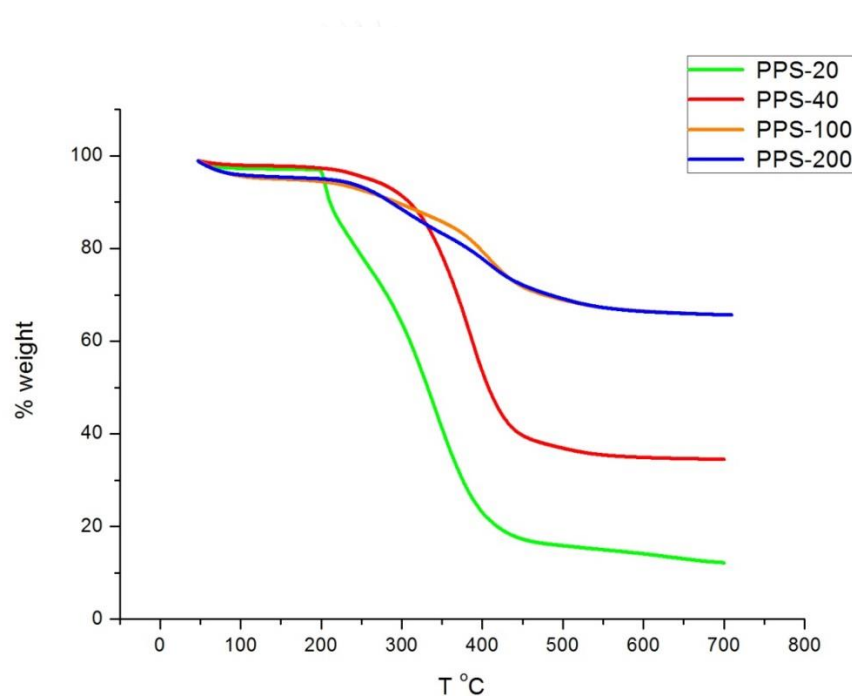


Figure 4.13 TGA curves of particles with PPEGMA coated on MNCs, PPEGMA-coated M@S MNCs PPEGMA-M@S MNCs (PPS-20 and PPS-40 for the sizes of 20 nm and 40 nm respectively), PPEGMA-S-M MNCs (PPS-100 and PPS-200 for the sizes of 100 nm and 200 nm respectively)

For the TGA curves of PPEGMA-coated MNCs, these curves showed a two-stage weight loss features as shown in Figure 4.13. The first stage suggested that the poly(ethylene glycol) side chains was eliminated in the range of 210 – 290°C, while in

the other stage, which in the range of 300 – 550 °C, the poly(methacrylate) was later eliminated[72]. The TGA curves of PPEGMA-MNCs showed the weight loss of 86%, 64%, 33%, and 30% for PPEGMA-M@S with the size of 20 nm (PPS-20) (green) PPEGMA-M@S with the size of 40 nm (PPS-40) (red) PPEGMA-S-M with the size of 100 nm (PPS-100) (orange) and PPEGMA-S-M with the size of 200 nm (PPS-200) (blue), respectively.

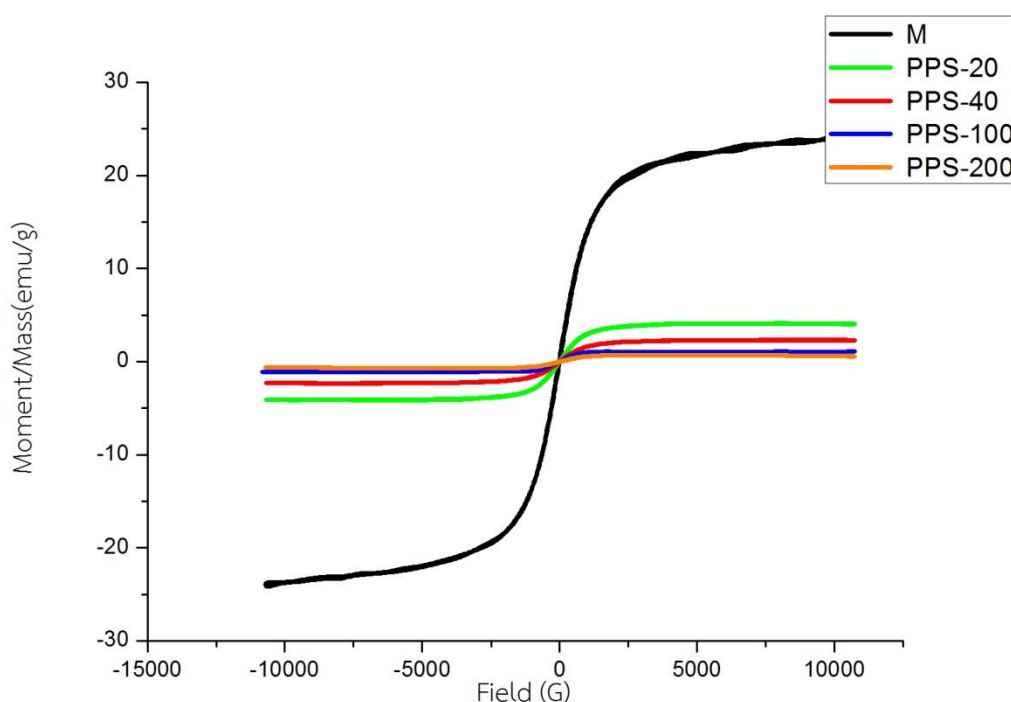


Figure 4.14 Show magnetization of pristine magnetites (M) (black) and PPEGMA-M@S MNCs (PPS-20 and PPS-40 for the sizes of 20 nm and 40 nm respectively), PPEGMA-S-M MNCs (PPS-100 and PPS-200 for the sizes of 100 nm and 200 nm respectively).

The saturation magnetization (M_s) value of magnetite (M) and PEGMA-coated MNCs (PEGMA-M@S and PEGMA-S-M) were determined by Vibrating-sample magnetometer (VSM) as shown in Figure 4.14. M_s of magnetite is 24.34 emu/g at 25°C and M_s of PEGMA-MNCs (PEGMA-M@S and PEGMA-S-M) are 4.13 emu/g, 2.33 emu/g, 1.09 emu/g and 0.73 emu/g at 25 °C for the sizes of 20, 40, 100 and 200 nm in diameter respectively. Figure 4.14 showed curves without hysteresis loop, which is the characteristic features of superparamagnetic behavior. Therefore, from hysteresis curves, it was indicated that magnetite, both of PEGMA-M@S MNCs sizes and both of PEGMA-S-M MNCs sizes are superparamagnetic material. Moreover, the M_s value curves showed that after the MNCs were coated with PEGMA, the M_s value significantly decreased when comparing with M_s of magnetite [82, 83]. Therefore, it indicated that all of PEGMA-MNCs had a much lower magnetism than pristine magnetite.

4.1.2 Preparation of dentine disc

The carious lesion without any sign of pulp exposure and the intact dentine were cut into discs. These discs were used for characterization via scanning electron microscopy (SEM) as shown in Figure 4.15. The SEM images showed that the different discs had different morphology. Moreover, in the same disc, they had at least two areas of different morphologies such as some area exhibited no tubules. This indicated the non-homogeneity nature of the dentine discs.

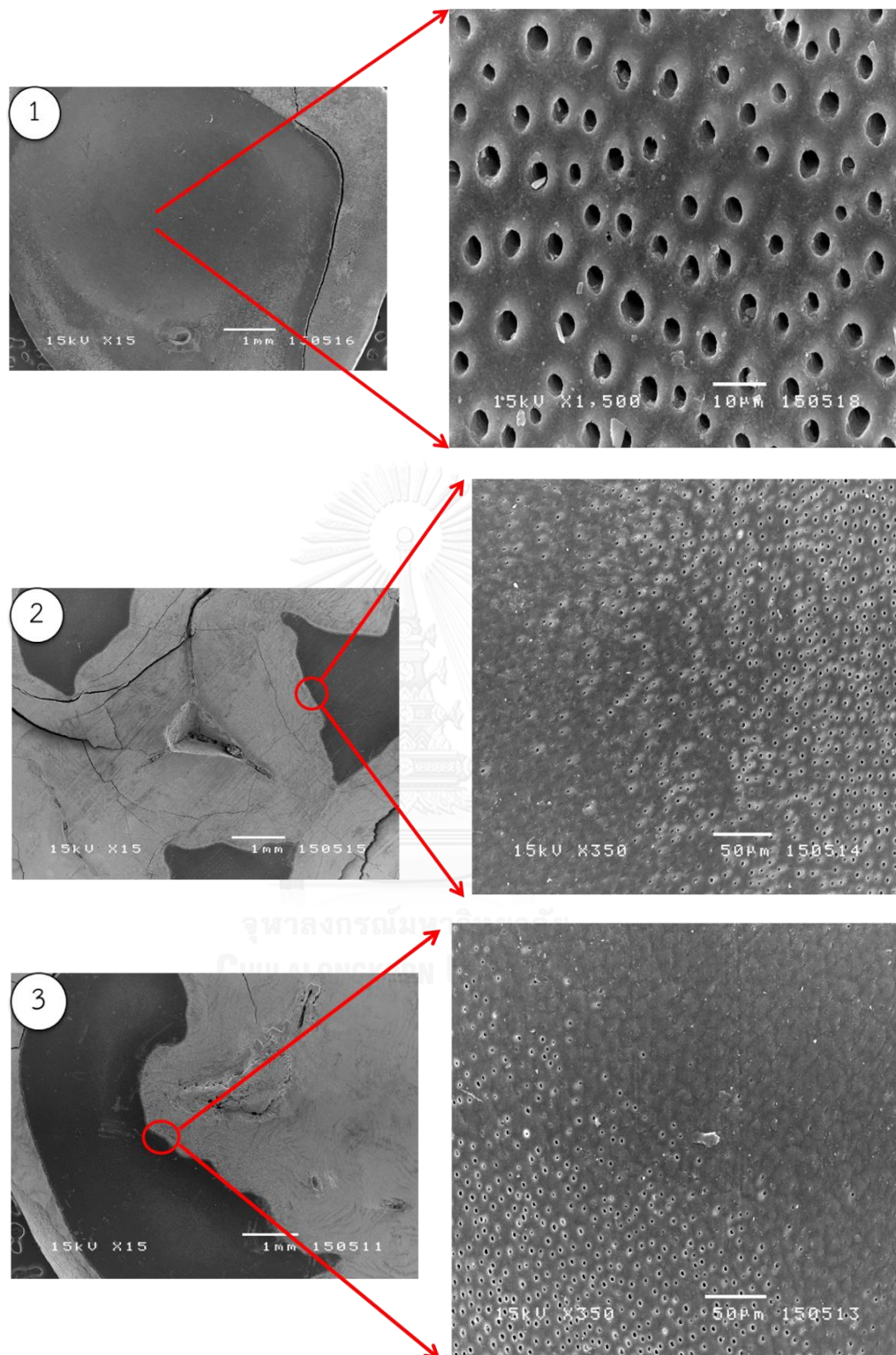


Figure 4.15 SEM images of the three dentine discs labelling (1), (2) and (3), respectively,

4.2 The investigation of the infiltration through dentine discs

4.2.1 The investigation of the infiltration through dentine discs of the two types of pristine magnetite samples

To investigate the effect of the dentine compatible solvent and the stabilizer on MNPs infiltration, two types of the pristine magnetite NPs (pMNPs) were prepared. The pristine magnetites were stabilized with oleic acid (Figure 4.16a) and AP (Figure 4.16b). The first one was dispersed in cyclohexane (M_c), while the last one was dispersed in ethanol (M_e). Cyclohexane is a nonpolar solvent, and it is not dentine compatible, while ethanol are more dentine compatible as it is a solvent with more polarity.

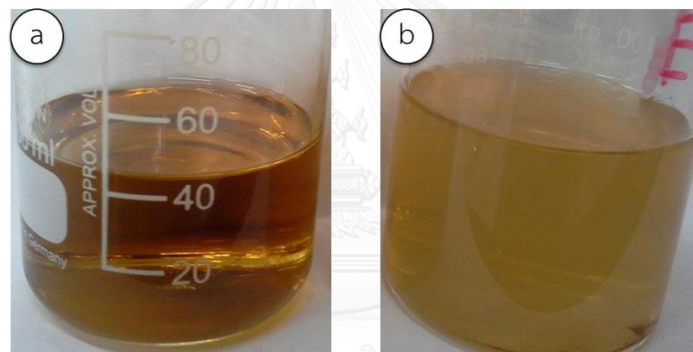


Figure 4.16 The dispersions of the pristine magnetites, a) the dispersion of M_c and b) the dispersion of M_e

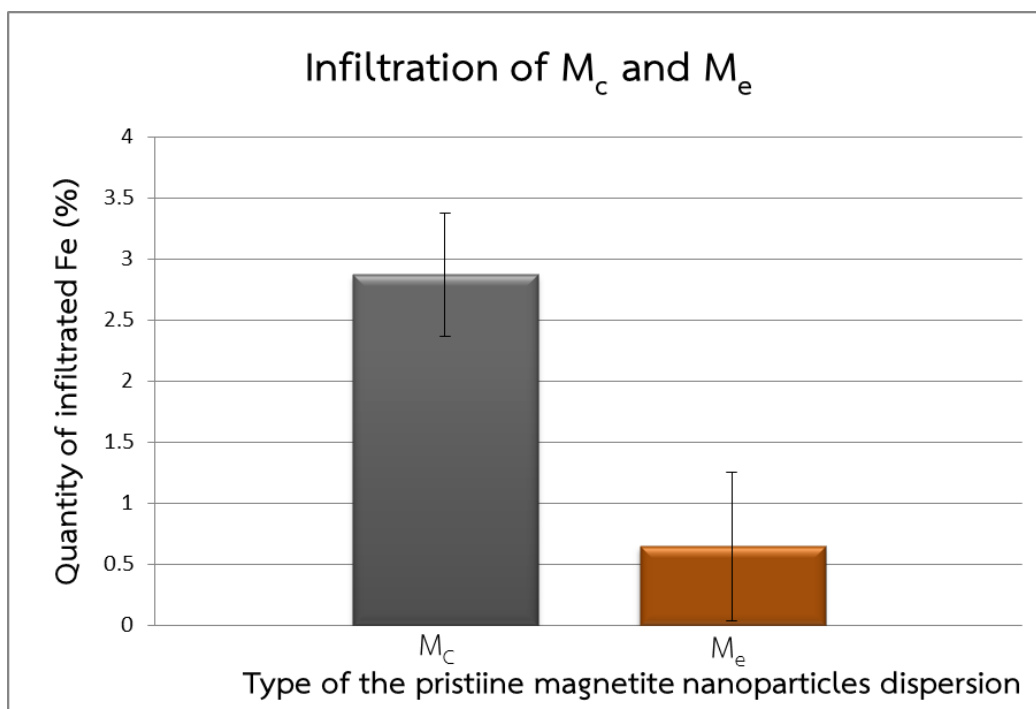






Figure 4.17 Diagram for the percent quantity of iron (Fe) when compare with the starting Fe that passed through dentine discs for 8.0 h starting from 0.453 mg of Fe in M_c and 0.505 mg of Fe in M_e injected to the apparatus.

These pristine magnetites were used for studying about NPs infiltration. M_c can pass through the dentine disc for 0.013 mg or 2.87% of the starting Fe quantity, while M_e can pass less than infiltration of M_c for only about 0.003 mg or 0.65% as shown in Figure 4.17. Although starting quantity of Iron (Fe) in M_c is less than M_e (independent t-test, $P < 0.05$), M_c can be infiltrated through the dentine discs more than M_e . The results showed that Although M_c which was dispersed in cyclohexane is dentine incompatible, it passed through the dentine better than M_e , which was in dentine compatible solvent. Therefore, the degree of infiltration was not depended much on the compatibility of solvents. We considered that dispersibility of the MNPs was more influential for the infiltration. M_c can be dispersed into cyclohexane using oleic acid better than M_e , which used AP to stabilize MNPs into ethanol. The images of the differences in the two dispersions were as shown in Figure 4.16. After 30 min, the particles precipitated in M_e dispersion, but the precipitation were not observed for M_c

dispersion. The effect might indicate that the infiltration through the dentine disc of the pristine magnetites was depended much on their dispersibility into the solvents.

4.2.2 The investigation of the infiltration through dentine disc of PPEGMA-MNC size series.

To study about infiltration through dentine discs of PPEGMA-MNCs of four different sizes, we studied for 8.0 h. All of them were induced by a strong magnet. After 8 h, quantity of Fe cannot be found by ICP as shown in Table 4.2. In addition, the dentine disc column in table 4.2 showed the pictures of dentine discs on the side that did not in contact with the PPEGMA-MNCs dispersion. The deposition of PPEGMA-MNCs cannot be observed on this side. The results indicated that PPEGMA-MNCs cannot be successfully passed the dentine disc using a magnet used in this experiment. In addition PPEGMA-MNCs with the size of less than 20 nm were studied for the infiltration. The result showed that it cannot be passed the dentine disc using a magnet similar to infiltration of PPEGMA-MNCs with the size of more than 20 nm. Although PPEGMA was claimed to be biocompatible, they caused a large decrease in magnetization of MNCs comparing to the pristine magnetite NPs (MNPs). Moreover, the result indicated that PPEGMA stabilizer on their MNCs might not be a good stabilizer for MNCs when compared to oleic acid and AP.

PPS	Amount of passed Fe	Used dentine discs
PPS-20	*	
PPS-40	*	
PPS-100	*	
PPS-200	*	

* The quantity of Fe cannot be measured.

Table 4.2 The summary for the infiltration of different sizes of PPEGMA-MNCs (PPS) through dentine discs (PPS-20, PPS-40, PPS-100 and PPS-200 with the MNC sizes of 20, 40 100 and 200 nm in diameters, respectively) for 8.0 h.

4.2.3 The investigation of the effect of time on the infiltration through dentine discs of the pristine magnetites

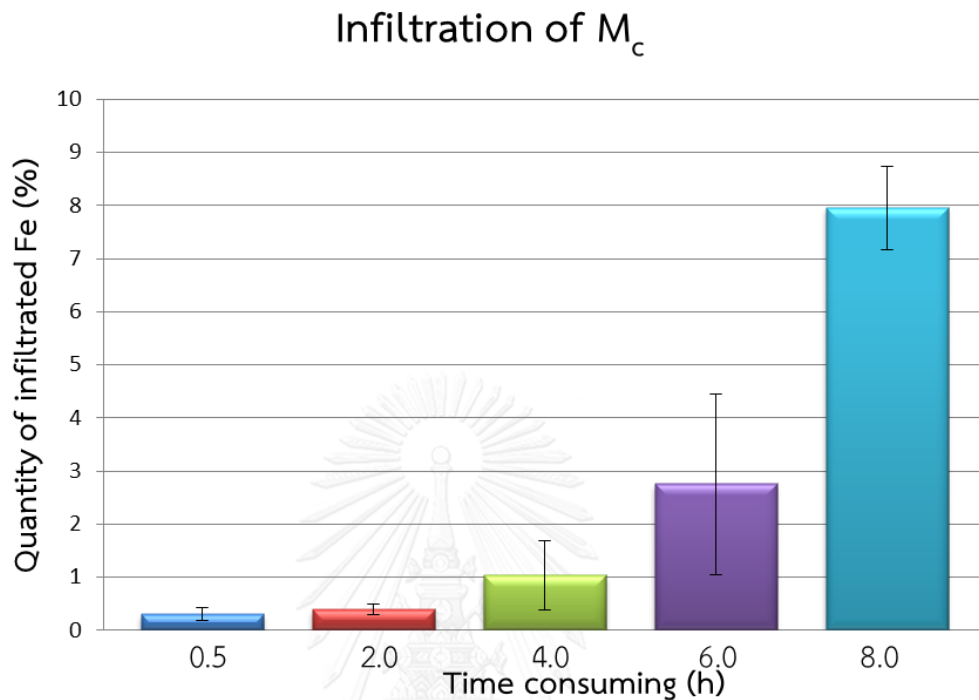


Figure 4.18 Diagram for the percent quantity of iron (Fe) in M_c that pass through dentine discs for 0.5, 2.0, 4.0, 6.0 and 8.0 h.

To investigate the effect of time used for infiltration through the dentine discs, 0.453 mg of starting Fe quantity was used for this study. The quantity of Fe can be found by ICP as shown in Figure 4.18. The percent of iron that passed through dentine discs which were different from the previous disc (4.2.1) is 0.30%, 0.39%, 1.03%, 2.75% and 8.00% for 0.5, 2.0, 4.0, 6.0 and 8.0 h respectively. The amount of iron that passed through the dentine disc increased when time used was increased (one-way ANOVA, $P < 0.05$). For the least time used (30 min in this case), it still allowed the infiltration of MNPs through dentine discs with an external magnet field. This study suggested that the new method for drug delivery to root canal using an external magnetic field could be achieved within 30 min.

4.2.4 The investigation of the effect from dentine thickness on the infiltration through the dentine disc of the pristine magnetites

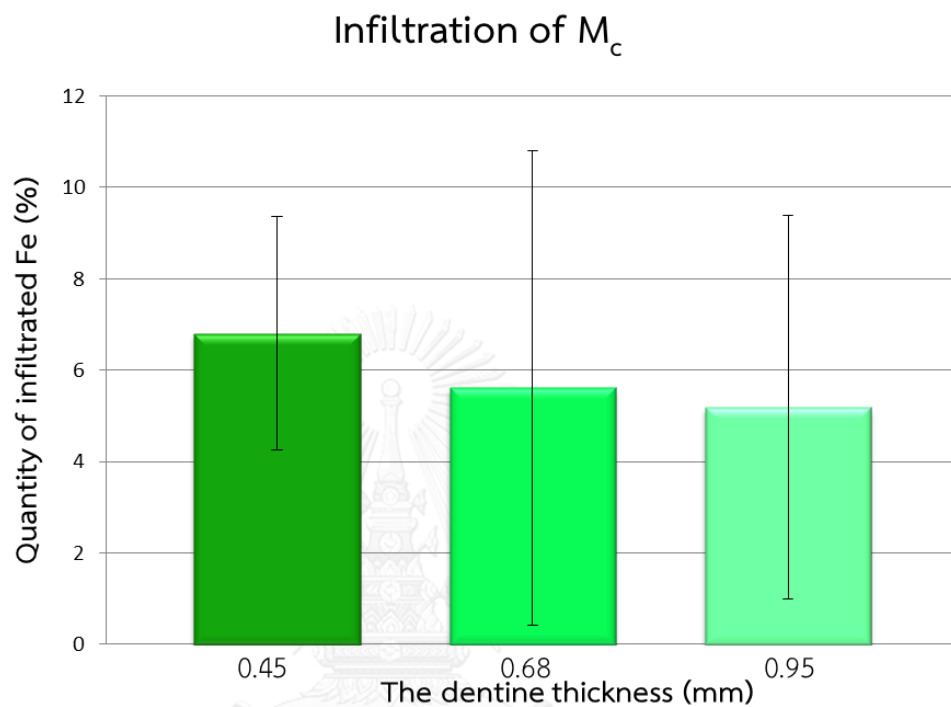


Figure 4.19 Diagram for the percent quantity of iron (Fe) in M_c that passed dentine disc using the different dentine discs (0.45, 0.68 and 0.95 mm) for 4.0 h with 0.453 mg of starting Fe quantity injected to apparatus as shown in Figure 3.3.

In order to apply in the real teeth, the dentine disc with different thickness in nature, the thickness was varied to investigation effect of thickness of the dentine disc. Dentine discs thickness of 0.45, 0.68 and 0.95 mm were used for studying the infiltration of M_c . Amount of iron that can pass through these dentine discs were 6.81%, 5.61% and 5.18%, respectively as shown in Figure 4.19. The results showed that M_c that was passed through the dentine discs when the discs were thinner were insignificantly different from those observed in the thicker discs (one-way ANOVA, $P < 0.05$). The results show that the disc thickness did not affect to the infiltration. Moreover, the dentine disc thickness of about 1.00 mm, the large amount of Fe was

still able to pass through the disc. This observation implied that if the dentine thickness is thicker than 1.00 mm, sufficient quantity of Fe might still be successfully passed through it.

4.2.5 The investigation of magnetic field strength on the infiltration through the dentine discs of the pristine magnetites

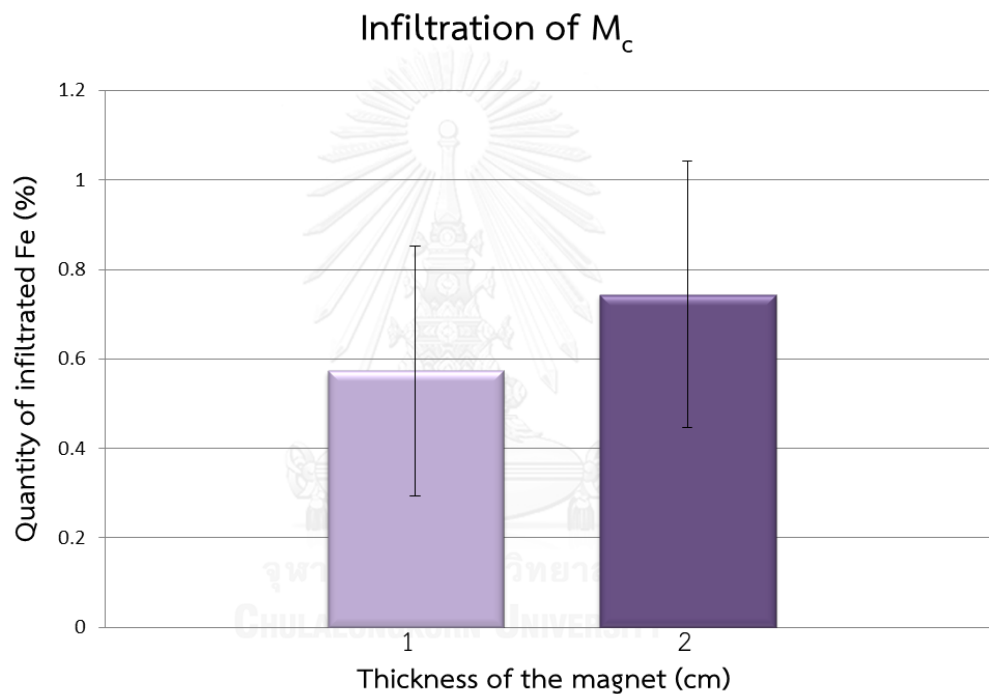


Figure 4.20 Diagram for the percent quantity of iron (Fe) in M_c that passed dentine disc using the same dentine discs with the thickness of 0.45 mm for 0.5 h and 1.287 mg of Fe injected to the apparatus.

In order to study the effect of magnetic strength, a thin (1 cm) magnet and a thick (2 cm) magnet were used for inducing MNPs through the dentine disc. The a thin magnet gave weaker magnetic field than thick magnet. The amount of Fe which passed the disc are 0.57% and 0.74% after inducing with the thin magnet

(32.59×10^2 gauss [84]) and the thick magnet (36.86×10^2 gauss[84]), respectively as shown in Figure 4.20. The results indicated that the strength of magnetic field insignificantly affected to infiltration of M_c in that the stronger magnetic field can induce M_c infiltration insignificantly more than the weaker one (independent t-test, $P < 0.05$). On the other hand, the results showed that the magnet that can induce magnetite did not need to be not very strong to achieve efficient infiltration, making sure this delivery system not too risky and not too complex to use.

4.2.6 The investigation of infiltration through different dentine discs of the pristine magnetites

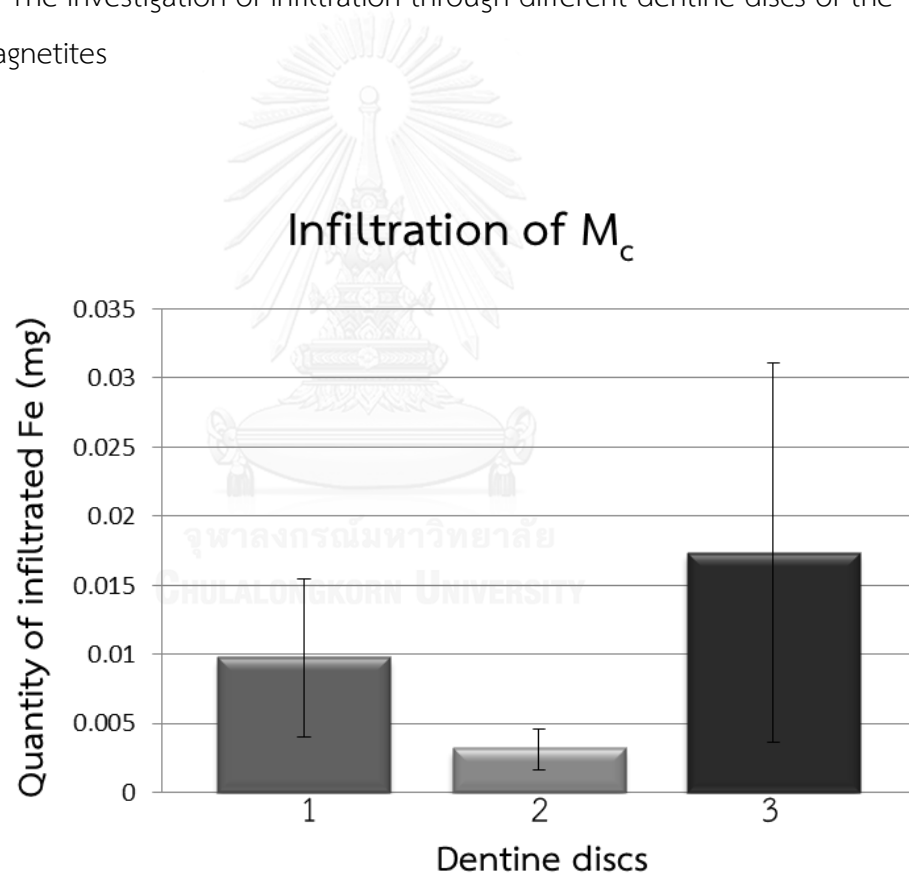


Figure 4.21 Diagram for the percent quantity of iron (Fe) in M_c that passed dentine disc using different dentine discs for 8.0 h with 0.453 mg of starting Fe injected to experiment setup.

The morphologies of dentine discs were different as shown in Figure 4.15. The different dentine discs were of concern in this study. To investigate effect of the different dentine disc, 0.453 mg of starting Fe quantity was used for each the dentine disc and all of the dentine disc thickness are 0.7 mm. The three dentine discs were randomly used for this investigation. The Fe quantity which can be passed the dentine disc number 1, 2 and 3 is 0.097 mg (2.14%), 0.0031 mg (0.69%), and 0.0173 mg (3.83 %), respectively, as shown in Figure 4.21. The amount of iron that passed through different discs was significantly different (one-way ANOVA, $P < 0.05$) because the dentine discs were cut from different teeth, the dentine discs are different in morphologies. In addition, M_c was several times infiltrated through the same disc, but amount of Fe was still so high in deviation for each infiltration experiment as shown in Figure 4.23. The results indicated that with the limit from the nature of the dentine disc, the quantity of Fe from the infiltration of M_c through dentine discs cannot be exactly controlled yet. For the use in the future, better control of MNP infiltration need to be done, or this current system can be applied in the delivery that require minimum threshold instead of require exact quantity.

CHAPTER V

CONCLUSION

For this work, magnetic nanocomposites (MNCs) in the forms of core-shell magnetite-silica MNCs (M@S) and magnetite-decorating silica nanocomposites (S-M) were synthesized successfully. Their sizes were controlled by adjusting the amount of TEOS. The M@SiO₂ MNCs with the sizes of 20 and 40 nm in diameter and the SiO₂-M MNCs with the sizes of 100 and 200 nm in diameter were obtained. All of MNCs were coated with PPEGMA via ATRP (PPEGMA-MNCs). PPEGMA-MNCs can protect the aggregation of MNCs, and they can disperse in water better than the uncoated PPEGMA MNCs.

This work study about infiltration of PPEGMA-MNCs and magnetite NPs through dentine disc with an external magnet. Four sizes of PPEGMA-MNCs were used for studying the effect of magnetic NPs sizes, and the results showed that they exhibited very low magnetic responses and worse dispersity than the pristine magnetite. As a result, PPEGMA-MNCs cannot pass through the dentine discs.

In contrast, magnetite NPs in the form of pristine magnetite NPs were induced by a strong magnet, and they can be passed through the discs. In addition, this work studies factors affecting the infiltration dentine discs of the pristine magnetite, which are dentine compatible solvent, time used, dentine disc thickness, magnet strength and the different dentine discs from different teeth. Although pristine magnetites were dispersed in different solvents, they still can pass through the dentine disc. This observation indicated that type and compatibility of solvent did not affect to their infiltration much, but the dispersity of MNP in the solvent was more important factor for the infiltration through the dentine discs. For the other factors, amount of magnetites infiltrated the dentine disc depended on the time used and the difference in dentine discs. However, the other two factors, dentine thickness and the magnetic field strength exhibited insignificant influences on the infiltration (one-way ANOVA and independent t-test, $P < 0.05$, respectively). From this

observation, it can be implied that MNC dispersity was an important factor for the infiltration through the dentine discs.

This work discovers newly delivery system through dentine discs. The system is a new choice for improvement of root canal treatment. The system is relied on the magnetic property for delivery. The advantages of this system can be that it is not risky and is not complex for dentistry. However, more improvement and development need to be done to increase the delivery efficiency.



REFERENCES

- [1] Lew, K.S.F., Klaseboer, E., and Khoo, B.C. A collapsing bubble-induced micropump: An experimental study. Sensors and Actuators A: Physical 133(1) (2007): 161-172.
- [2] Puapichartdumrong, P., Ikeda, H., and Suda, H. Facilitation of iontophoretic drug delivery through intact and caries-affected dentine. International Endodontic Journal 36(10) (2003): 674-681.
- [3] Shrestha, A., Fong, S.-W., Khoo, B.-C., and Kishen, A. Delivery of Antibacterial Nanoparticles into Dentinal Tubules Using High-intensity Focused Ultrasound. Journal of Endodontics 35(7) (2009): 1028-1033.
- [4] Bedanta, S., Petravic, O., and Kleemann, W. Chapter 1 - Supermagnetism. in Buschow, K.H.J. (ed.) Handbook of Magnetic Materials, pp. 1-83: Elsevier, 2015.
- [5] Coey, J.M.D. Magnetism and Magnetic Materials. Cambridge University Press, 2010.
- [6] Coey, J.M.D. magnetism and magnetic materials. Cambridgeshire, England.: Cambridge University Press, 2012.
- [7] Wei, W., Zhaohui, W., Taekyung, Y., Changzhong, J., and Woo-Sik, K. Recent progress on magnetic iron oxide nanoparticles: synthesis, surface functional strategies and biomedical applications. Science and Technology of Advanced Materials 16(2) (2015): 023501.
- [8] O'Brien, F.J. Biomaterials & scaffolds for tissue engineering. Materials Today 14(3) (2011): 88-95.
- [9] Gowd, G.S., et al. Synthesis of Fe₃O₄@Y₂O₃:Eu³⁺ core-shell multifunctional nanoparticles and their magnetic and luminescence properties. Optical Materials 35(9) (2013): 1685-1692.
- [10] Ye, Y., Kuai, L., and Geng, B. A template-free route to a Fe₃O₄-Co₃O₄ yolk-shell nanostructure as a noble-metal free electrocatalyst for ORR in alkaline media. Journal of Materials Chemistry 22(36) (2012): 19132-19138.

- [11] Sperling, R.A. and Parak, W.J. Surface modification, functionalization and bioconjugation of colloidal inorganic nanoparticles. Vol. 368, 2010.
- [12] Wang, G., et al. Multifunctional Fe₃O₄-CdTe@SiO₂-carboxymethyl chitosan drug nanocarriers: synergistic effect towards magnetic targeted drug delivery and cell imaging. New Journal of Chemistry 38(2) (2014): 700-708.
- [13] Neoh, K.G. and Kang, E.T. Functionalization of inorganic nanoparticles with polymers for stealth biomedical applications. Polymer Chemistry 2(4) (2011): 747-759.
- [14] Tsai, Z.-T., Wang, J.-F., Kuo, H.-Y., Shen, C.-R., Wang, J.-J., and Yen, T.-C. In situ preparation of high relaxivity iron oxide nanoparticles by coating with chitosan: A potential MRI contrast agent useful for cell tracking. Journal of Magnetism and Magnetic Materials 322(2) (2010): 208-213.
- [15] Kloust, H., et al. In Situ Functionalization and PEO Coating of Iron Oxide Nanocrystals Using Seeded Emulsion Polymerization. Langmuir 29(15) (2013): 4915-4921.
- [16] Li, L., et al. Superparamagnetic iron oxide nanoparticles as MRI contrast agents for non-invasive stem cell labeling and tracking. Theranostics 3(2013), 595-615 DOI: 10.7150/thno.5366.
- [17] Lai, S.-M., et al. Polyethylene glycol-based biocompatible and highly stable superparamagnetic iron oxide nanoclusters for magnetic resonance imaging. Journal of Materials Chemistry 22(30) (2012): 15160-15167.
- [18] Miyamoto, D., Oishi, M., Kojima, K., Yoshimoto, K., and Nagasaki, Y. Completely Dispersible PEGylated Gold Nanoparticles under Physiological Conditions: Modification of Gold Nanoparticles with Precisely Controlled PEG-b-polyamine. Langmuir 24(9) (2008): 5010-5017.
- [19] Jon, S., Seong, J., Khademhosseini, A., Tran, T.-N.T., Laibinis, P.E., and Langer, R. Construction of Nonbiofouling Surfaces by Polymeric Self-Assembled Monolayers. Langmuir 19(24) (2003): 9989-9993.
- [20] Fan, Q.-L., Neoh, K.-G., Kang, E.-T., Shuter, B., and Wang, S.-C. Solvent-free atom transfer radical polymerization for the preparation of poly(poly(ethyleneglycol) monomethacrylate)-grafted Fe₃O₄ nanoparticles:

- Synthesis, characterization and cellular uptake. Biomaterials 28(36) (2007): 5426-5436.
- [21] Poly(methyl methacrylate) particulate carriers in drug delivery. Journal of Microencapsulation (2012): 1.
- [22] Wu, X., et al. Water-soluble dendritic-linear triblock copolymer-modified magnetic nanoparticles: preparation, characterization and drug release properties. Journal of Materials Chemistry 21(35) (2011): 13611-13620.
- [23] Tailoring magnetic PLGA nanoparticles suitable for doxorubicin delivery. Journal of Nanoparticle Research 16(1) (2014).
- [24] Qi, Y., et al. Hollow superparamagnetic PLGA/Fe₃O₄ composite microspheres for lysozyme adsorption. Nanotechnology 25(8) (2014): 085702.
- [25] Chen, H., Yuan, L., Song, W., Wu, Z., and Li, D. Biocompatible polymer materials: Role of protein-surface interactions. Progress in Polymer Science 33(11) (2008): 1059-1087.
- [26] Ashish kalthane. slide share enamel, dentin and pulp [Online]. 2015. Available from: <http://www.slideshare.net/ashish1801/1-enamel-dentin-pulp?related=1>
- [27] Britannica. Encyclopædia britannica dentin [Online]. 2015. Available from: <http://global.britannica.com/EBchecked/topic/158066/dentin>
- [28] 123rf. ROYALTY FREE STOCK PHOTOS, VECTORS AND ILLUSTRATIONS Dentin Stock Vectors, Clipart and Illustrations [Online]. 2015. Available from: <http://www.123rf.com/clipart-vector/dentin.html>
- [29] Schwertmann, U. and Cornell, R.M. Ferrihydrite. in Iron Oxides in the Laboratory, pp. 103-112: Wiley-VCH Verlag GmbH, 2007.
- [30] Gupta, A.K. and Gupta, M. Synthesis and surface engineering of iron oxide nanoparticles for biomedical applications. Biomaterials 26(18) (2005): 3995-4021.
- [31] Park, J., et al. Ultra-large-scale syntheses of monodisperse nanocrystals. Nat Mater 3(12) (2004): 891-895.
- [32] Sun, S. and Zeng, H. Size-Controlled Synthesis of Magnetite Nanoparticles. Journal of the American Chemical Society 124(28) (2002): 8204-8205.

- [33] Li, Z., Tan, B., Allix, M., Cooper, A.I., and Rosseinsky, M.J. Direct Coprecipitation Route to Monodisperse Dual-Functionalized Magnetic Iron Oxide Nanocrystals Without Size Selection. Small 4(2) (2008): 231-239.
- [34] Woo, K., et al. Easy Synthesis and Magnetic Properties of Iron Oxide Nanoparticles. Chemistry of Materials 16(14) (2004): 2814-2818.
- [35] Wang, Y., Zhu, Z., Xu, F., and Wei, X. One-pot reaction to synthesize superparamagnetic iron oxide nanoparticles by adding phenol as reducing agent and stabilizer. Journal of Nanoparticle Research 14(4) (2012): 1-7.
- [36] Bronstein, L.M., et al. Influence of Iron Oleate Complex Structure on Iron Oxide Nanoparticle Formation. Chemistry of Materials 19(15) (2007): 3624-3632.
- [37] Rockenberger, J., Scher, E.C., and Alivisatos, A.P. A New Nonhydrolytic Single-Precursor Approach to Surfactant-Capped Nanocrystals of Transition Metal Oxides. Journal of the American Chemical Society 121(49) (1999): 11595-11596.
- [38] Liang, X., Wang, X., Zhuang, J., Chen, Y., Wang, D., and Li, Y. Synthesis of Nearly Monodisperse Iron Oxide and Oxyhydroxide Nanocrystals. Advanced Functional Materials 16(14) (2006): 1805-1813.
- [39] Hu, M., Jiang, J.-S., Bu, F.-X., Cheng, X.-L., Lin, C.-C., and Zeng, Y. Hierarchical magnetic iron (iii) oxides prepared by solid-state thermal decomposition of coordination polymers. RSC Advances 2(11) (2012): 4782-4786.
- [40] Hu, M., Jiang, J.-S., and Zeng, Y. Prussian blue microcrystals prepared by selective etching and their conversion to mesoporous magnetic iron(iii) oxides. Chemical Communications 46(7) (2010): 1133-1135.
- [41] Amara, D. and Margel, S. Solventless thermal decomposition of ferrocene as a new approach for the synthesis of porous superparamagnetic and ferromagnetic composite microspheres of narrow size distribution. Journal of Materials Chemistry 21(39) (2011): 15764-15772.
- [42] Maity, D., Choo, S.-G., Yi, J., Ding, J., and Xue, J.M. Synthesis of magnetite nanoparticles via a solvent-free thermal decomposition route. Journal of Magnetism and Magnetic Materials 321(9) (2009): 1256-1259.

- [43] Liu, S. and Han, M.-Y. Silica-Coated Metal Nanoparticles. Chemistry – An Asian Journal 5(1) (2010): 36-45.
- [44] Rao, K.S., El-Hami, K., Kodaki, T., Matsushige, K., and Makino, K. A novel method for synthesis of silica nanoparticles. Journal of Colloid and Interface Science 289(1) (2005): 125-131.
- [45] Rahman, I.A., et al. An optimized sol–gel synthesis of stable primary equivalent silica particles. Colloids and Surfaces A: Physicochemical and Engineering Aspects 294(1–3) (2007): 102-110.
- [46] Park, S.K., Kim, K.D., and Kim, H.T. Preparation of silica nanoparticles: determination of the optimal synthesis conditions for small and uniform particles. Colloids and Surfaces A: Physicochemical and Engineering Aspects 197(1–3) (2002): 7-17.
- [47] He, W., et al. Bifunctional nanoparticles with magnetism and NIR fluorescence: controlled synthesis from combination of AGET ATRP and ‘click’ reaction. Nanotechnology 25(4) (2014): 045602.
- [48] Zayat, M., Garcia-Parejo, P., and Levy, D. Preventing UV-light damage of light sensitive materials using a highly protective UV-absorbing coating. Chemical Society Reviews 36(8) (2007): 1270-1281.
- [49] Guerrero-Martínez, A., Pérez-Juste, J., and Liz-Marzán, L.M. Recent Progress on Silica Coating of Nanoparticles and Related Nanomaterials. Advanced Materials 22(11) (2010): 1182-1195.
- [50] Chaikin, Y., Kedem, O., Raz, J., Vaskevich, A., and Rubinstein, I. Stabilization of Metal Nanoparticle Films on Glass Surfaces Using Ultrathin Silica Coating. Analytical Chemistry 85(21) (2013): 10022-10027.
- [51] Kobayashi, Y., Katakami, H., Mine, E., Nagao, D., Konno, M., and Liz-Marzán, L.M. Silica coating of silver nanoparticles using a modified Stöber method. Journal of Colloid and Interface Science 283(2) (2005): 392-396.
- [52] Jana, N.R., Earhart, C., and Ying, J.Y. Synthesis of Water-Soluble and Functionalized Nanoparticles by Silica Coating. Chemistry of Materials 19(21) (2007): 5074-5082.

- [53] Yi, D.K., Lee, S.S., Papaefthymiou, G.C., and Ying, J.Y. Nanoparticle Architectures Templated by SiO₂/Fe₂O₃ Nanocomposites. Chemistry of Materials 18(3) (2006): 614-619.
- [54] Ladj, R., et al. Individual inorganic nanoparticles: preparation, functionalization and in vitro biomedical diagnostic applications. Journal of Materials Chemistry B 1(10) (2013): 1381-1396.
- [55] Wongwailikhit, K. and Horwongsakul, S. The preparation of iron (III) oxide nanoparticles using W/O microemulsion. Materials Letters 65(17-18) (2011): 2820-2822.
- [56] Han, L.-H., Liu, H., and Wei, Y. In situ synthesis of hematite nanoparticles using a low-temperature microemulsion method. Powder Technology 207(1-3) (2011): 42-46.
- [57] Malik, M.A., Wani, M.Y., and Hashim, M.A. Microemulsion method: A novel route to synthesize organic and inorganic nanomaterials: 1st Nano Update. Arabian Journal of Chemistry 5(4) (2012): 397-417.
- [58] Tai, H.-Y., Fu, E., and Don, T.-M. Calcium phosphates synthesized by reverse emulsion method for the preparation of chitosan composite membranes. Carbohydrate Polymers 88(3) (2012): 904-911.
- [59] Meador, M.A.B., Nguyen, B.N., and Guo, H. Highly porous ceramic oxide aerogels having improved flexibility. 2011, Google Patents.
- [60] Pandey, S. and Mishra, S. Sol-gel derived organic-inorganic hybrid materials: synthesis, characterizations and applications. Journal of Sol-Gel Science and Technology 59(1) (2011): 73-94.
- [61] Facile synthesis of complex multi-component organic and organic-magnetic inorganic nanocomposite particles. Journal of Materials Chemistry 22(47) (2012): 24744.
- [62] Magnetite fine particles highly loaded PMMA microspheres for hyperthermia of deep-seated cancer. Journal of the Ceramic Society of Japan 121(1417) (2013): 802.

- [63] Yang, X., Tian, H., Ho, C.-T., and Huang, Q. Stability of Citral in Emulsions Coated with Cationic Biopolymer Layers. Journal of Agricultural and Food Chemistry 60(1) (2012): 402-409.
- [64] Swee Kuan Yen, Parasuraman Padmanabhan, and Selvan, S.T. Multifunctional Iron Oxide Nanoparticles for Diagnostics, Therapy and Macromolecule Delivery. Theranostics 3(12) (2013): 986-1003.
- [65] He, W., Jiang, H., Zhang, L., Cheng, Z., and Zhu, X. Atom transfer radical polymerization of hydrophilic monomers and its applications. Polymer Chemistry 4(10) (2013): 2919-2938.
- [66] Matyjaszewski, K., Shipp, D.A., Wang, J.-L., Grimaud, T., and Patten, T.E. Utilizing Halide Exchange To Improve Control of Atom Transfer Radical Polymerization. Macromolecules 31(20) (1998): 6836-6840.
- [67] Peng, C.-H., Kong, J., Seeliger, F., and Matyjaszewski, K. Mechanism of Halogen Exchange in ATRP. Macromolecules 44(19) (2011): 7546-7557.
- [68] Wei, W., Quanguo, H., and Hong, C. Silane Bridged Surface Tailoring on Magnetite Nanoparticles. in Bioinformatics and Biomedical Engineering, 2007. ICBBE 2007. The 1st International Conference on, pp. 76-79, 2007.
- [69] Blogger. Human Biochemistry , Mcqs , Quizzes and Postgraduation entrance preparation 43 - Ninhydrin test or Ninhydrin reagent [Online]. 2015. Available from: <http://ourbiochemistry.blogspot.com/2010/07/43-ninhydrin-test-or-ninhydrin-reagent.html> [23 JULY 23]
- [70] Flesch, C., Unterfinger, Y., Bourgeat-Lami, E., Duguet, E., Delaite, C., and Dumas, P. Poly(ethylene glycol) Surface Coated Magnetic Particles. Macromolecular Rapid Communications 26(18) (2005): 1494-1498.
- [71] Kanhakeaw, P., Rutnakornpituk, B., Wichai, U., and Rutnakornpituk, M. Surface-Initiated Atom Transfer Radical Polymerization of Magnetite Nanoparticles with Statistical Poly(tert-butyl acrylate)-poly(poly(ethylene glycol) methyl ether methacrylate) Copolymers. Journal of Nanomaterials 2015 (2015): 10.
- [72] Hu, Neoh, K.G., Cen, L., and Kang, E.-T. Cellular Response to Magnetic Nanoparticles “PEGylated” via Surface-Initiated Atom Transfer Radical Polymerization. Biomacromolecules 7(3) (2006): 809-816.

- [73] Colombo, M., et al. Biological applications of magnetic nanoparticles. Chemical Society Reviews 41(11) (2012): 4306-4334.
- [74] Lehmann, A.D., et al. Fluorescent-magnetic hybrid nanoparticles induce a dose-dependent increase in proinflammatory response in lung cells in vitro correlated with intracellular localization. Small 6(6) (2010): 753-62.
- [75] Yang, Y., et al. Enzyme-Responsive Multifunctional Magnetic Nanoparticles for Tumor Intracellular Drug Delivery and Imaging. Chemistry – An Asian Journal 6(6) (2011): 1381-1389.
- [76] Karakoti, A.S., Das, S., Thevuthasan, S., and Seal, S. PEGylated Inorganic Nanoparticles. Angewandte Chemie International Edition 50(9) (2011): 1980-1994.
- [77] Lutz, J.-F., Stiller, S., Hoth, A., Kaufner, L., Pison, U., and Cartier, R. One-Pot Synthesis of PEGylated Ultrasmall Iron-Oxide Nanoparticles and Their in Vivo Evaluation as Magnetic Resonance Imaging Contrast Agents. Biomacromolecules 7(11) (2006): 3132-3138.
- [78] Musi, S., Filipovi -Vincekovi, N., and Sekovani, L. Precipitation of amorphous SiO₂ particles and their properties. Brazilian Journal of Chemical Engineering 28 (2011): 89-94.
- [79] Li, H. and Li, Y. Synthesis of highly luminescent cobalt(ii)-bis(8-hydroxyquinoline)nanosheets as isomeric aromatic amine probes. Nanoscale 1(1) (2009): 128-132.
- [80] Blogger. Spectroscopy data amide infrared spectra [Online]. 2012. Available from: <http://chemistrytextbookcrawl.blogspot.com/2012/12/amide-infrared-spectra.html>
- [81] Tschamner, W. Photon Correlation Spectroscopy in Particle Sizing. in Encyclopedia of Analytical Chemistry: John Wiley & Sons, Ltd, 2006.
- [82] Wu, W., Changzhong, J., and Roy, V.A.L. Recent progress in magnetic iron oxide-semiconductor composite nanomaterials as promising photocatalysts. Nanoscale 7(1) (2015): 38-58.

- [83] Reddy, L.H., Arias, J.L., Nicolas, J., and Couvreur, P. Magnetic Nanoparticles: Design and Characterization, Toxicity and Biocompatibility, Pharmaceutical and Biomedical Applications. *Chemical Reviews* 112(11) (2012): 5818-5878.
- [84] Elmhurst, a. Adams magnetic product. in *Gauss and Pull Calculators for Magnets*. 2015.





APPENDIX

จุฬาลงกรณ์มหาวิทยาลัย
CHULALONGKORN UNIVERSITY

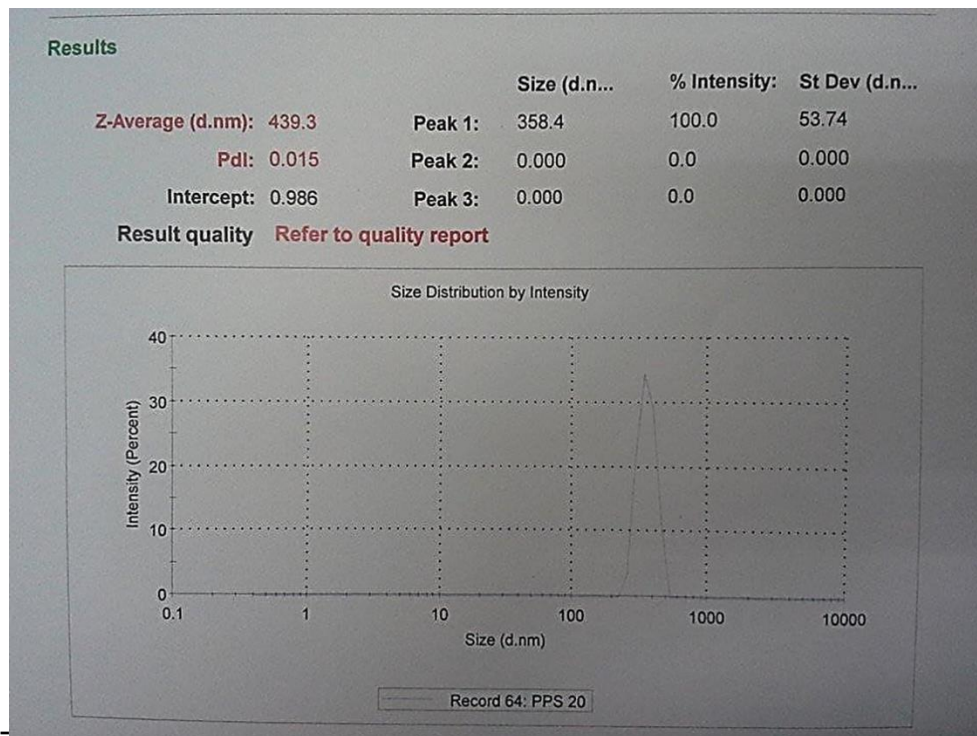


Figure A1 Distribution graph of PPS-20 from DLS analysis

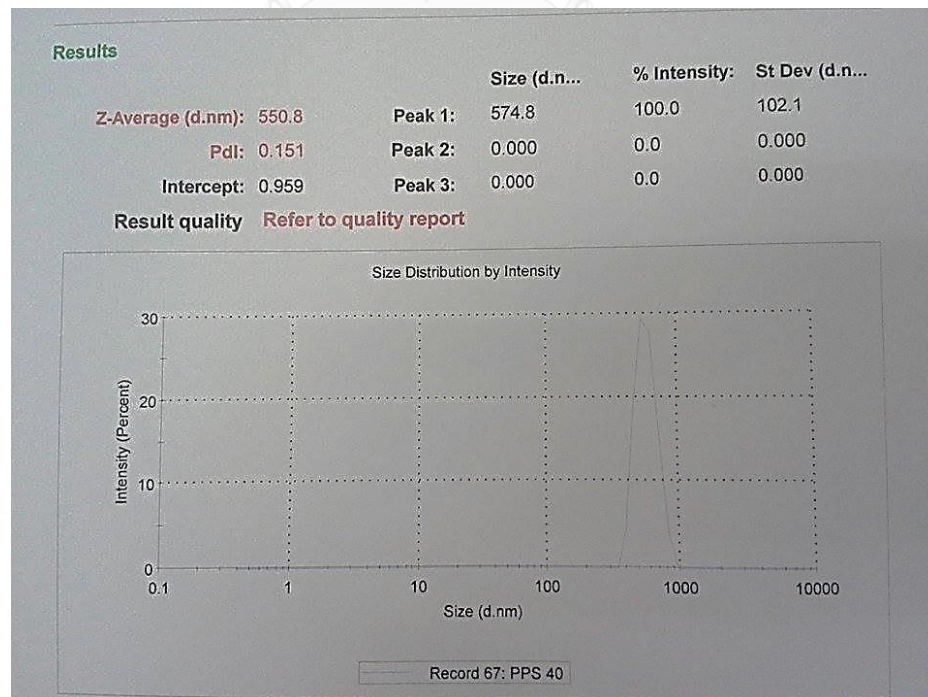


Figure A2 Distribution graph of PPS-40 from DLS analysis

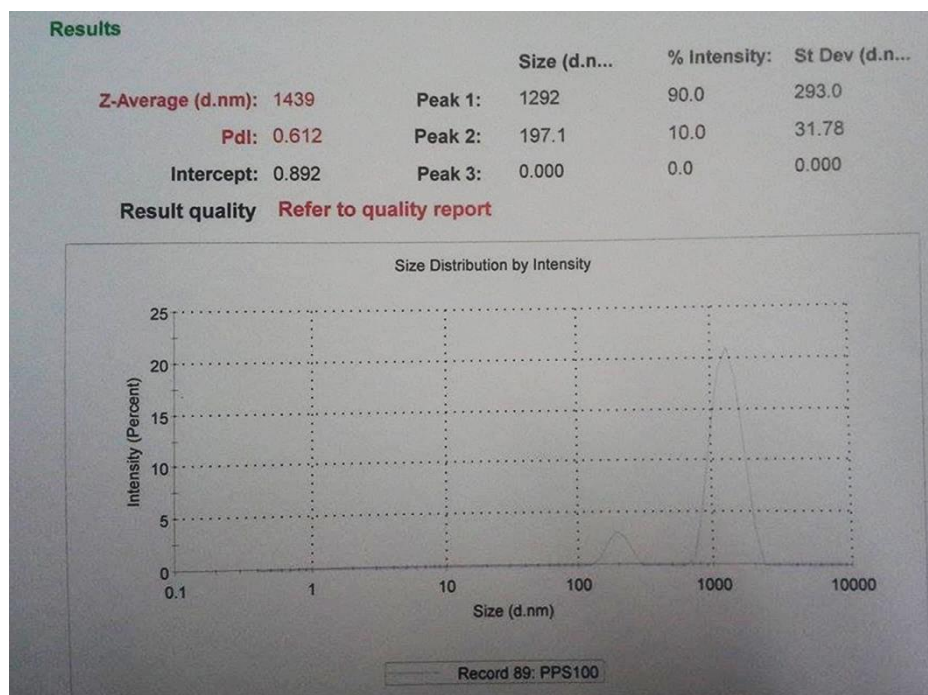


Figure A3 Distribution graph of PPS-100 from DLS analysis

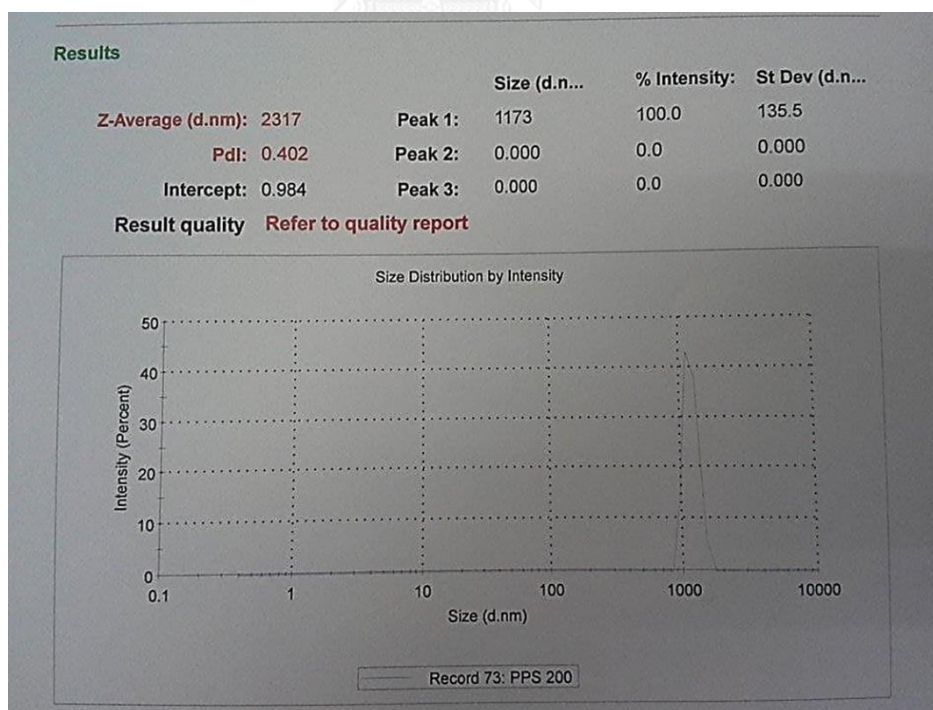


Figure A4 Distribution graph of PPS-200 from DLS analysis

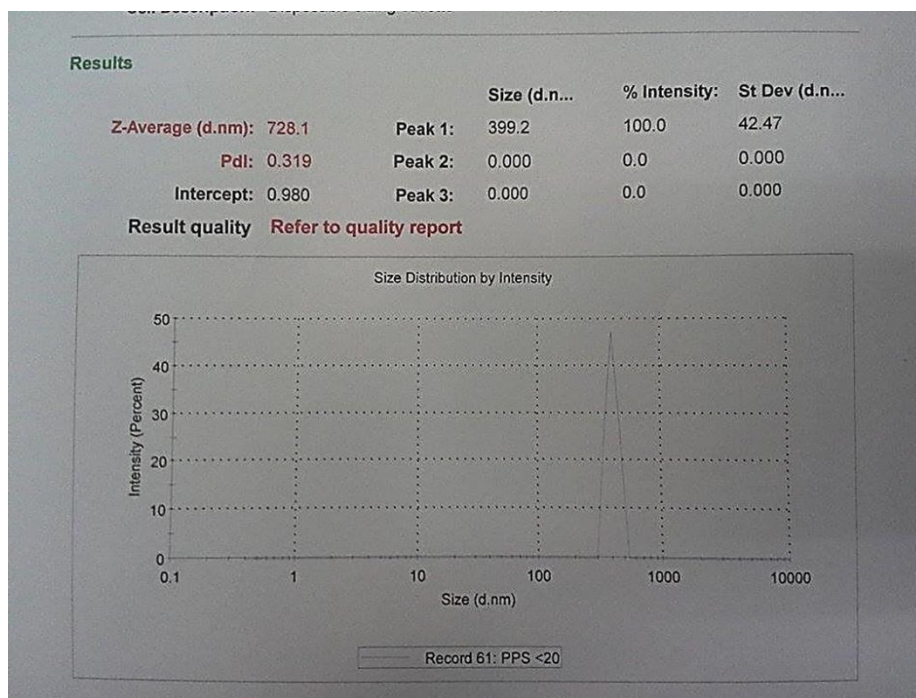


Figure A5 Distribution graph of PPS<20 from DLS analysis

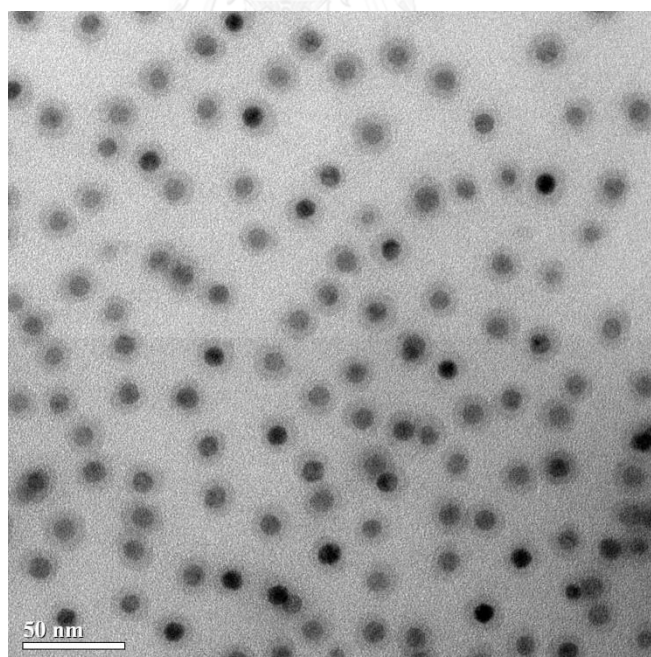


Figure A6 TEM image of PPS<20

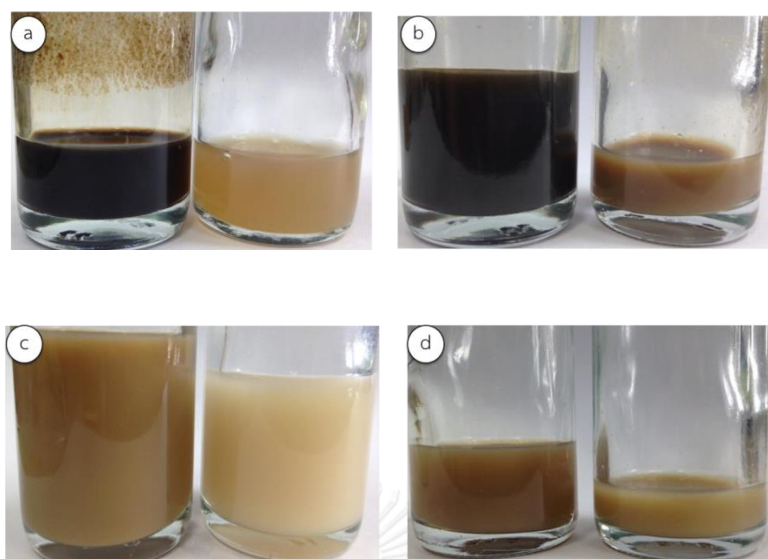


Figure A7 Photographs comparing the dispersibility of MNCs (left) and PPEGMA coated MNCs dispersions (right); figures (a), (b), (c), and (d) are for NPs of the size 20, 40, 100 and 200 nm in diameter, respectively.

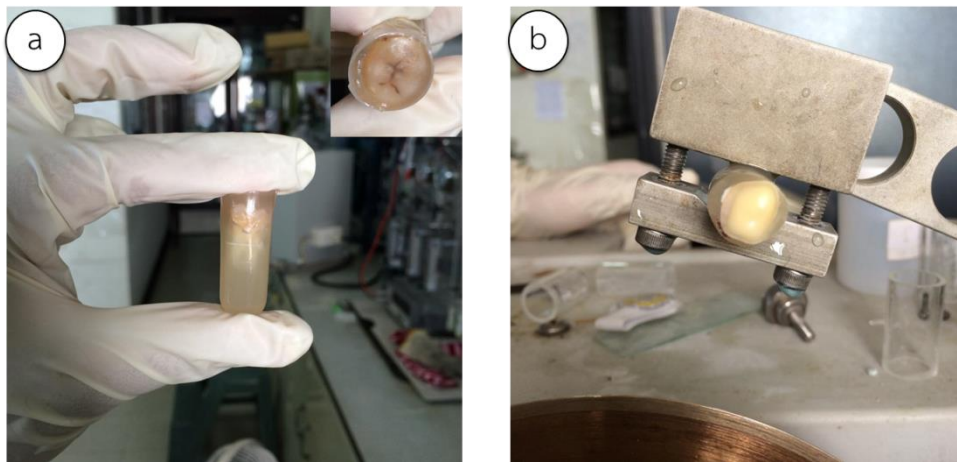


Figure A8 Photographs of the preparation process of the dentine discs, (a) The dentine disc casting in a resin and (b) the dentine disc cutting

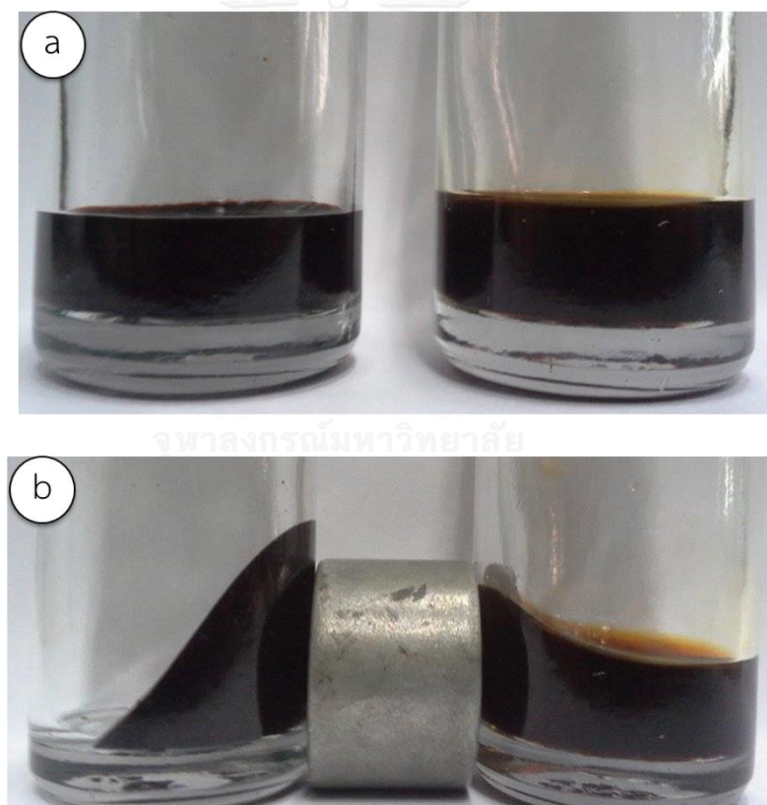


Figure A9 Images of the pristine magnetite dispersion (M_c , left) and (M_e right), (a) without a strong magnet and (b) with a strong magnet.

VITA

Miss Wishulada Injumba was born on September 23, 1990 in Sakonnakorn, Thailand. She graduated in Bachelor Degree of Science in Chemistry from Khonkaen University in 2012. She continued her Master's Degree of Science in Chemistry at Chulalongkorn University. She became a member of Materials Chemistry and Catalysis Research Unit under the supervision of Dr. Numpon Insin. On 21-23 January 2015, she attended the 15th Pure and Applied Chemistry International Conference 2015 in the title of "SYNTHESES OF MAGNETIC NANOCOMPOSITES SIZE SERIES" by poster presentation.

Her present address is 107 Rama4 road, Bangruk, Bangkok, Thailand 10500

E-mail address: Wishu_lada@hotmail.com

